GEORGIA INSTITUTE OF TECHNOLOGY
Engineering Experiment Station

PROJECT INITIATION

Date: April 5, 1974

Project Title: Solar Furnace Cross-Calibration Program Analysis

Project No.: A-1620

Project Director: Dr. Steve H. Bomar

Sponsor: U.S. Army, White Sands Missile Range, New Mexico

Effective March 26, 1974 Estimated to run until March 25, 1975

Type Agreement: Contract No. DAAD07-74-C-0145 (Fixed Price) Amount: $ 16,183.40

Reports Required: Letter Progress Report; Interim Technical Report; Technical Report (Final)

Sponsor Contact Person (s):

Technical Matters

Commanding General
ATTN: Mr. Marvin Squires
STEWS-TE-NT
White Sands Missile Range
New Mexico 88002

Phone: (915)678-1161

Contractual Matters
(Thru GTRI)
Procurement Directorate
ATTN: Mr. Charles P. Cutler
Contract Administrator
STEWS-PR-A, Building 1830
White Sands Missile Range
New Mexico 88002

Phone: (915)678-3338

DEFENSE PRIORITY RATING: DO-S1 under DMS Reg. 1.

Assigned to HIGH TEMPERATURE MATERIALS Division

COPIES TO:

- ☐ Project Director
- ☐ Director
- ☐ Assistant Director
- ☐ GTRI
- ☐ Division Chief (s)
- ☐ Branch Heads
- ☐ Service Groups
- ☐ Patent Coordinator
- ☐ Photographic Laboratory
- ☑ Security, Property, Reports Coordinator
- ☐ EES Accounting
- ☐ EES Supply Services
- ☐ Library
- ☐ Office of Computing Services
- ☐ Project File
- ☐ Other _____

RA-73

Posted
A65

GEORGIA INSTITUTE OF TECHNOLOGY
ENGINEERING EXPERIMENT STATION

PROJECT TERMINATION

Date: October 1, 1975

Project Title: Solar Furnace Cross-Calibration Program Analysis

Project No.: A-1633

Project Director: Dr. S. H. Bomar

Sponsor: U. S. Army, White Sands Missile Range, New Mexico

Effective Termination Date: 3/23/75 (Contract Expiration)

Clearance of Accounting Charges: all charges have cleared

Grant/Contract Closeout Actions Remaining:
1. Final Report of Inventions
2. Gov't. Property Inventory & Cert.
3. Classified Material Cert.

Assigned to: Energy & Materials Technology Division

COPIES TO:

Project Director
Director, EES
Director, ORA/GTRI
Assistant Director
Division Chief
EES Accounting
Patent Coordinator

EES Supply Services
Photographic Laboratory
Security—Reports—Property Office
General Office Services
Library, Technical Reports Section
Office of Computing Services
Project File
Other _____

Form EES 402 (R3—75)

A-1620

ENGINEERING EXPERIMENT STATION
GEORGIA INSTITUTE OF TECHNOLOGY • ATLANTA, GEORGIA 30332

June 11, 1974

TE-PM, Bldg. 1504
Attn: Mr. William Frye
M/F: PR&C 3340-301
Contract DAAD07-74-C-0145
White Sands Missile Range,
New Mexico 88002

Subject: Letter Progress Report, Contract DAAD07-74-C-0145,
"Solar Furnace Cross-Calibration Program Analysis"
(Georgia Tech Project A-1620)

Gentlemen:

In accordance with the provisions of the Contract, J. D. Walton, Jr. and S. H. Bomar, Jr. visited the White Sands Solar Furnace (WSSF) Facility on 20-21 May 1974, for the purpose of completing program Phase 1. We have also reviewed material in the technical literature pertaining directly to this facility (References 1-3), studied photographs provided by Mr. Marvin Squires, and conducted numerous telephone conversations with Mr. Squires and members of his staff. This letter report sets forth our recommended analysis plan to accomplish program Phases 2 and 3.

Our completion of Phase 1 is approximately one month later than specified in the Contract; this results from difficulty in scheduling a mutually acceptable time for the Georgia Tech personnel to visit the WSSF. However, it is anticipated that this delay will not affect timing of the remainder of the program.

PHASE 2 - INITIAL ANALYSIS AND RECOMMENDATIONS

The objectives of Phase 2 are to determine the best types of instruments and procedures to be used for measurement of certain operating parameters of the WSSF. We are concerned with calibration during the initial startup period and with furnace operations after startup is completed. Georgia Tech will submit recommendations dealing with instruments and operations as well as new techniques and opportunities which become known to us during the course of the program.

Phase 2 is scheduled for completion seven months after initiation of the contract. An interim technical report will be submitted by 25 October 1974, covering the Phase 2 effort and an updated work plan for Phase 3. Specific

approaches for completing the program tasks are given in the following sections. Since it is necessary that the solar furnace be operated while some of these procedures are conducted and it is desirable that a Georgia Tech investigator be present to participate, the timing of the work will require coordination with the WSSF staff.

1. Total Thermal Fluence

It is recommended that a particular plane normal to the optical axis of the solar furnace be designated the "focal plane" and carefully mapped by the techniques described below. It is also desirable that the three dimensional region in the vicinity of the focal plane be mapped both forward and back from this plane; this three dimensional region will be called the "focal zone." There are two basic types of calorimeters with which the focal plane should be mapped. The first is a cavity-shaped water-cooled calorimeter and the second is a disk radiometer; the two instruments each give "absolute" measurements and should therefore permit cross checks to be established. After the heat flux distribution at the focal plane is established, other methods of measurement might simplify the experimental procedures for mapping the entire focal zone.

a. Cavity Shaped Water Cooled Calorimeter. This method will serve as one of the primary standards for mapping the focal plane. A calorimeter of the type described by Glaser (Reference 4) or Trombe and Le Phat Vinh (Reference 5) should be employed. These cavity shaped instruments are preferred over a blackened flat-plate calorimeters because their geometry approaches that of a black body, and they absorb substantially all of the energy incident on the aperture. If two aperture sizes are available, for example one inch and four inches, it will be possible to calculate the total heat from a distribution curve and measure the total heat directly over a relatively large area.

b. Disk Radiometer. This method is the second choice for a primary standard, and employs instruments of the type described by Gardon (Reference 6) and Trombe and Le Phat Vinh (Reference 5). These devices are sold by Hy-Cal Engineering under the nomenclature "Asymtotic Calorimeter" and are already being considered by White Sands personnel for heat flux measurements. Only the water cooled variety appear suitable for use in the WSSF environment. In disk radiometers, water cooling is used to protect the equipment; heat input is measured by a differential thermocouple. The active measurement area is small, usually in the range of 0.1 to 0.5 inch diameter, so that they must be used to determine a heat flux distribution rather than a total flux over a large area. The cavity shaped water cooled calorimeters and disk radiometers together should permit the heat flux at the focal plane to be mapped with a high level of confidence, since cross checking is possible.

c. Thermal Fluence Mapping of the Focal Zone. After the heat flux in the focal plane has been established as a function of direct incident sunlight intensity and position in the plane, it is desirable that the three dimensional focal zone be mapped. Water cooled disk radiometers are suitable for this purpose and it is expected that they will be easier to operate than the cavity shaped calorimeters since careful monitoring of the water flow rate is not required. Measurements forward and back from the focal plane will be referred to previously established heat fluxes in the focal plane to confirm the values measured by the radiometer. In addition to this conventional technique, two other methods of measuring relative heat fluxes might be applicable and offer experimental advantages. In the first of these, the light from a full moon would be directed to the focal zone as a substitute for sunlight. A grid inked on translucent paper would be placed in the plane where measurements were to be made, and light intensity within the grid squares would be determined with a small-spot photographic light meter. This scheme would permit a large number of measurements to be made quickly, without coping with the hazard of intense radiation in the focal zone. If successful, it might be especially useful for future verification of the focal zone characteristics after changes in the optical system. In the second alternate measurement method, a magnesium-oxide-smoked, water-cooled plate would be placed at the plane where measurements were to be made. Various positions on the plate would then be viewed from the open area in the concentrating mirror array using a monochromatic optical pyrometer. Since powdered magnesium oxide has a diffuse reflectivity approaching one, and the plate would be maintained near room temperature, the optical pyrometer would observe reflected sunlight at its operating wavelength. It should be a straightforward task to correlate the pyrometer's output with the heat flux arriving at a particular location on the plate. Brief investigations of both these alternate techniques have been conducted at the CNRS solar furnace, and they appear to be workable.

d. Georgia Tech Participation. It is recommended that a Georgia Tech investigator participate in the thermal fluence mapping to assist the WSSF staff. After the necessary equipment has been assembled and assuming favorable weather, it is estimated that this work could be accomplished in about one week.

2. Pulse Rise Time and Pulse Shape

On the basis of Reference 3, it is estimated that pulse rise times on the order of 0.1 second must be resolved and that the instruments must have time constants in the range of 1 to 5 milliseconds to adequately record the pulse shape. At the Natick installation pulse shape and rise time were measured with a gas phototube; however, present technology will permit development of a much simpler and probably more reliable system. Radiometers or photoelectric detectors are the best candidates for this application and photographic recording from an oscilloscope screen is recommended.

a. Radiometers. Hy-Cal Engineering offers a line of radiometers which have "rapid response time." Detailed data on these will be requested by Georgia Tech to determine their suitability for this application.

b. Semiconductor Photoelectric Detector. An electronics engineer consulted at Georgia Tech has indicated that a number of solid state photoelectric detectors are available which should be suitable for measuring pulse rise time and shape under the requirements of this program. Their response to varying light levels is usually a change in internal resistance, and a simple circuit can be set up to use this output to drive an oscilloscope or recording oscillograph. Photographic recording of an oscilloscope trace is recommended because it is easy to accomplish and the equipment is probably alreay on hand at the WSSF. A trigger pulse is necessary to start the oscilloscope trace and can be provided from the mechanism that opens the shutter at the focal plane. For shorter pulses, the power line frequency provides a convenient check on the time base calibration before each test.

c. Improved Pulse Shaping System. The use of Kerr cells or other electro-optical pulse shaping methods will be investigated. The CNRS Solar Energy Laboratory has designed and built a mechanical shutter for simulating nuclear pulses under a U. S. Army contract; the possibility of adapting this design to the WSSF will be investigated.

d. Georgia Tech Participation. It is recommended that an electronics engineer at Georgia Tech be assigned to devise a photoelectric pulse measurement circuit if in his judgment this can be done in 30 to 40 man-hours. The circuit will be tested at Georgia Tech and delivered to White Sands. Other work within this task will be conducted before and during the visit for thermal fluence mapping.

3. Temperatures in Test Objects

It is desired that both internal and surface temperatures be measured in a great variety of materials which might be tested at the WSSF. Metal wire thermocouples are the most satisfactory method of measuring internal temperatures, but are not desirable for measuring the temperatures of surfaces exposed to radiant heat fluxes. Optical pyrometry is the preferred method of measuring surface temperatures if the fundamental difficulty of accounting for reflected energy can be overcome.

a. Internal Temperatures. Thermocouples of Chromel:Alumel or Platinum: Platinum-Rhodium are recommended for internal temperature measurements. However, the thermocouple wire diameter should be made as small as possible and the bead should be essentially the same diameter as the wire. These precautions minimize disruption of the specimen and assure negligible

heat capacity of the thermocouple junction. The choice of thermocouple metals depends on the anticipated temperature; Chromel:Alumel is useable to 2400° F and Platinum:Platinum-Rhodium is useable to 3000° F. Above 3000° F, alloys of Tungsten and Rhenium can be employed, although they oxidize in air at elevated temperature. In most material response tests conducted in the solar furnace, in-depth sample temperatures will not exceed the capabilities of Chromel:Alumel and exposure times will be on the order of a few seconds. Placement of thermocouples depends on the nature of the specimens; in soft materials they can be installed with a sewing needle, and in ceramics and metals they must be placed in saw cuts. Thermocouple wire diameters of 0.005 to 0.015 inch are available.

b. Optical Pyrometry. The use of thermocouples on surfaces exposed to radiant heat fluxes presumes that the absorption characteristics of the thermocouple match those of the specimen. Our experience indicates that such an assumption is untenable in many situations; for example, translucent materials absorb energy in depth as well as on the surface and the emittance of a thermocouple may be quite different from that of the sample. Therefore, optical pyrometry is preferred for surface temperature measurements. In order to use optical pyrometry however, one must devise a means of accounting for the reflected incident radiation and separating it from the thermally emitted radiation which is to be measured. This separation can be accomplished by optically filtering the incident radiation at the operating wavelength of the pyrometer or by mechanically chopping the incident radiation for brief time intervals and obtaining optical temperature data while the incident beam is cut off (References 7,8). Either of these schemes involves the sacrifice of a portion of the incident energy from the concentrator of the solar furnace. Mechanical chopping is unacceptable during nuclear pulse simulation tests because the pulse time is the same order of magnitude as the chopping time. The spectral absorption bands which occur in glass have provided automatic filtering at the CNRS solar furnace since back surfaced mirrors are used in that facility. It has been established that such filtering does not occur in the WSSF because most of the mirrors are front surfaced.

Use of a filter in the incident beam will be considered and the various alternatives presented to WSSF personnel. Rough estimates suggest that a 36-inch square Pyrex window located near the front wall of the focal building would be a satisfactory filter and would survive the environment. Plexiglas has an absorption band at 1.7 μm; an eight foot square panel placed near the plane of the attenuator might give the required filtering and survive the environment. If one or two filtering methods which are acceptable to WSSF personnel can be identified, then compatible pyrometry equipment can be chosen.

c. Other Optical Pyrometry Techniques. Methods for operating optical pyrometers without the use of filters or choppers can be envisioned,

but their feasibility has not been proven. For example, signal conditioning techniques might permit subtraction of the reflected component from a pyrometer output if the reflected component could be measured during the test. The reflected radiation component is directly proportional to the incident energy and specimen emittance. It may be possible to operate in a wavelength band where the emittance is constant, and the incident energy level will normally be measured during each test. Another possibility is the use of atmospheric absorption bands for filtering. Solar spectrum information is needed for another part of this program, and will be checked to determine whether atmospheric absorption bands can be used for optical pyrometry.

d. Light Amplification. A light amplification device, also called an optical transformer, has recently come to our attention (References 9,10). The device was originally intended to collect photons for scintillation counting, but may also be useful for increasing the energy level available in a solar furnace. It is roughly funnel shaped, non-focusing, and must have a particular wall curvature for maximum efficiency. Other work at Georgia Tech is underway to investigate the use of light amplifiers, and the resulting information will be furnished to White Sands.

e. Georgia Tech Participation. Georgia Tech will propose several filter and pyrometer combinations which may be suitable for optical pyrometry. Considerations will include: (1) the penalty in lost incident energy, (2) the size and cost of filters capable of withstanding the environment, and (3) pyrometer characteristics such as sensitivity and inherent accuracy at the available filter wavelengths.

4. Intensity versus Wavelength Spectrum

Two spectroradiometers capable of measuring the spectrum of solar radiation have been identified up to now. These instruments are manufactured by International Light, Inc., Newburyport, Massachusetts, and Instrumentation Specialties Company, Lincoln, Nebraska. Based on their product literature, it appears that a spectral monitoring system can be set up for three to five thousand dollars, depending on accessories selected. These suppliers will be asked to supply literature directly to the WSSF. Purchase of such a system would be highly desirable in order to permit correlation of the solar furnace spectral distribution with atmospheric haze and weather conditions.

5. Insolation Data

It is necessary that direct incident sunlight be measured during solar furnace operation to provide checks on radiometers and calorimeters. Also, the collection of permanent direct and indirect insolation data over a period of at least one year is important for research related to solar energy utilization; if we can assume that the U. S. Army might perform energy related

research in the future, collection of insolation data should begin as soon as possible. Thus, we recommend that a pyranometer and a pyroheliometer be installed and operated on a continuous basis. The Eppley Laboratory, Inc., Newport, Rhode Island manufactures several instruments that are considered standards in this field. An insolation measurement station with automatic data collection capability is being set up at Georgia Tech, and information will be provided to the WSSF.

PHASE 3 - ANALYSIS CONTINUATION AND FINAL REPORT

The objectives of Phase 3 are to assist in the cross-calibration of the WSSF and the CNRS solar furnace, and other thermal facilities; to analyze all cross-calibration data and account for differences, and to prepare a final report.

Phase 3 is scheduled for completion twelve months after initiation of the contract. Detailed planning of this phase will depend on the results achieved in Phase 2, and will be included in the Interim Technical Report. However, cross-calibration is the major requirement and assistance on other topics will be continued as appropriate.

Respectfully submitted,

Steve H. Bomar, Jr.
Project Director

jw

REFERENCES

1. John M. Davies and Eugene S. Cotton, "Design of the Quartermaster Solar Furnace," Solar Energy, 1, 16-22 (1957).

2. Eugene S. Cotton, et al., "Image Quality and Use of the United States Army Quartermaster Solar Furnace," Proceedings of the United Nations Conference on New Sources of Energy, paper S/79, Rome, Italy (1961).

3. Frederic G. Penniman et al., "A Pulse Shaper for the Natick Laboratories Solar Furnace," Solar Energy, 12, 85-94 (1968).

4. Peter E. Glaser, "High Radiation-Flux, Absolute, Water-Flow Calorimeter," The Review of Scientific Instruments, 28, 1084-1086 (1957).

5. F. Trombe and A. Le Phat Vinh, "Mesure de L'energie au Foyer des Systemes de Concentration," Association Francaise pour L'etude et le Developpement des Applications de L'energie Solaire -A.F.E.D.E.S., No. 3, 78-80 (1971).

6. Robert Gardon, "An Instrument for the Direct Measurement of Intense Thermal Radiation," The Review of Scientific Instruments, 24, 366-370 (1953).

7. M. Foex, "Temperature Measurements in the Solar Furnace," Proceedings of the United Nations Conference on New Sources of Energy, paper S/66, Rome, Italy (1961).

8. Peter E. Glaser and Henry H. Blau, Jr., "A New Technique for Measuring the Spectral Emissivity of Solids at High Temperatures," Transactions of the ASME, Series C, Journal of Heat Transfer, 81, 92-94 (1959).

9. H. Hinterberger and R. Winston, "Use of a Solid Light Funnel to Increase Phototube Aperture without Restricting Angular Acceptance," The Review of Scientific Instruments, 39, 1217-1218 (1968).

10. R. Winston and J. M. Enoch, "Retinal Cone Receptor as an Ideal Light Collector," Journal of the Optical Society of America, 61, 1120-1121 (1971).

A-1620

INTERIM TECHNICAL REPORT

SOLAR FURNACE CROSS-CALIBRATION PROGRAM ANALYSIS

WHITE SANDS SOLAR FURNACE
WHITE SANDS MISSILE RANGE, NEW MEXICO

December 1974

By

S. H. Bomar, Jr.
C. T. Brown

Engineering Experiment Station
Georgia Institute of Technology
Atlanta, Georgia 30332

Contract DAAD07-74-C-0145
Georgia Tech Project A-1620

December 17, 1974

TE-PM, Bldg. 1504
Attn: Mr. William Frye
M/F: PR&C 3340-301
Contract DAAD07-74-C-0145
White Sands Missile Range,
New Mexico 88002

Subject: Interim Technical Report, Contract DAAD07-74-C-0145,
"Solar Furnace Cross-Calibration Program Analysis"
(Georgia Tech Project A-1620)

Gentlemen:

In accordance with the provisions of the contract, S. H. Bomar, Jr., C. T. Brown and J. H. Murphy visited the White Sands Solar Furnace (WSSF) facility on 21-22 November 1974 for the purpose of conducting experiments to determine the best types of instruments and procedures to be used for the measurement of certain operating parameters of the WSSF. This effort was made in an attempt to satisfy in part the Phase 2 work statement as outlined in our previous letter progress report dated June 11, 1974.

Phase 2 of the current program involves the exploration of techniques and instrumentation for:

(1) the mapping of the heat flux distribution in the vicinity of the focal zone of the WSSF;

(2) the characterization of pulse shapes available from the fast focal plane shutter and the nuclear burst simulator shutter at the WSSF;

(3) the measurement of internal and surface temperatures of test objects under concentrated solar irradiation;

(4) the determination of intensity versus wavelength information for the concentrated solar energy at the WSSF; and

(5) the collection of site insolation data.

The most recent visit to the WSSF had as its goal the mapping of the flux zone of the furnace, the characterization of the pulse shapes available

from both the focal plane shutter and the nuclear burst shutter, and further experimentation with the two Winston optical transformers. Due to heavy cloud cover on the second day of the visit it was not possible to perform the flux mapping. However, using the light from a half moon on the first night and sky shine on the second day, it was possible to characterize the pulse shapes available from both of the WSSF shutters. Qualitative optical gain information was also obtained for the two optical transformers.

Characterization of Pulse Shapes

Several devices have been suggested as candidates to measure the optical/thermal pulse shapes available at the WSSF. These include rapid response calorimeters, semiconductor photoelectric detectors, and photomultiplier tube (PMT) detectors. Rapid response calorimeters as typified by the Hy-Cal Asymptotic® calorimeter are electrically simple, rugged, quite small in size, but suffer from a relatively long thermal response time ($\sim$ 100 milliseconds). Thus, the calorimetric radiometer is satisfactory only for very slow rise time pulse shape work.

Of the photoelectric detector and the photomultiplier tube detector, the photoelectric detector is much smaller, is less expensive, and does not require a source of high voltage as does the PMT detector. The photomultiplier tube is, however, a much more sensitive device and its dynamic range (range of linearity) is much greater than that of the photodiode. Also, with the use of fiber optics the PMT detector can be used to probe quite small areas.

A photomultiplier tube apparatus was assembled on the Georgia Tech campus and transported to the White Sands Solar Furnace for evaluation. The experimental arrangement shown in Figure 1 was used to evaluate the apparatus and, at the same time, calibrate and characterize the optical/thermal pulse shapes produced by the various WSSF shutter arrangements. A list of the equipment used in these experiments is given in Table I.

During normal pulse mode operation light from the concentrator mirror is gated on and off by one or both of two pulse shaping shutters located in the focal building. The fast focal plane shutter was designed to give a square shaped pulse of known duration. When such a pulse shape is desired the vane type nuclear burst shutter is removed from the path of the incident light.

Operation of the WSSF nuclear burst shutter is intended to simulate the thermal effects associated with a nuclear weapon (Ref. 1). This shutter is cam driven and runs continuously when placed in operation. The selection of a single pulse is made by synchronizing the opening and closing of the fast focal plane shutter with a single pulse from the vane type shutter.

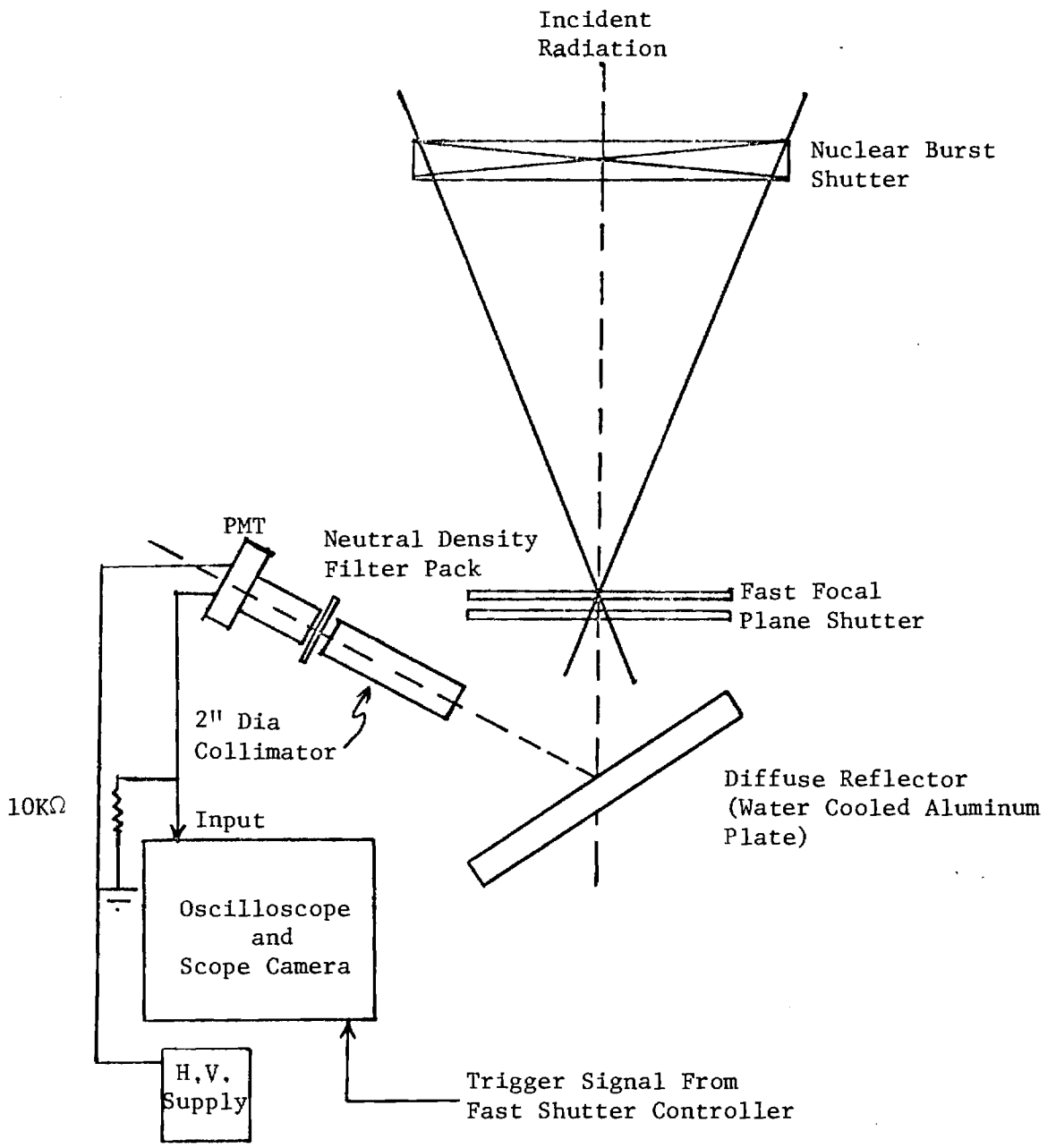

Figure 1. Experimental Arrangement for Characterizing Optical/ Thermal Pulse Shapes from the White Sands Solar Furnace.

TABLE I

LIST OF EQUIPMENT USED TO CHARACTERIZE
OPTICAL/THERMAL PULSE SHAPES FROM THE WSSF

Item	Manufacturer and Model No.
2" Photomultiplier Tube	Amperex, Model 56AVP
H. V. Power Supply	ORTEC, Model 456
Oscilloscope	Tektronix, Model 502
Scope Camera	Unknown
WRATTEN Gelatin Filters	Kodak, No. 96; N.D. 0.10, 0.70 1.00, 2.00, 3.00 and 4.00

Characterization of the pulse shapes available from these shutters was accomplished by placing a diffusely reflecting water-cooled aluminum plate behind the focal plane shutter and viewing the scattered radiation with a photomultiplier tube. A 2-inch diameter by approximately 14-inch long collimator was used to eliminate stray radiation, and neutral density filters were used as necessary to attenuate the light incident on the cathode of the PMT. The output of the PMT was displayed by an oscilloscope and photographed. Proper triggering of the oscilloscope was accomplished with the aid of an output from the fast shutter timer.

Fast focal plane shutter data were collected for nominal pulse widths of 100 and 500 milliseconds. The width of the pulse, its rise time and its fall time were of interest in these experiments. The raw data for these two pulse widths are shown in Figures 2 through 7. Table II summarizes the pulse shape information obtained from these data. The measured pulse widths (Full Width at Half Maximum) were found to agree quite well with their nominal values. Pulse rise times for the four sets of data were self consistant and yielded an average rise time of approximately 26 milliseconds. The average decay time for the 100 millisecond pulse is approximately 28 milliseconds. The decay time of the 500 millisecond pulse is of the order of 25 to 40 milliseconds. A more accurate estimate of this decay time will require the use of a delayed trigger signal from the shutter timer to the

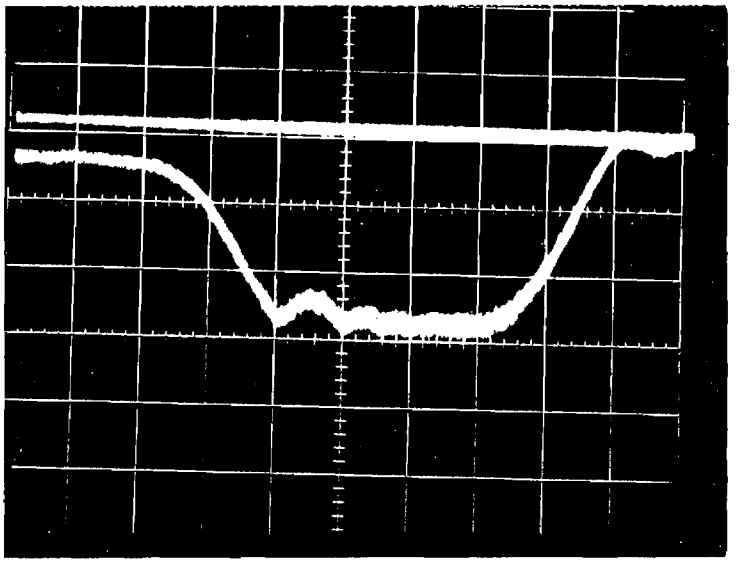

Figure 2. Square Pulse from Fast Focal Plane Shutter. Nominal Pulse Width of 100 Milliseconds. 20 msec/cm Sweep.

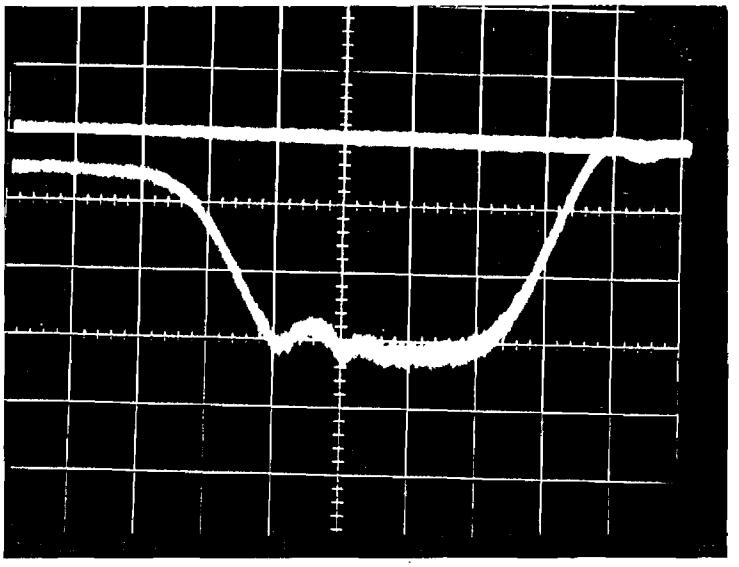

Figure 3. Square Pulse from Fast Focal Plane Shutter. Nominal Pulse Width of 100 Milliseconds. 20 msec/cm Sweep.

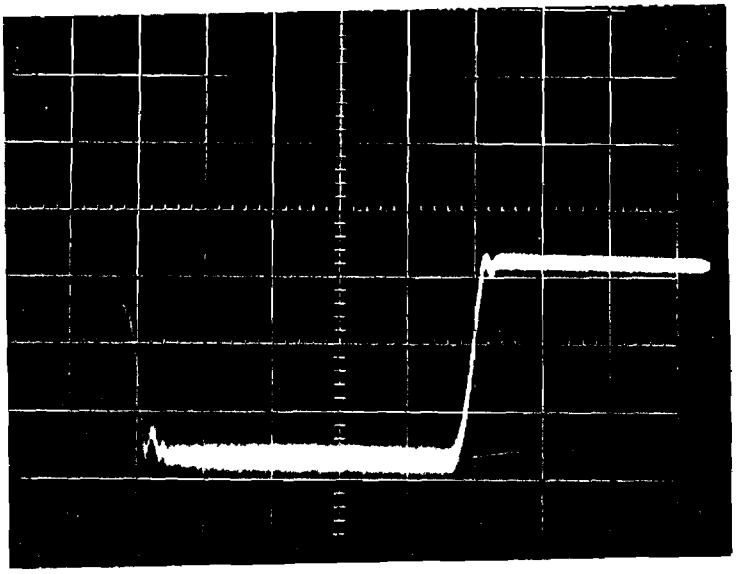

Figure 4. Square Pulse from Fast Focal Plane Shutter. Nominal Pulse Width of 500 Milliseconds. 100 msec/cm Sweep.

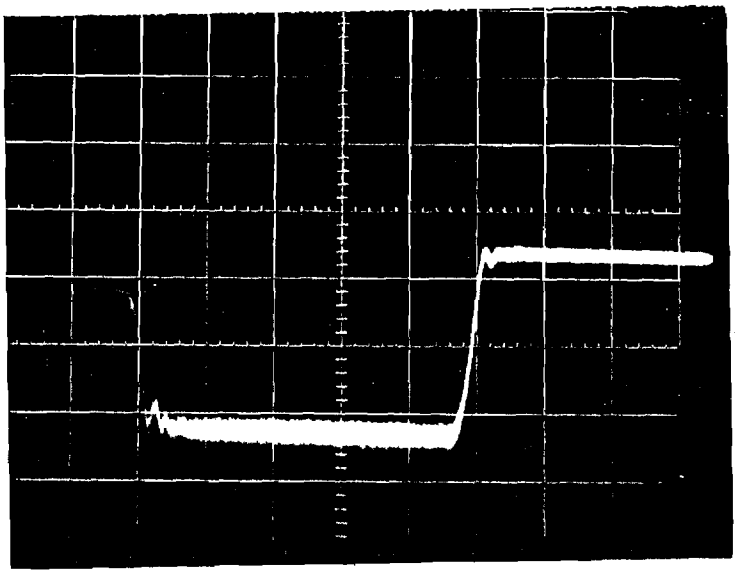

Figure 5. Square Pulse from Fast Focal Plane Shutter. Nominal Pulse Width of 500 Milliseconds. 100 msec/cm Sweep.

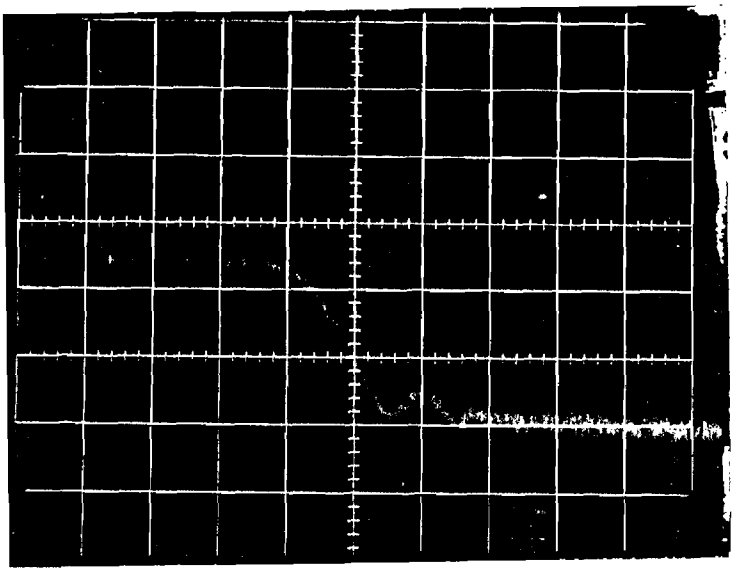

Figure 6. Pulse Rise Time for Square Pulse. Nominal Pulse Width of 500 Millseconds. 20 msec/cm Sweep.

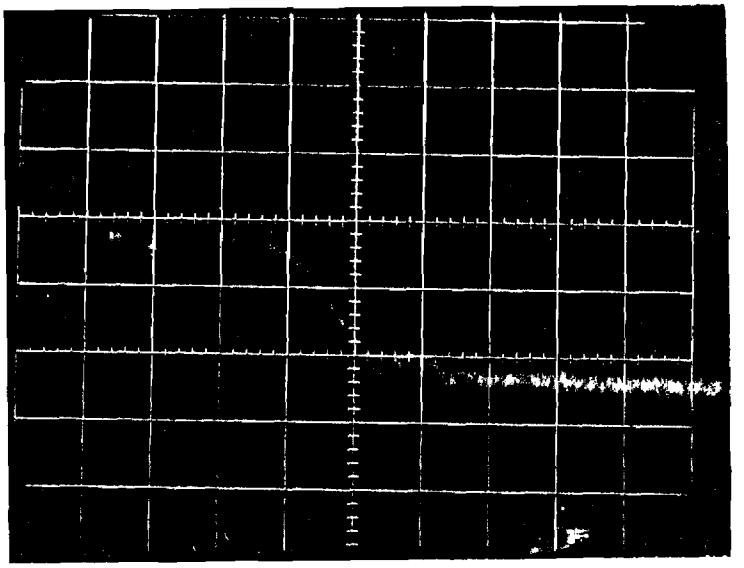

Figure 7. Pulse Rise Time for Square Pulse. Nominal Pulse Width of 500 Milliseconds. 20 msec/cm Sweep.

TABLE II

SUMMARY OF PULSE SHAPE DATA FOR FAST FOCAL PLANE SHUTTER

Nominal Pulse Width (milliseconds)	Reference Figure Number	Measured: Pulse Width, FWHM (milliseconds)	Measured: Pulse Rise Time, 10% - 90% (milliseconds)	Measured: Pulse Fall Time, 90% - 10% (milliseconds)
100	2	99	28	29
	3	93	27	27
500	4	495	-	35 ± 5*
	5	490	-	30 ± 5*
	6	-	23	-
	7	-	25	-

*These errors represent only the error in reading the data from the photograph.

oscilloscope. The compressed air supply used to drive the shutters was set at 87 psig for these experiments.

Pulse shape data were also collected for the characterization of the nuclear burst shutter. These data were collected at nominal shutter speeds of 5, 14 and 25 revolutions per minute. Three sets of data were collected for each shutter speed. The first set depicted two consecutive pulses and was used to check the speed of the nuclear burst shutter. The second set was used to characterize the complete pulse shape and the third set was used to characterize the leading edge of the pulse. Representative samples of the raw data appear in Figures 8 through 14. The fast focal plane shutter was not used during the collection of these data.

A comparison of the nominal and measured shutter speeds was made and the results are summarized in Table III. The probable error in these experiments is of the order of three percent. Only the 14 rpm shutter speed with its six percent difference fell outside of these error limits.

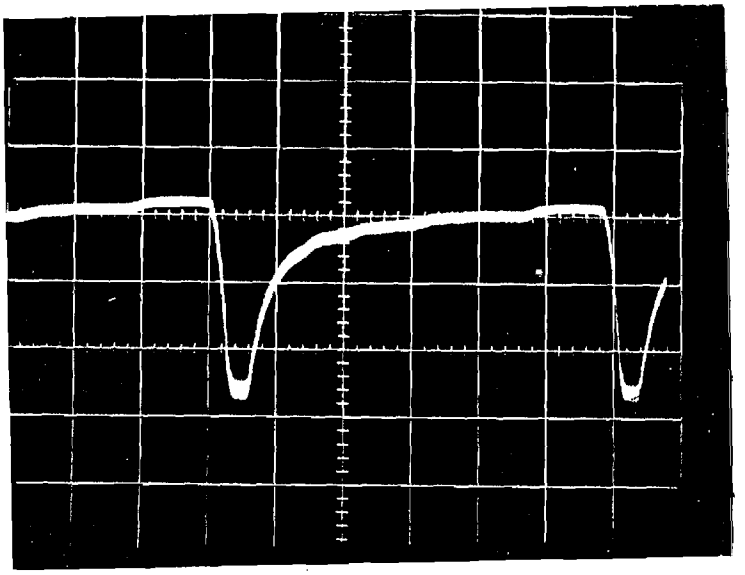

Figure 8. Pulse Shape from Nuclear Burst Shutter Operating at 5 rpm. 2 sec/cm Sweep.

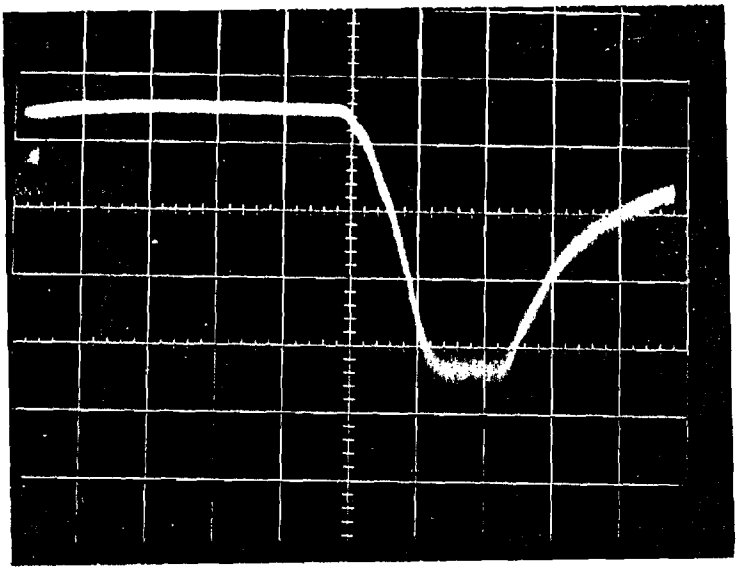

Figure 9. Rise Time of Pulse from Nuclear Burst Shutter Operating at 5 rpm. 100 msec/cm Sweep.

Figure 10. Pulse Shape from Nuclear Burst Shutter Operating at 14.8 rpm 500 msec/cm Sweep.

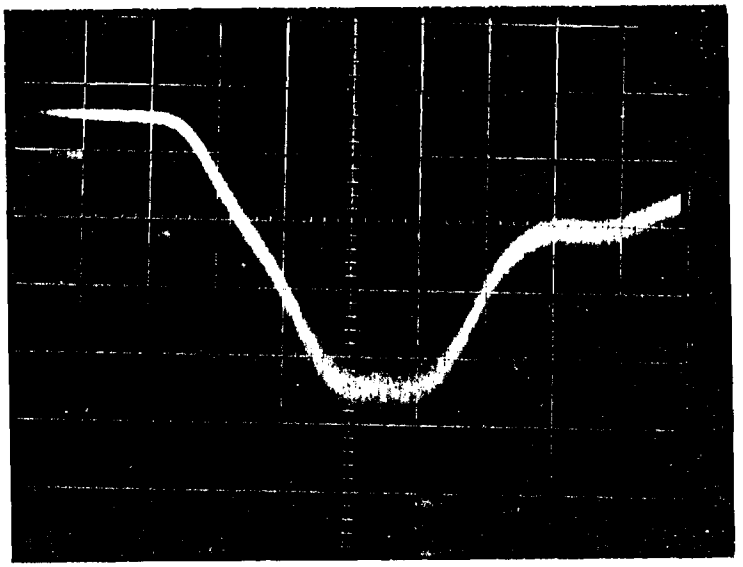

Figure 11. Rise Time of Pulse from Nuclear Burst Shutter Operating at 14.8 rpm. 100 msec/cm Sweep.

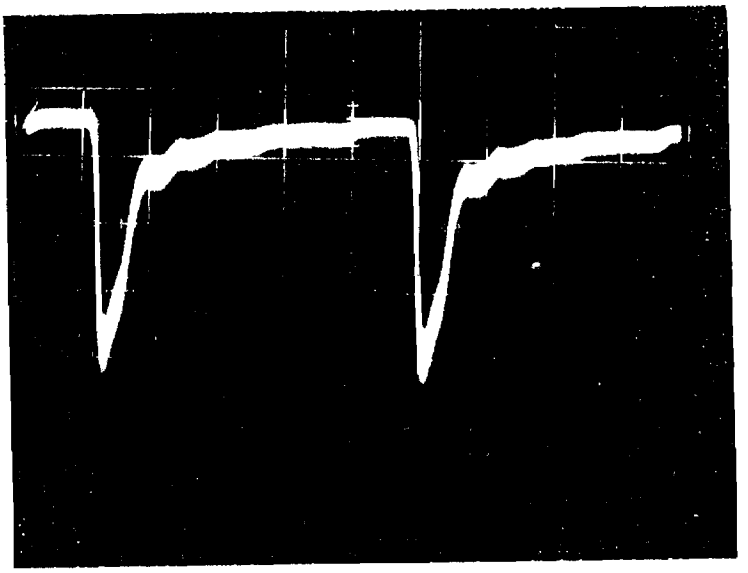

Figure 12. Pulse Pair from Nuclear Burst Shutter Operating at 25 rpm. 500 msec/cm Sweep.

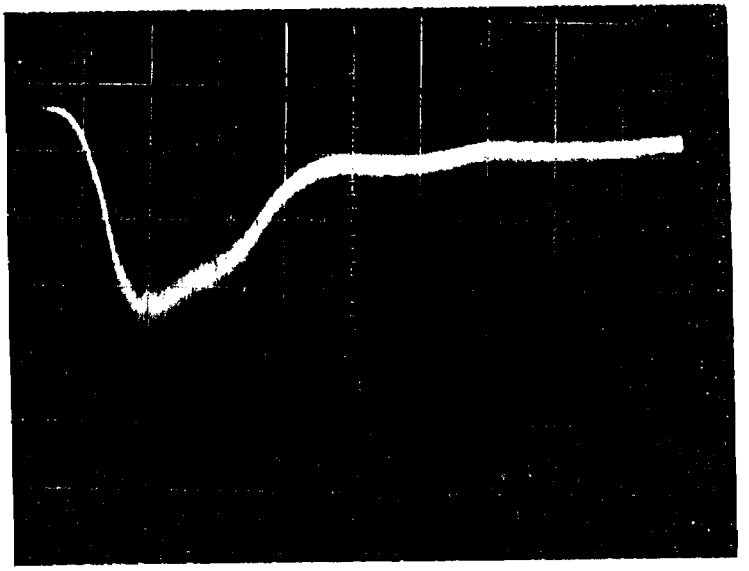

Figure 13. Pulse Shape from Nuclear Burst Shutter Operating at 25 rpm. 100 msec/cm Sweep.

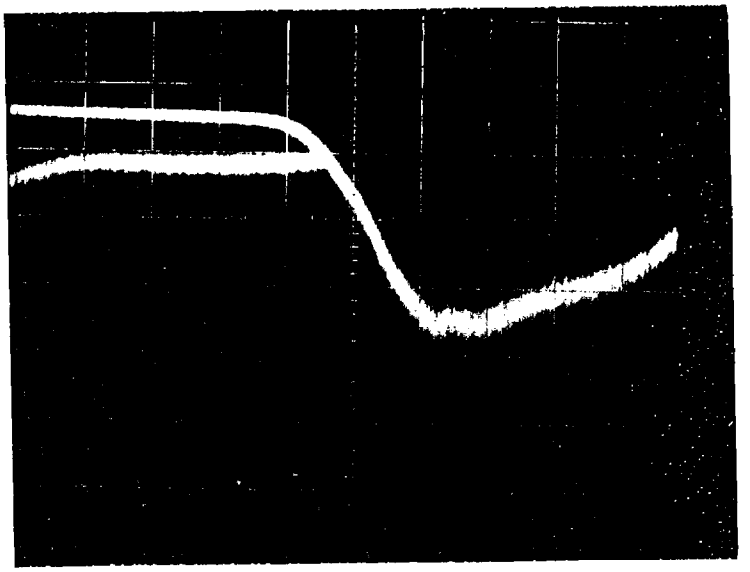

Figure 14. Rise Time of Pulse from Nuclear Burst Shutter Operating at 25 rpm. 50 msec/cm Sweep.

TABLE III

COMPARISON OF NOMINAL AND MEASURED SHUTTER SPEEDS
FOR THE WSSF NUCLEAR BURST SHUTTER

Nominal Shutter Speed (rpm)	Measured Shutter Speed (rpm)
5	5.1 ± 0.2
14	14.8 ± 0.4
25	25.3 ± 0.7

Glasstone (Ref. 2) has indicated that for reasonable weapon sizes, the thermal pulses from all weapons are similar in shape and can be represented by the standard pulse shown in Figure 15. It consists of a very rapid rise and a much slower decline. The WSSF nuclear burst shutter was designed to simulate this shape for a variety of weapon sizes. Note that this standard pulse has been normalized to H_m, the maximum irradiance, and to t_m, the time to reach that maximum irradiance. The time t_m is related to the size of the weapon by the expression

$$t_m = 0.032\ W^{\frac{1}{2}},$$

where t_m is in seconds and W is in kilotons.

The pulse shapes available from the WSSF for shutter speeds of 5, 14, and 25 rpm were compared with Glastone's standard shape. The results of the comparison are shown in Figures 16 through 18. The theoretical and experimental curves compare quite favorably for shutter speeds of 5 and 14 rpm. Such is not the case for the 25 rpm data-the shutter appears to be closing much slower than required for this case. Furthermore, there is evidence at all three shutter speeds that the vanes are somewhat erratic in their rate of closing.

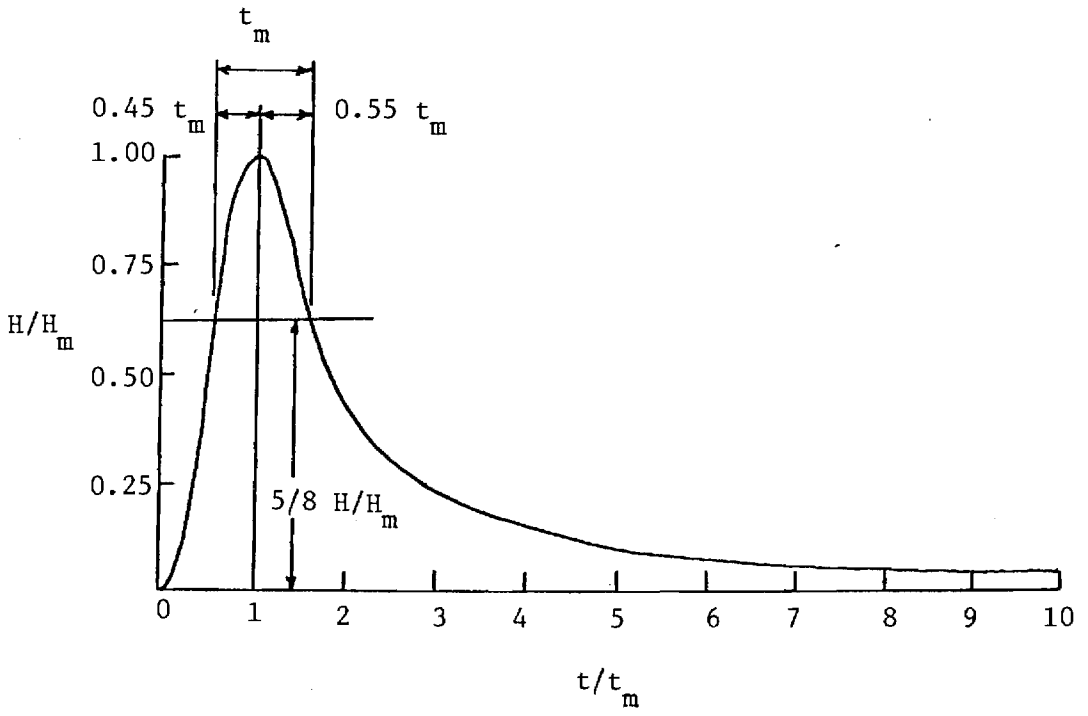

Figure 15. Normalized Thermal Pulse from Glasstone.

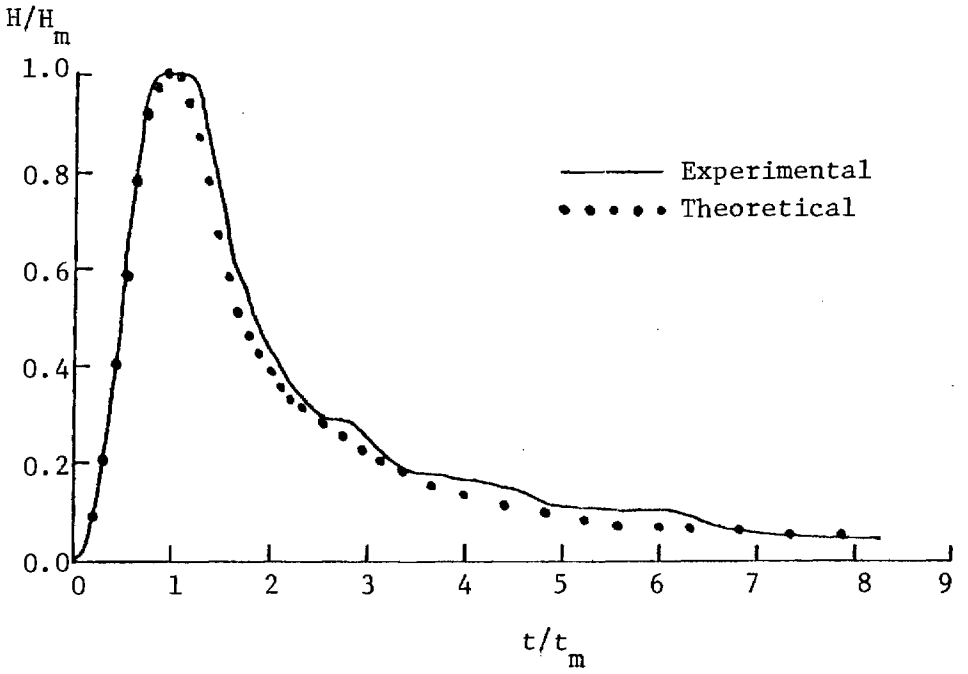

Figure 16. Experimental and Theoretical Pulse Shapes for Shutter Speed of 5 rpm.

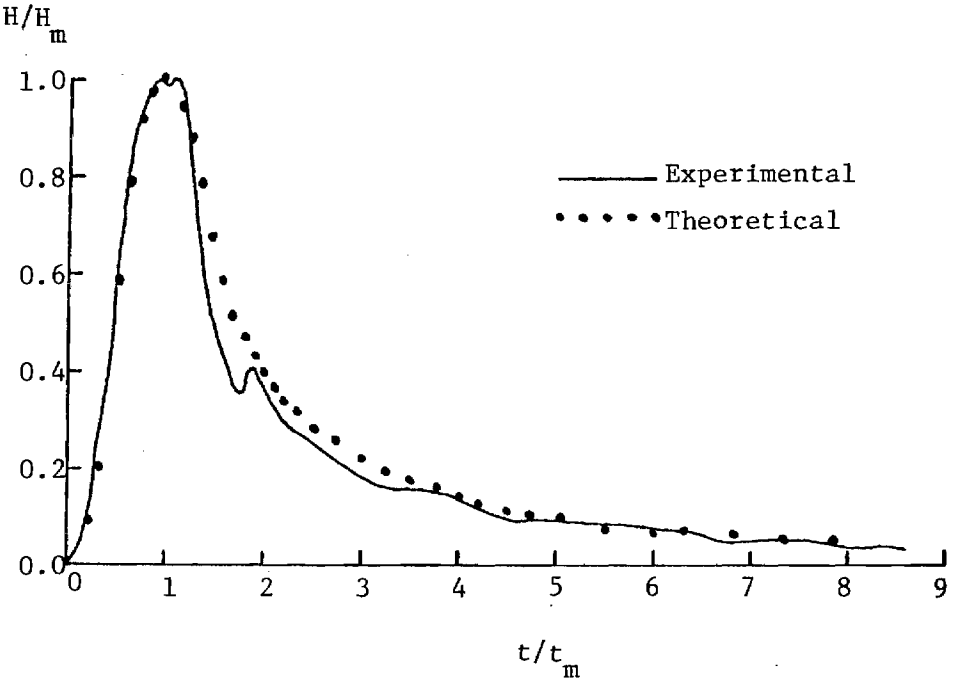

Figure 17. Experimental and Theoretical Pulse Shapes for Shutter Speed of 14.8 rpm.

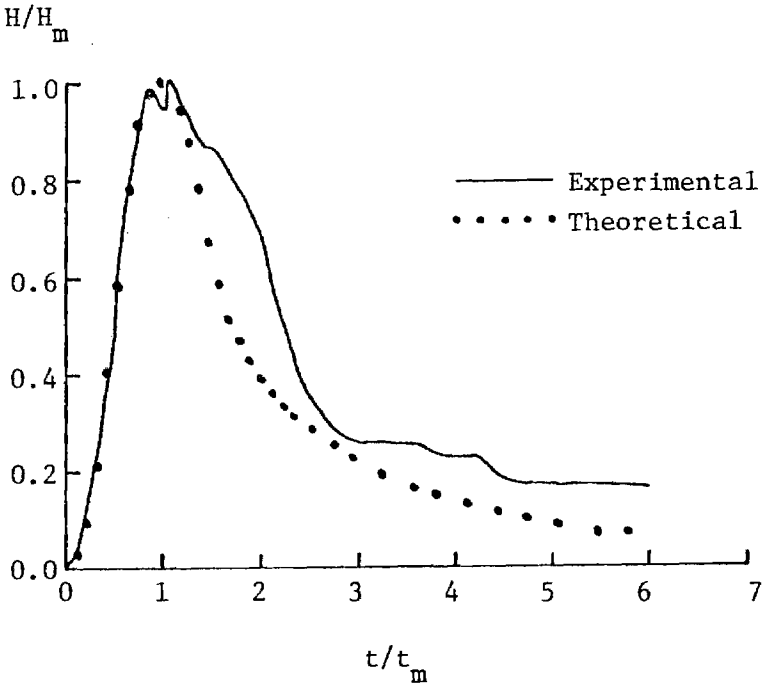

Figure 18. Experimental and Theoretical Pulse Shapes for Shutter Speed of 25 rpm.

Values were determined for t_m, the time to reach maximum power, for each of the three shutter speeds, and these values were then used to calculate the corresponding weapon sizes. The results of these calculations are summarized in Table IV. The data are in violent disagreement with the results given by Penniman, et al. (Ref.1) for the operation of the shutter at Natick. A comparison of the Natick data and the Georgia Tech data appears as Table V. Note that for a given shutter speed the pulse rise time measured by Georgia Tech is approximately 1.7 to 2.3 times faster than that reported by the Natick group. This yields weapon sizes that are from 1/3 to 1/5 the sizes reported at Natick. According to WSSF personnel the shutter assembly has not been modified since leaving Natick.

TABLE IV

SIMULATED WEAPON SIZE AS A FUNCTION OF SHUTTER SPEED

Shutter Speed (rpm)	Time to Maximum Power (seconds)	Weapon Size (kilotons)
5	1.1	1180
14.8	0.30	88
25	0.17	28

In an attempt to reconcile the two sets of data, the product of the shutter speed with the pulse rise time was formed for each set of data. This product should be a constant since the pulse rise time is inversely proportional to the shutter speed. That is,

$$t_m = \frac{k}{(rpm)},$$

where k is some constant. The results of these calculations appear as Table VI.

TABLE V

COMPARISON OF NATICK AND GEORGIA TECH PULSE SHAPE AND WEAPON SIZE DATA

Shutter Speed (rpm)	Natick Data		Georgia Tech Data	
	t_m (sec)	W (kilotons)	t_m (sec)	W (kilotons)
5			1.1	1180
10	1.58	2440		
14.8-15	0.69	468	0.30	88
25	0.29	82	0.17	28

The Georgia Tech data is reasonably self-consistant with respect to the t_m (rpm) product. Such is not the case with the Natick data. The Georgia Tech product is constant within 14 percent for the three shutter speeds. The Natick product is constant only within 48 percent over an even smaller dynamic range of shutter speeds. The implication is that there is an error in the data as published by Penniman et al., or the time base of the oscilloscope used to collect the Georgia Tech data is incorrect by a factor of approximately two for some but not all sweep rates. Having an uncalibrated scope in the most recent experiment would not, however, explain the relatively large t_m (rpm) product spread exhibited by the Natick data.

Optical Transformers

A light amplification device known as an optical transformer came to our attention earlier this year (Ref. 3,4). It is roughly a funnel-shaped device with a highly reflecting inner surface; it should have a particular wall curvature for maximum efficiency although even a straight sided funnel can give some amplification. In theory, the radiant flux arriving at the larger end is directed through the aperture at the smaller end with minimum losses, thereby giving an amplification of flux at the expense of illuminated area. It is a non-focussing device, and it may have considerable value in nuclear and laser effects testing.

TABLE VI

PRODUCT OF SHUTTER SPEED AND PULSE RISE TIME AS A FUNCTION OF SHUTTER SPEED FOR THE NATICK DATA AND THE GEORGIA TECH DATA

Source of Data	Shutter Speed	t_m (rpm) Product
Georgia Tech:	5	5.5
	14.8	4.44
	25	4.13
Natick:	10	15.8
	15	10.35
	20	8.0
	25	7.25
	35	5.6

In October 1974, two simple versions of the optical transformer were constructed at Georgia Tech for preliminary tests at the White Sands Solar Furnace. These were made by wrapping aluminum foil around a mandrel, covering the foil with epoxy-impregnated glass tape, and curing the structure at elevated temperature. The resulting device had thin glass reinforced plastic walls with a shiny but crinkled inner surface formed by the aluminum foil. No cooling was provided. The two optical transformers were inspected briefly at very low power levels in the solar furnace during the trip in October, and amplification of flux was detected.

Further experimentation designed to measure the optical gain of the two Georgia Tech optical transformers was conducted during the November visit to the WSSF. This work was carried out at night while manually tracking a half moon. First, the photomultiplier tube was placed at the focal point of the concentrator and a light intensity recorded. Then each optical transformer was placed with its mouth at the focal point and the light intensity at the small end recorded. In each case the intensity after amplification was lower than the original intensity. Various alignment positions were tried, but without success.

In retrospect the above results appear to be reasonable. With the photomultiplier at the focal point of the concentrator, it was receiving

approximately 65 percent of the incident radiation. With the photomultiplier/ optical transformer in position the amount of direct radiation falling on the photomultiplier tube was only 10 to 20 percent of the incident radiation. Thus, for the optical transformer to have an apparent gain of one in the above experiments it would have had to redirect the remaining 80 to 90 percent of the radiation from the concentrator onto the photomultiplier with an efficiency of approximately 50 percent. Since optical gains approaching one were obtained, it follows that the transformer was redirecting the scattered radiation through the rear aperature with an efficiency of approximately 50 percent. Further experimentation with these devices will be undertaken to quantitatively establish their optical gain.

Optical Pyrometry

The use of thermocouples on surfaces exposed to radiant heat fluxes presumes that the absorption characteristics of the thermocouple match those of the specimen. Our experience indicates that such an assumption is untenable in many situations; for example, translucent materials absorb energy in depth as well as on the surface and the emittance of a thermocouple may be quite different from that of the sample. Therefore, optical pyrometry is preferred for surface temperature measurements. In order to use optical pyrometry however, one must devise a means of accounting for the reflected incident radiation and separating it from the thermally emitted radiation which is to be measured. This separation can be accomplished by optically filtering the incident radiation at the operating wavelength of the pyrometer or by mechanically chopping the incident radiation for brief time intervals and obtaining optical temperature data while the incident beam is cut off. Either of these schemes involves the sacrifice of a portion of the incident energy from the concentrator of the solar furnace. Mechanical chopping is unacceptable during nuclear pulse simulation tests because the pulse time is the same order of magnitude as the chopping time.

It is sometimes possible to let natural phenomena accomplish the optical filtering at the pyrometer's operating wavelength so that temperature measurements can be made. At the CNRS 1000 kW furnace in southern France, we have used this technique with pyrometers operating at wavelengths around 5μ in the infrared portion of the spectrum. Glass absorbs radiation strongly in this wavelength range, and all the mirrors at the CNRS installation are back-silvered glass. Therefore, energy reaching the focal point of that solar furnace contains no 5μm radiation and the pyrometer observes no reflected solar energy at its operating wavelength. The pyrometer response can be attributed entirely to emitted radiation from the specimen and temperature can thus be measured.

During a visit to the White Sands Solar Furnace in May 1974, Georgia Tech investigators brought a pyrometer which operates at 5.1 μm. All the concentrator mirrors and many of the heliostat mirrors at the WSSF are front-silvered glass, so that much of the energy in the focal area of the White Sands facility has not been filtered through glass. The pyrometer measured apparent temperatures of about 2000° F on a water cooled aluminum shutter plate, leading to the conclusion that pyrometry at 5 μm is not feasible at the WSSF because of interference by reflected radiation at that wavelength.

During the NSF International Seminar on Large Scale Solar Test Facilities in November 1974, Professor Sakuari, who operates the Japanese Solar Furnace noted that he had made temperature measurements with pyrometers operating in water absorption bands at 1.38 and 1.8 μm. The success of this approach depends upon having strong absorption by water vapor in the atmosphere, and this in turn depends to some extent on local weather conditions. Solar spectrum measurements made recently at White Sands Missile Range did not cover wavelengths higher than 1.1 μm, so that it is not yet possible to determine whether pyrometry at the 1.38 and 1.8 μm bands will be successful.

Solar Spectrum Measurements

In August 1974, a representative of the Tektronix, Incorporated demonstrated a spectrometer at the White Sands Solar Furnace and made solar spectrum measurements covering the range from 0.3 μm to 1.1 μm. Although this work was not done by Georgia Tech, it is shown in this report for reference. Figures 19 through 21 show the measured curves for direct sunlight, the reflected beam from the heliostat, and the reflected radiation from the concentrator. Figure 22 shows a set of curves published by Thekaekara (Ref. 5).

The spectra measured at White Sands are probably on a logarithmic scale, although this is not known for certain. Considering this probable difference in scales, they have an appearance similar to the "sea level" curve in Figure 22 except that they peak at a higher wavelength. An oxygen absorption band at about 0.76 μm and a water absorption band at about 0.94 μm are visible on the White Sands curves at relative intensities similar to Figure 22; thus it appears that the water absorption bands at 1.38 and 1.8 μm may be strong enough to permit optical pyrometry at those wavelengths.

Respectfully submitted,

Steve H. Bomar, Jr.,
Project Director

jw

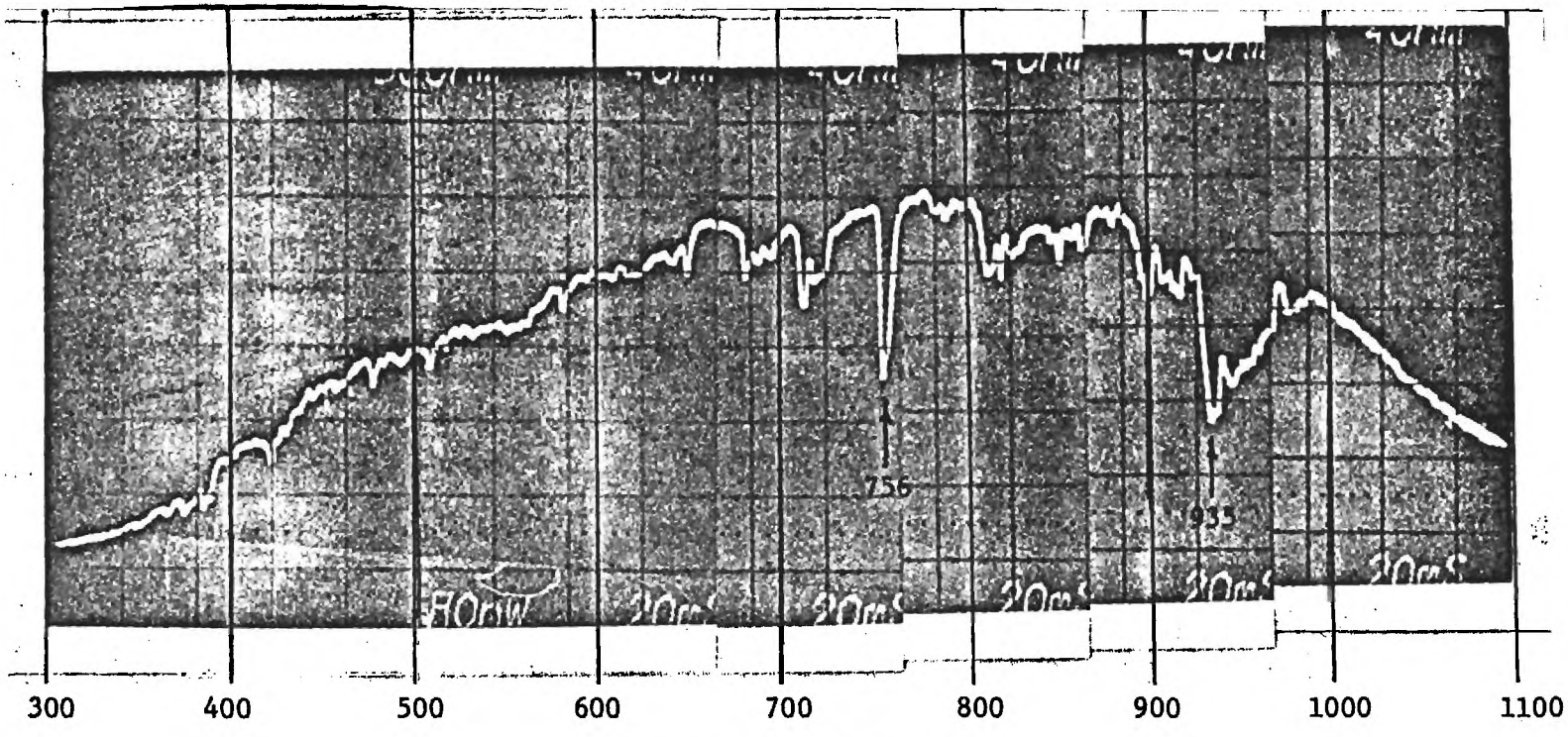

Figure 19. Solar Spectrum Taken at White Sands Solar Furnace, August 1, 1974.

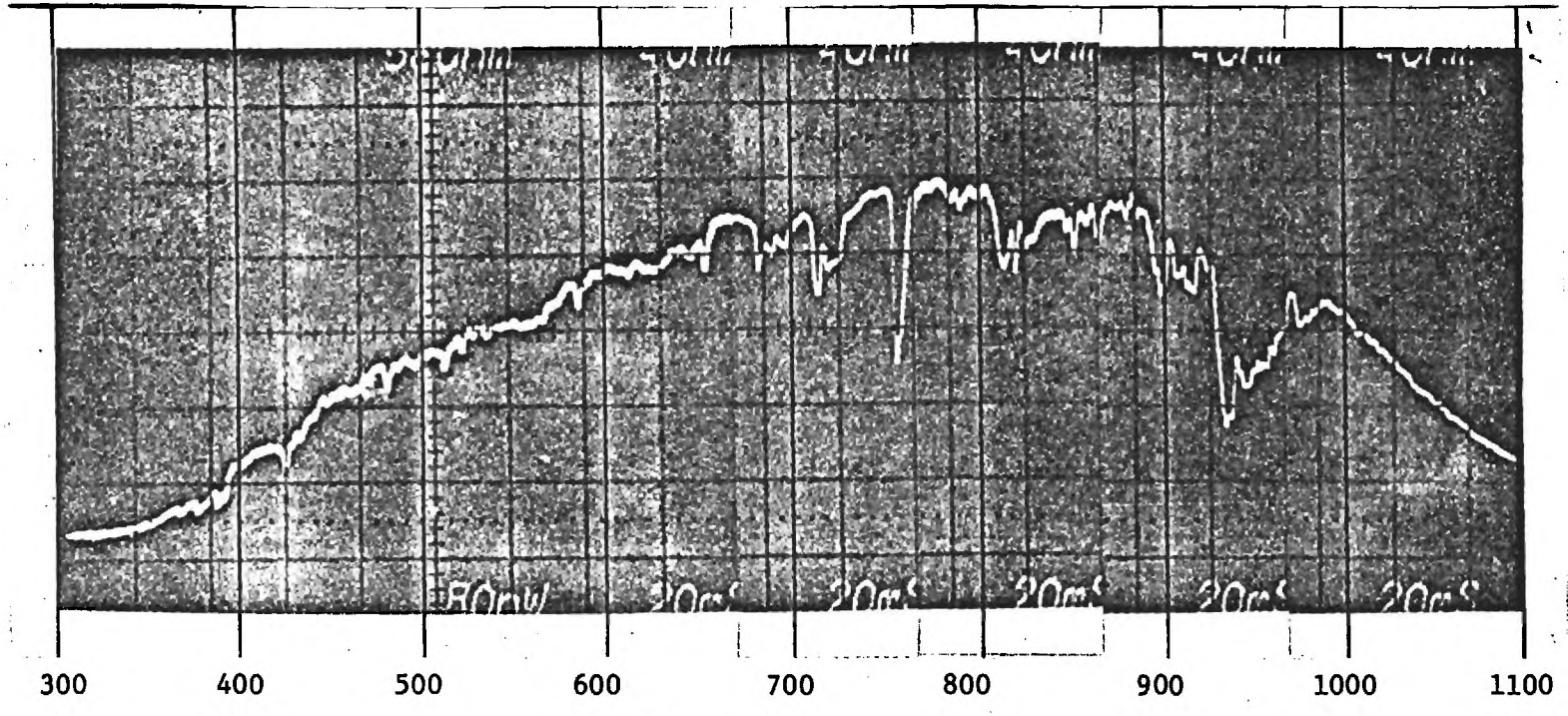

Figure 20. Spectrum of Solar Radiation Reflected from WSSF Heliostat, August 1, 1974.

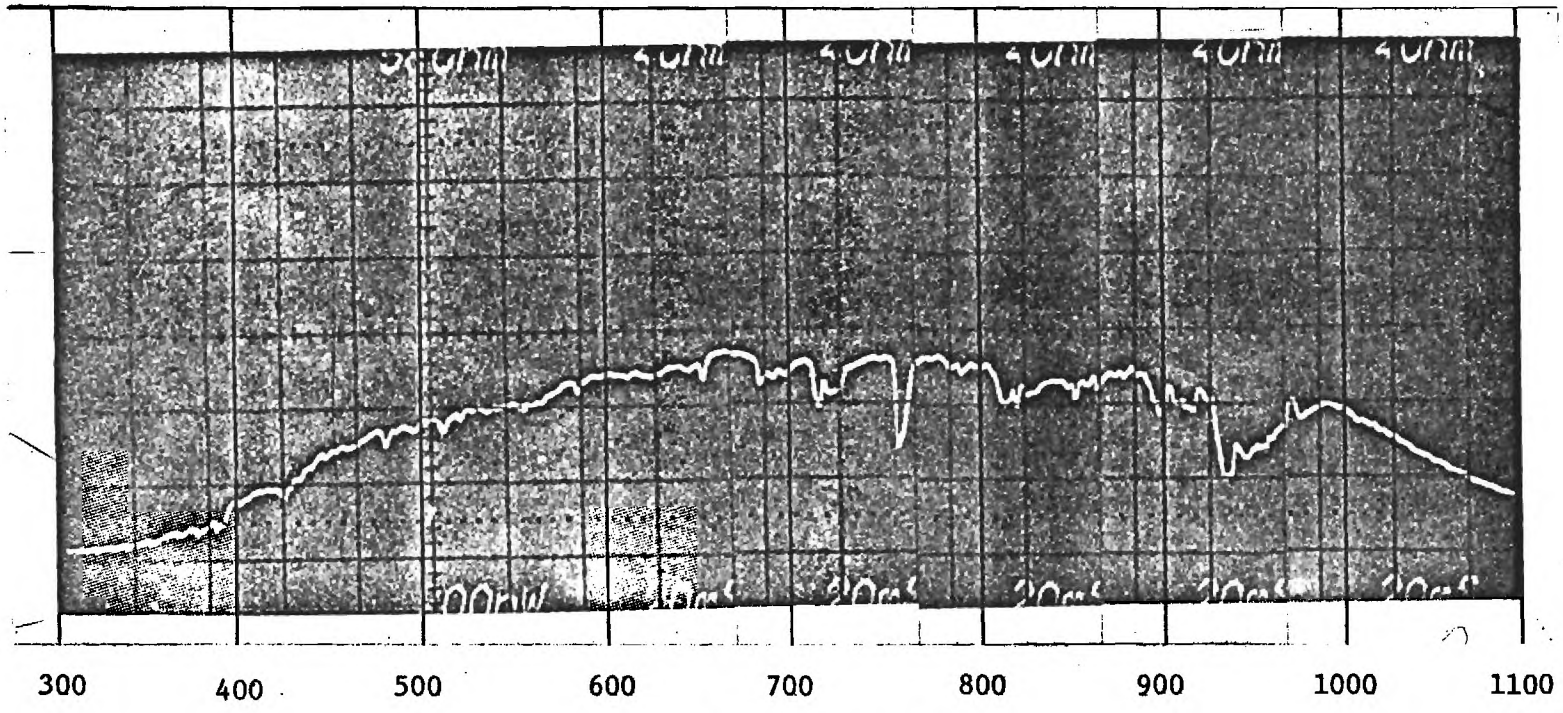

Figure 21. Spectrum of Solar Radiation Reflected from WSSF Concentrator, August 1, 1974.

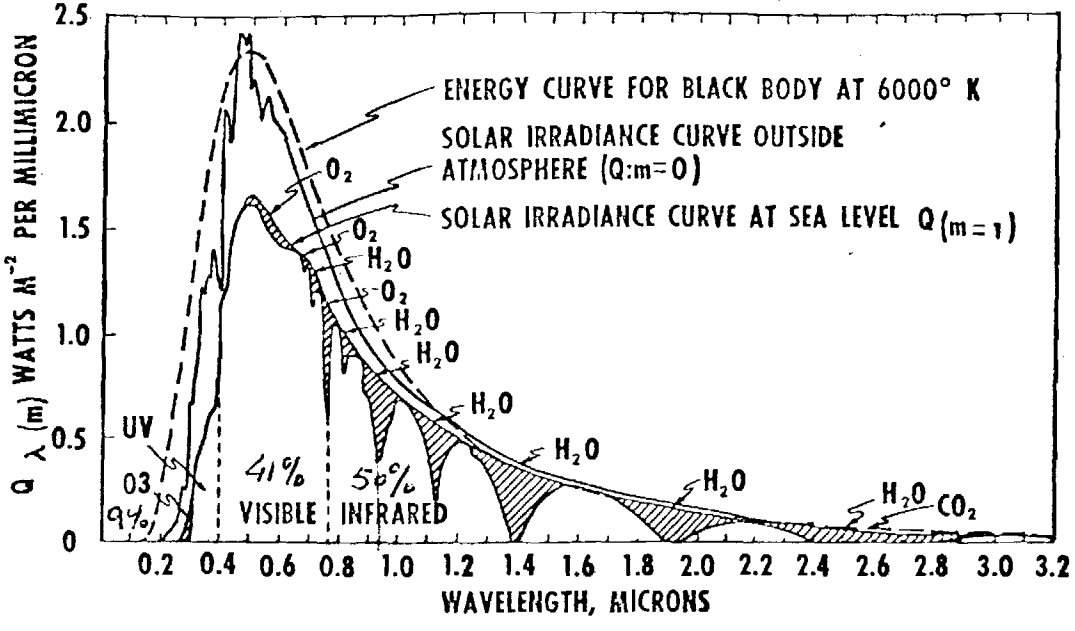

Figure 22. Solar Spectrum Data Published by Thekaekara.

REFERENCES

1. Frederick G. Penniman et al., "A Pulse Shaper for the Natick Laboratories Solar Furnace," Solar Energy , 12, 85-94 (1968).

2. Samuel Glasstone, The Effects of Nuclear Weapons, Revised Edition, U. S. Government Printing Office, April 1962.

3. H. Hinterberger and R. Winston, "Use of a Solid Light Funnel to Increase Phototube Aperture without Restricting Angular Acceptance," The Review of Scientific Instruments, 39, 1217-1218 (1968).

4. R. Winston and J. M. Enoch, "Retinal Cone Receptor as an Ideal Light Collector," Journal of the Optical Society of America, 61, 1120-1121 (1971).

5. Matthew P. Thekaekara, "The Solar Constant and Spectral Distribution of Solar Radiant Flux," Solar Energy, 9, 7-20 (1965).

FINAL REPORT

SOLAR FURNACE CROSS–CALIBRATION PROGRAM ANALYSIS

WHITE SANDS SOLAR FURNACE
WHITE SANDS MISSLE RANGE, NEW MEXICO

By
C.T. Brown
S.H. Bomar, Jr.

Contract DAAD07–74–C–0145
Georgia Tech Project A–1620

May 1975

1975

Engineering Experiment Station
GEORGIA INSTITUTE OF TECHNOLOGY
Atlanta, Georgia

FINAL REPORT

SOLAR FURNACE CROSS-CALIBRATION PROGRAM ANALYSIS

WHITE SANDS SOLAR FURNACE
WHITE SANDS MISSILE RANGE, NEW MEXICO

May 1975

By

C. T. Brown
S. H. Bomar, Jr.

Engineering Experiment Station
Georgia Institute of Technology
Atlanta, Georgia 30332

Contract DAAD07-74-C-0145
Georgia Tech Project A-1620

TABLE OF CONTENTS

SECTION I

INTRODUCTION

The largest solar furnace located in the United States is the U. S. Army White Sands Solar Furnace. This 35 kW facility was originally constructed in 1958 at Natick, Massachusetts by the Quartermaster Corps 1,2,3/, but has since been moved to the Nuclear Weapon Effects Laboratory, White Sands Missile Range, New Mexico. The purpose of the facility was, and still is, to provide a high radiant flux facility that can be used to simulate the thermal effects of nuclear weapons in order to evaluate the performance of protective clothing and other equipment used by the Army. Additionally, consideration is presently being given to the use of the facility to aid in the development of solar energy as a viable natural resource.

A photograph of the facility as it presently exists is shown in Figure 1. The major components (see Figure 2) are: (1) the tracking heliostat composed of 356 segments of flat mirrors each 24 inches by 24 inches, (2) a spherical concentrator composed of 180 concave mirror segments, one-half of which are 24 inches by 24 inches and the remainder 25 inches x 26 inches, (3) an attenuator which contains 17 rows of rotating blades which control the solar energy being directed onto the concentrator by the heliostat, and (4) a focal room with a working space approximately 6 feet cubed and into which the collected solar energy is concentrated.

Reconstruction of the original Natick furnace at White Sands Missile Range (WSMR) began in 1973, and was substantially complete by the middle of 1974. In 1974, the High Temperature Materials Division of the

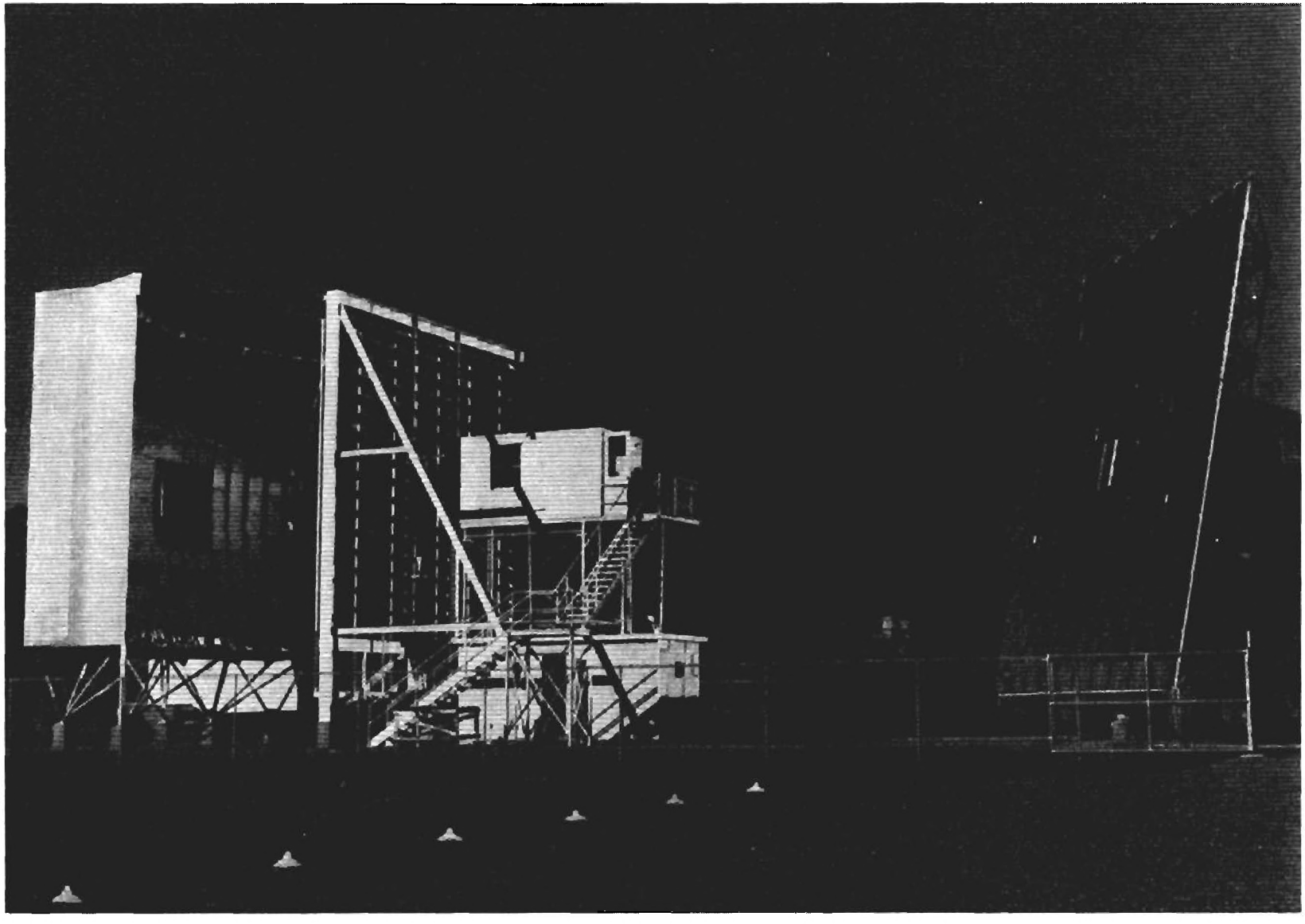

Figure 1. Photograph of the White Sands Solar Furnace.

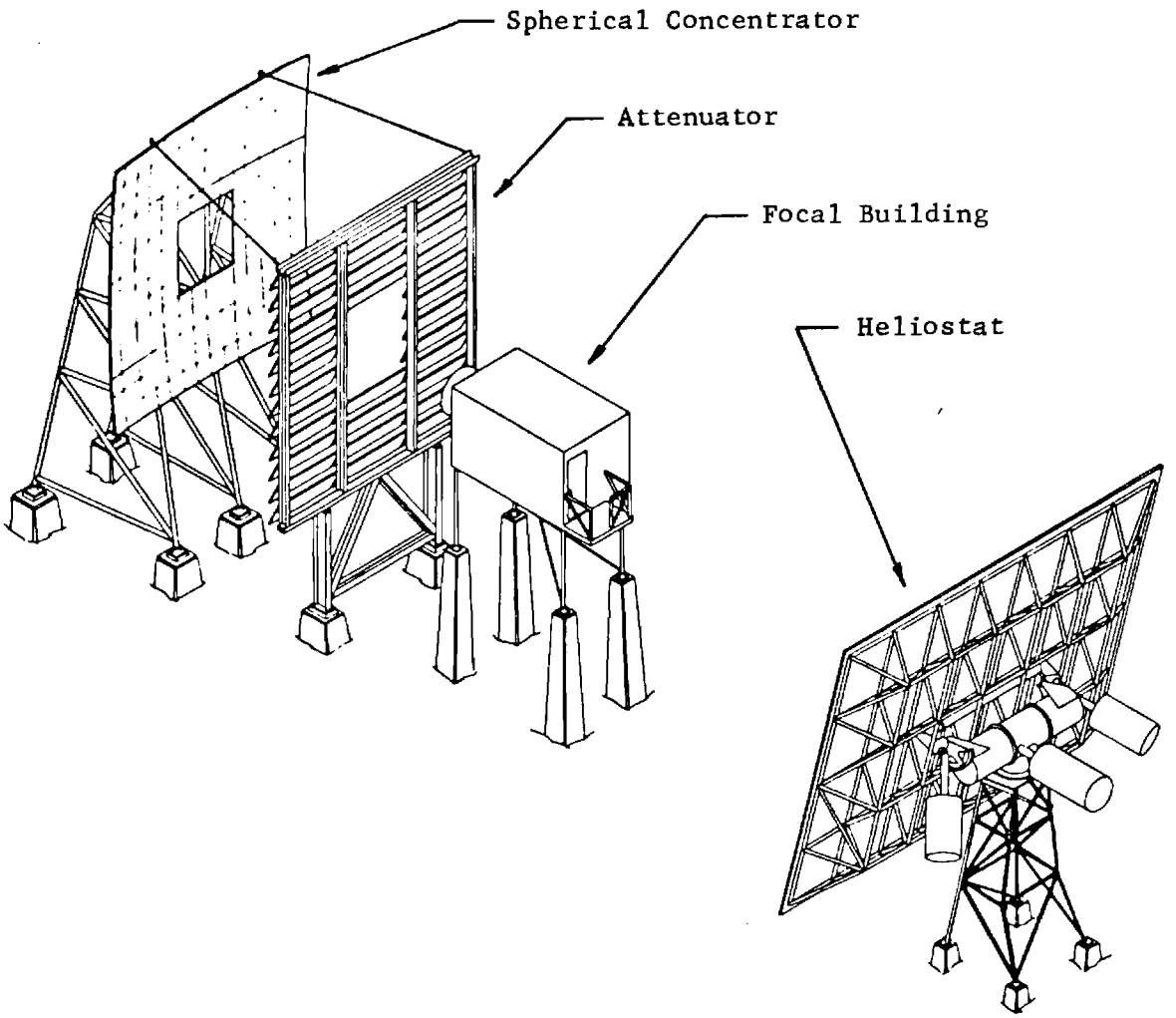

Figure 2. Sketch of White Sands 35 kW Solar Furnace.

Engineering Experiment Station, Georgia Institute of Technology began an evaluation and calibration study of the White Sands Solar Furnace (WSSF) under contract DAAD07-74-C-0145 with the U. S. Army. The objectives of this study were to determine the performance characteristics of the WSSF, to assist in its calibration, and to recommend appropriate test methods and instrumentation for future solar energy programs. Data were collected by Georgia Tech personnel in support of this program on three separate visits to the facility. These visits occurred on May 20-21, 1974, November 21-22, 1974 and February 25-March 1, 1975.

This document, divided into four sections, is the final report for that program. Section II of the report describes the experimental effort to characterize the furnace and the results of that effort. Specific topics discussed include: (1) characterization of pulse shapes available from the fast focal plane shutter and the nuclear burst shutter, (2) characterization of the flux distribution in the vicinity of the focal point, and (3) evaluation in part of the heliostat tracking system. Experimentation conducted in support of the development of test instrumentation and methods for the WSSF is described in Section III. Conclusions of this program and recommendations for future work are outlined in the final section of this report.

SECTION II

CHARACTERIZATION OF THE WHITE SANDS SOLAR FURNACE

A. Pulse Shape Determinations

Several devices have been suggested as candidates to measure the optical/thermal pulse shapes available at the WSSF. These include rapid response calorimeters, semiconductor electro-optical detectors, and photomultiplier tube (PMT) detectors. Rapid response calorimeters as typified by the Hy-Cal Asymptotic® calorimeter are electrically simple, rugged, quite small in size, but suffer from a relatively long thermal/optical response time ($\sim$ 100 milliseconds). Thus, the calorimetric radiometer is satisfactory only for very slow risetime pulse shape work.

Of the semiconductor detector and the photomultiplier tube detector, the semiconductor detector is much smaller, is less expensive, and does not require a source of high voltage as does the PMT detector. The photomultiplier tube is, however, a much more sensitive device and its dynamic range (range of linearity) is much greater than that of the photodiode. Also, with the use of fiber optics the PMT detector can be used to probe quite small areas.

During the course of the program experiments were conducted at the WSSF with both a PMT detector and a phototransister detector. The first series of experiments, involving a PMT detector, were carried out during the November visit. A solid state detector based on the use of a phototransistor was designed, constructed, and checked-out on the Georgia Tech Campus and evaluated during the February visit to the furnace. The

details of the experimentation with these two detectors are discussed in turn.

Photomultiplier Tube Detector. A photomultiplier tube apparatus was assembled on the Georgia Tech campus and transported to the White Sands Solar Furnace for evaluation. The experimental arrangement shown in Figure 3 was used to evaluate the apparatus and, at the same time, calibrate and characterize the optical/thermal pulse shapes produced by the various WSSF shutter arrangements. A list of the equipment used in these experiments is given in Table I.

TABLE I

LIST OF EQUIPMENT USED TO CHARACTERIZE
OPTICAL/THERMAL PULSE SHAPES FROM THE WSSF

Item	Manufacturer and Model No.
2" Photomultiplier Tube	Amperex, Model 56AVP
H. V. Power Supply	ORTEC, Model 456
Oscilloscope	Tektronix, Model 502
Scope Camera	Unknown
WRATTEN Gelatin Filters	Kodak, No. 96; N.D. 0.10, 0.70 1.00, 2.00, 3.00 and 4.00

During normal pulse mode operation light from the concentrator mirror is gated on and off by one or both of two pulse shaping shutters located in the focal building. The fast focal plane shutter was designed to give a square shaped pulse of known duration. When such a pulse shape is

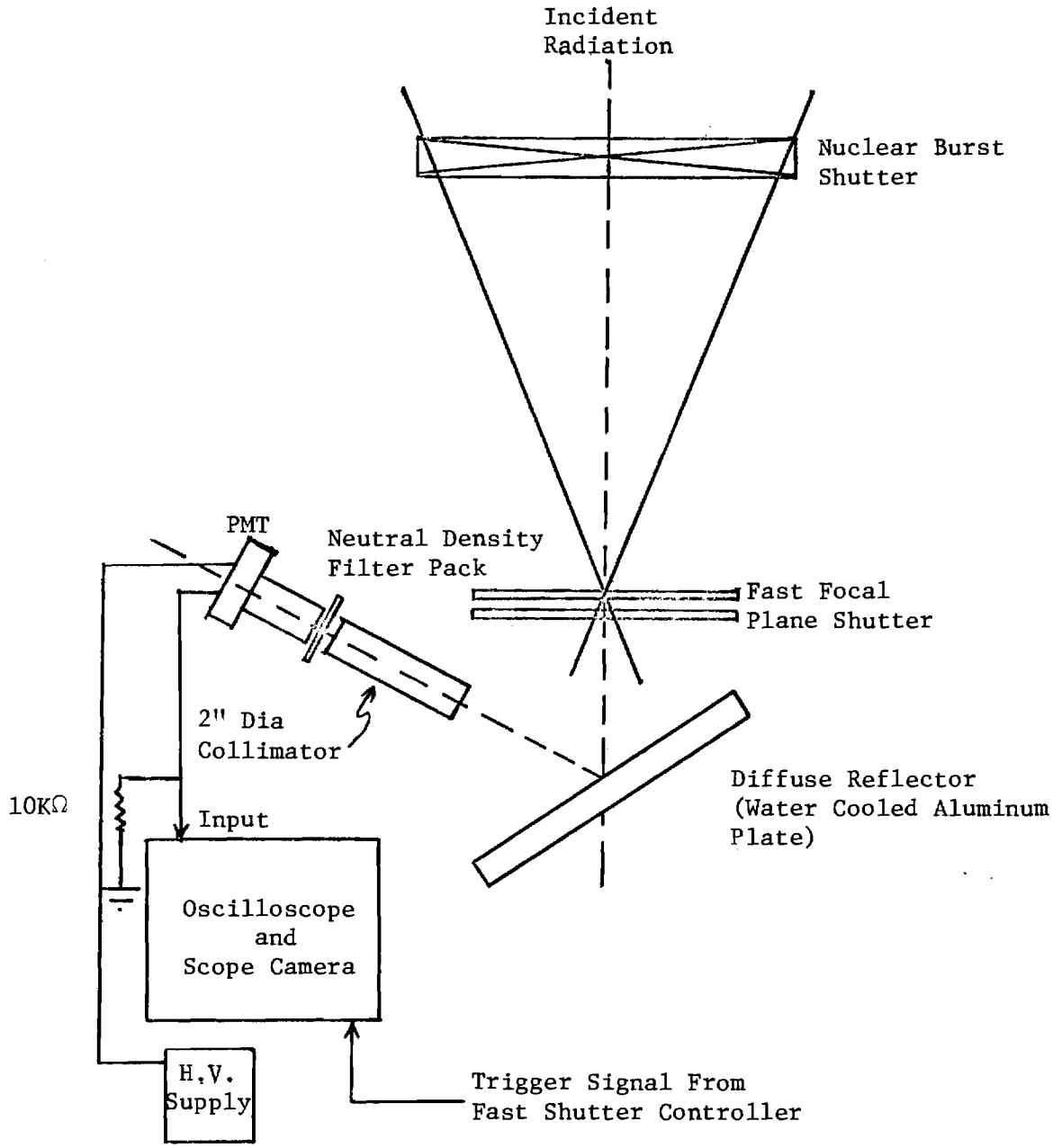

Figure 3. Experimental Arrangement for Characterizing Optical/ Thermal Pulse Shapes from the White Sands Solar Furnace.

desired the vane type nuclear burst shutter is removed from the path of the incident light.

Operation of the WSSF nuclear burst shutter is intended to simulate the thermal effects associated with a nuclear weapon 3/. This shutter is cam driven and runs continuously when placed in operation. The selection of a single pulse is made by synchronizing the opening and closing of the fast focal plane shutter with a single pulse from the vane type shutter.

Characterization of the pulse shapes available from these shutters was accomplished by placing a diffusely reflecting water-cooled aluminum plate behind the focal plane shutter and viewing the scattered radiation with a photomultiplier tube. A 2-inch diameter by approximately 14-inch long collimator was used to eliminate stray radiation, and neutral density filters were used as necessary to attenuate the light incident on the cathode of the PMT. The output of the PMT was displayed by an oscilloscope and photographed. Proper triggering of the oscilloscope was accomplished with the aid of an output from the fast shutter timer.

Fast focal plane shutter data were collected for nominal pulse widths of 100 and 500 milliseconds. The width of the pulse, its rise time and its fall time were of interest in these experiments. The raw data for these two pulse widths are shown in Figures 4 through 9. Table II summarizes the pulse shape information obtained from these data. The measured pulse widths (Full Width at Half Maximum) were found to agree quite well with their nominal values. Pulse rise times for the four sets of data were self consistant and yielded an average rise time of approximately 26 milliseconds. The average decay time for the 100 millisecond pulse was approximately 28

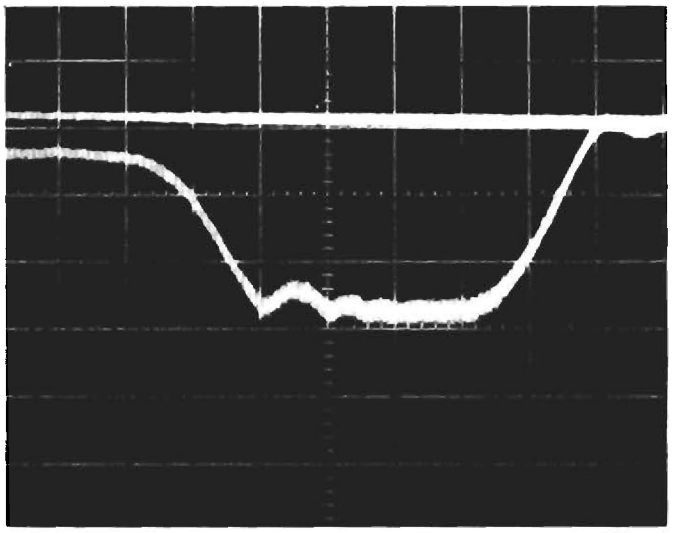

Figure 4. Square Pulse from Fast Focal Plane Shutter. Nominal Pulse Width of 100 Milliseconds. 20 msec/cm Sweep.

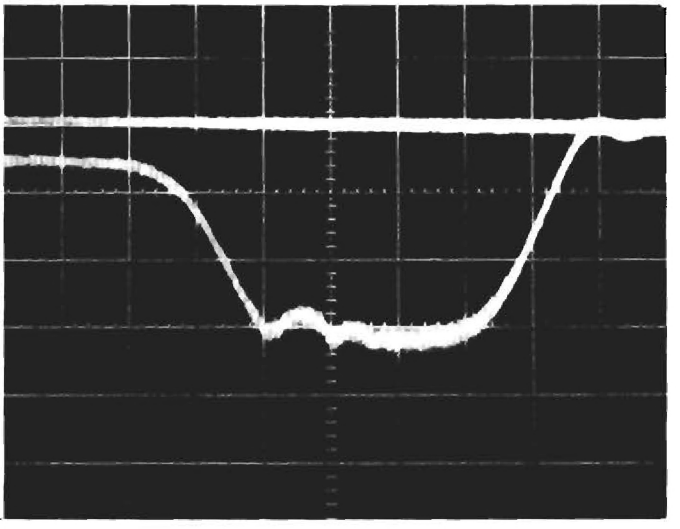

Figure 5. Square Pulse from Fast Focal Plane Shutter. Nominal Pulse Width of 100 Milliseconds. 20 msec/cm Sweep.

Figure 6. Square Pulse from Fast Focal Plane Shutter. Nominal Pulse Width of 500 Milliseconds. 100 msec/cm Sweep.

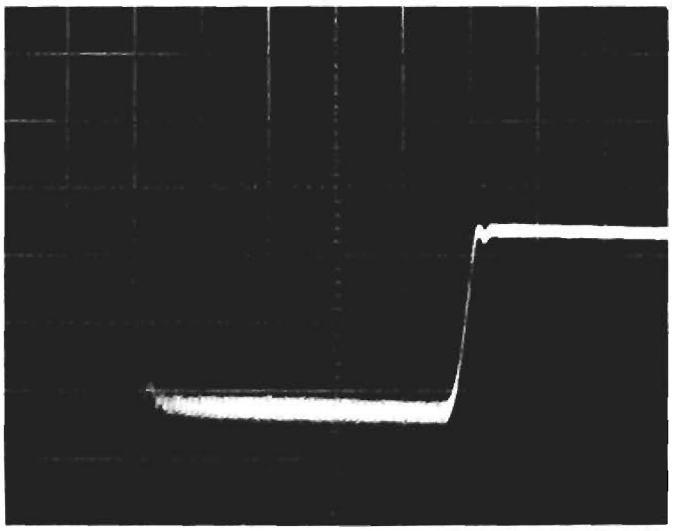

Figure 7. Square Pulse from Fast Focal Plane Shutter. Nominal Pulse Width of 500 Milliseconds. 100 msec/cm Sweep.

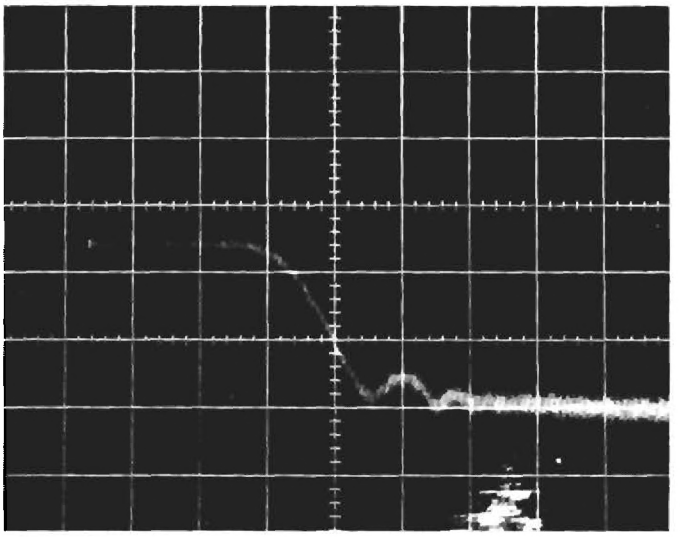

Figure 8. Pulse Rise Time for Square Pulse. Nominal Pulse Width of 500 Milliseconds. 20 msec/cm Sweep.

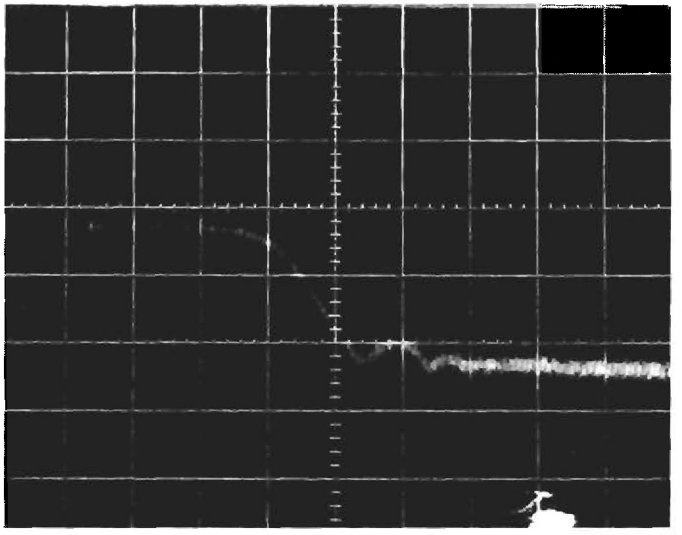

Figure 9. Pulse Rise Time for Square Pulse. Nominal Pulse Width of 500 Milliseconds. 20 msec/cm Sweep.

TABLE II

SUMMARY OF PULSE SHAPE DATA FOR FAST FOCAL PLANE SHUTTER

Nominal Pulse Width (milliseconds)	Reference Figure Number	Pulse Width, FWHM (milliseconds)	Pulse Rise Time, 10% - 90% (milliseconds)	Pulse Fall Time 90% - 10% (milliseconds)
100	4	99	28	29
	5	93	27	27
500	6	495	-	35 ± 5*
	7	490	-	30 ± 5*
	8	-	23	-
	9	-	25	-

*These errors represent only the error in reading the data from the photograph.

milliseconds. The decay time of the 500 millisecond pulse is of the order of 25 to 40 milliseconds. A more accurate estimate of this decay time will require the use of a delayed trigger signal from the shutter timer to the oscilloscope. The compressed air supply used to drive the shutters was set at 87 psig for these experiments.

Pulse shape data were also collected for the characterization of the nuclear burst shutter. These data were collected at nominal shutter speeds of 5, 14 and 25 revolutions per minute. Three sets of data were collected for each shutter speed. The first set depicted two consecutive pulses and was used to check the speed of the nuclear burst shutter. The second set was used to characterize the complete pulse shape and the third set was

used to characterize the leading edge of the pulse. Representative samples of the raw data appear in Figures 10 through 16. The fast focal plane shutter was not used during the collection of these data.

A comparison of the nominal and measured shutter speeds was made and the results are summarized in Table III. The probable error in these experiments is of the order of three percent. Only the 14 rpm shutter speed with its six percent difference fell outside of these error limits.

TABLE III

COMPARISON OF NOMINAL AND MEASURED SHUTTER SPEEDS
FOR THE WSSF NUCLEAR BURST SHUTTER

Nominal Shutter Speed (rpm)	Measured Shutter Speed (rpm)
5	5.1 ± 0.2
14	14.8 ± 0.4
25	25.3 ± 0.7

Glasstone 4/ has indicated that for reasonable weapon sizes, the thermal pulses from all weapons are similar in shape and can be represented by the standard pulse shown in Figure 17. It consists of a very rapid rise and a much slower decline. The WSSF nuclear burst shutter was designed to simulate this shape for a variety of weapon sizes. Note that this standard pulse has been normalized to H_m, the maximum irradiance, and to t_m, the time to reach that maximum irradiance. The time t_m is related to the size of the weapon by the expression

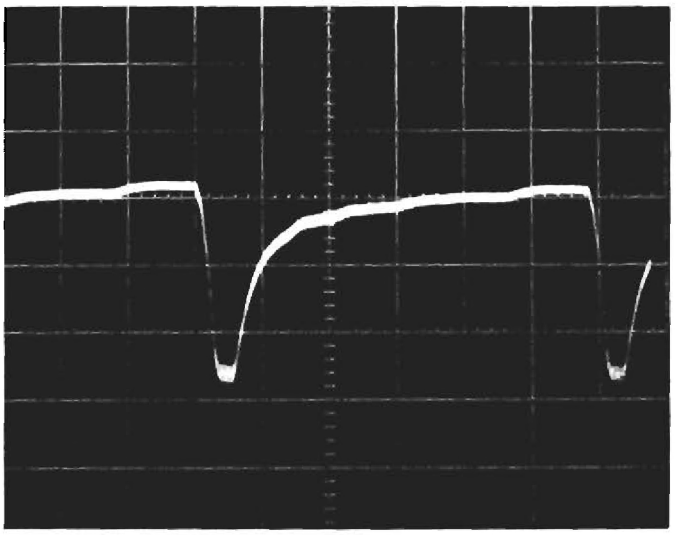

Figure 10. Pulse Shape from Nuclear Burst Shutter Operating at 5 rpm. 2 sec/cm Sweep.

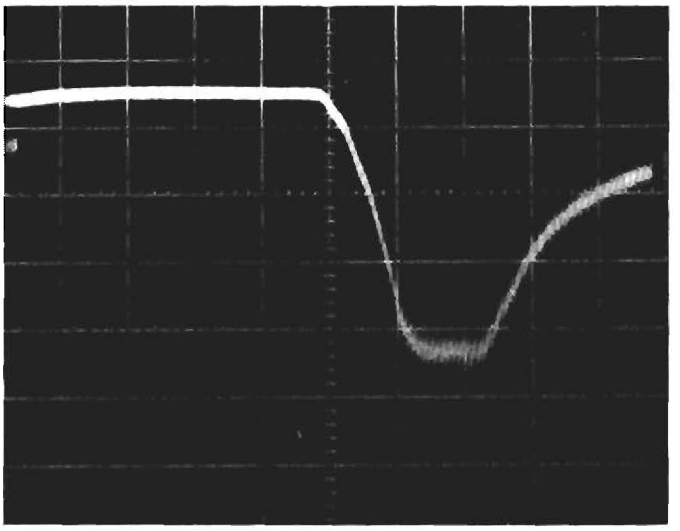

Figure 11. Rise Time of Pulse from Nuclear Burst Shutter Operating at 5 rpm. 100 msec/cm Sweep.

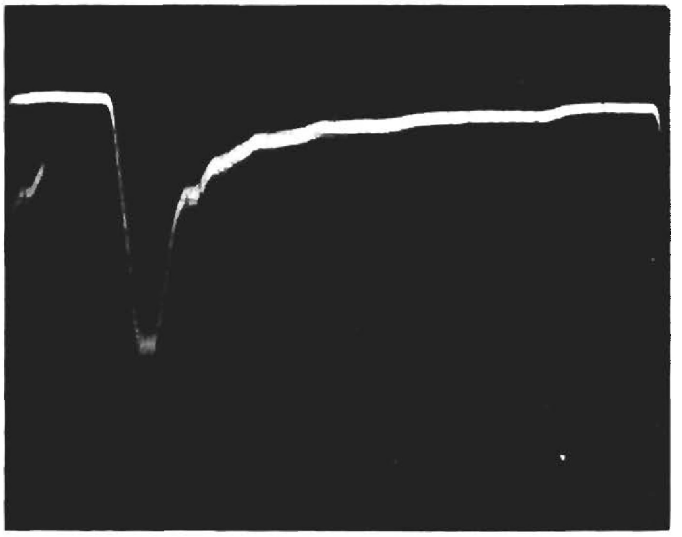

Figure 12. Pulse Shape from Nuclear Burst Shutter Operating at 14.8 rpm 500 msec/cm Sweep.

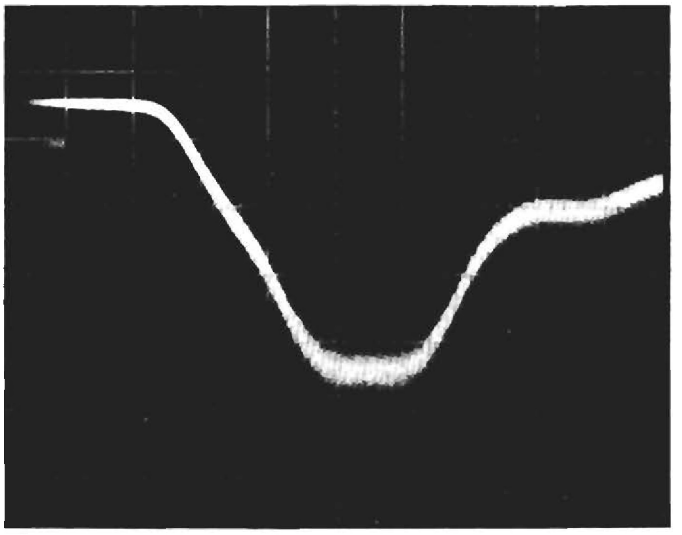

Figure 13. Rise Time of Pulse from Nuclear Burst Shutter Operating at 14.8 rpm. 100 msec/cm Sweep.

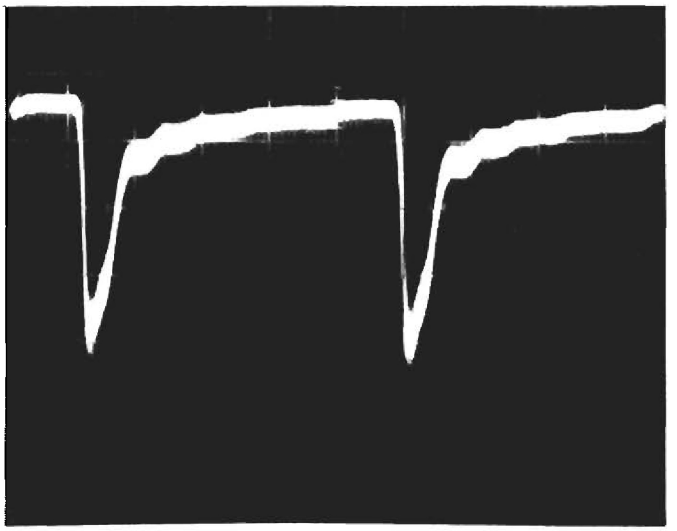

Figure 14. Pulse Pair from Nuclear Burst Shutter Operating at 25 rpm. 500 msec/cm Sweep.

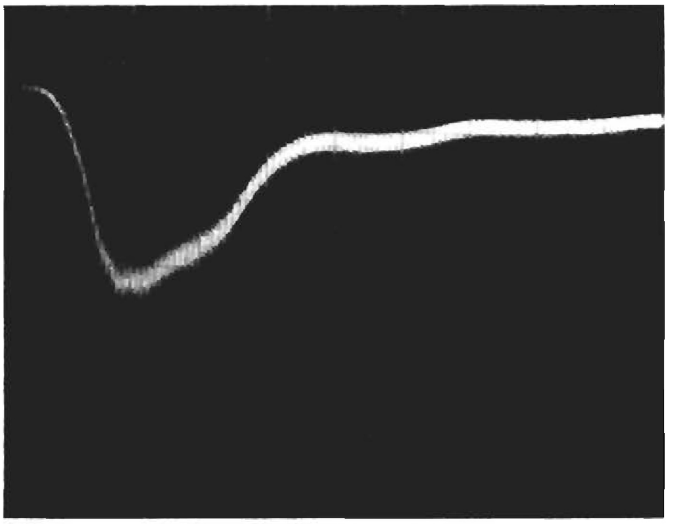

Figure 15. Pulse Shape from Nuclear Burst Shutter Operating at 25 rpm. 100 msec/cm Sweep.

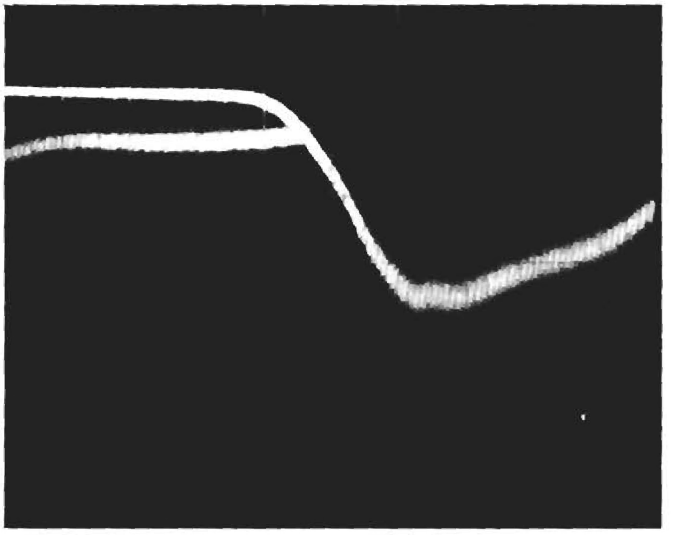

Figure 16. Rise Time of Pulse from Nuclear Burst Shutter Operating at 25 rpm. 50 msec/cm Sweep.

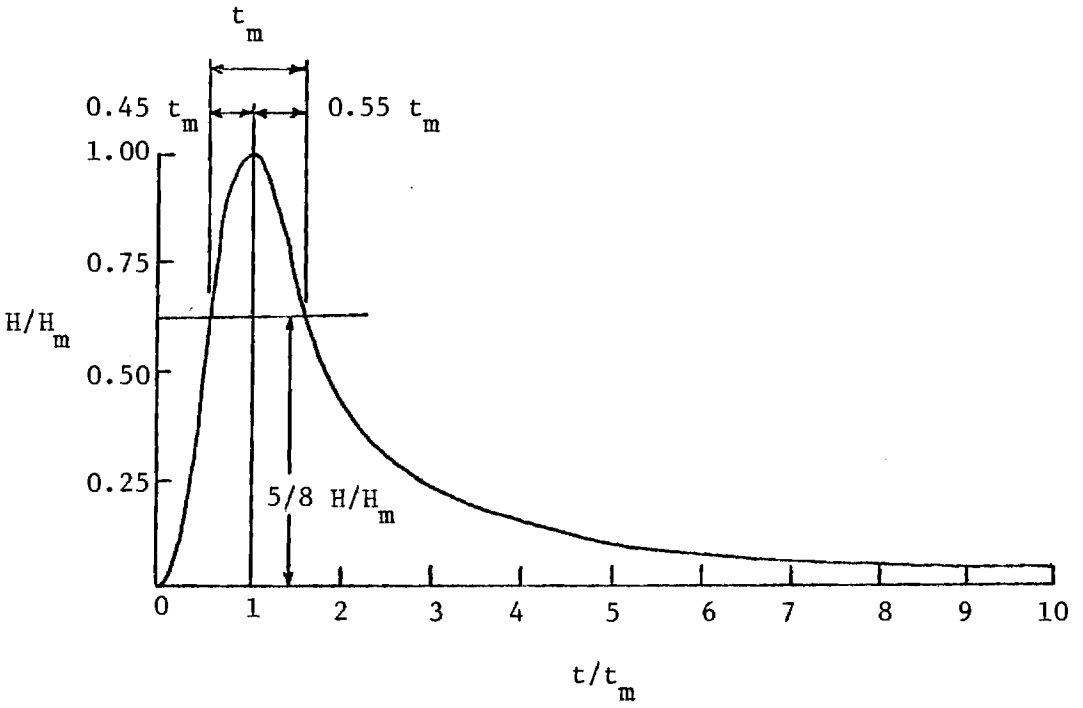

Figure 17. Normalized Thermal Pulse from Glasstone 4/.

$$t_m = 0.032\ W^{\frac{1}{2}},$$

where t_m is in seconds and W is in kilotons.

The pulse shapes available from the WSSF for shutter speeds of 5, 14, and 25 rpm were compared with Glasstone's standard shape. The results of the comparison are shown in Figures 18 through 20. The theoretical and experimental curves compare quite favorably for shutter speeds of 5 and 14 rpm. Such is not the case for the 25 rpm data - the shutter appears to be closing much slower than required for this case. Furthermore, there is evidence at all three shutter speeds that the vanes are somewhat erratic in their rate of closing.

Values were determined for t_m, the time to reach maximum power, for each of the three shutter speeds, and these values were then used to calculate the corresponding weapon sizes. The results of these calculations are summarized in Table IV. These data are in violent disagreement with the results given by Penniman, et al. (Ref. 3) for the operation of the shutter at Natick. A comparison of the Natick data and the Georgia Tech data appears as Table V. Note that for a given shutter speed the pulse risetime measured by Georgia Tech is approximately 1.7 to 2.3 times faster than that reported by the Natick group. This yields weapon sizes that are from 1/3 to 1/5 the sizes reported at Natick. According to WSSF personnel the shutter assembly has not been modified since leaving Natick.

In an attempt to reconcile the two sets of data, the product of the shutter speed with the pulse rise time was formed for each set of data.

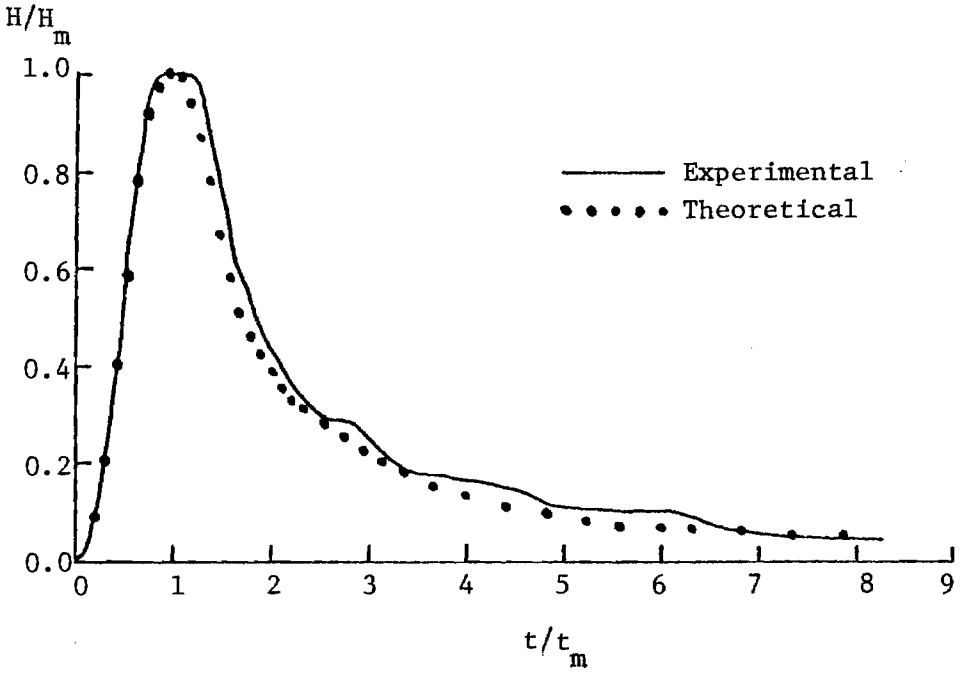

Figure 18. Experimental and Theoretical Pulse Shapes for Shutter Speed of 5 rpm.

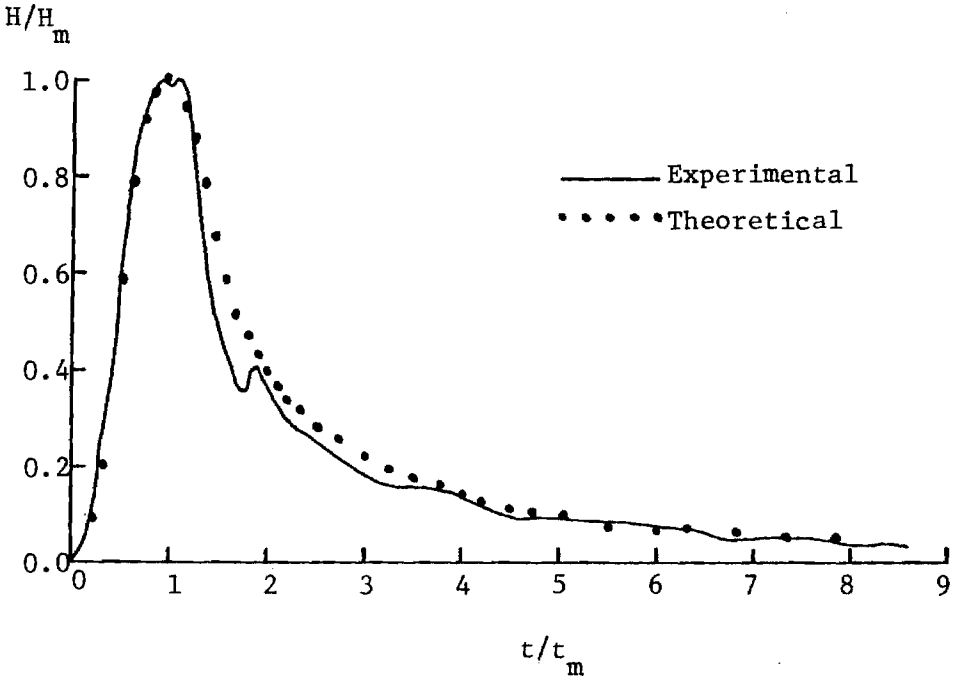

Figure 19. Experimental and Theoretical Pulse Shapes for Shutter Speed of 14.8 rpm.

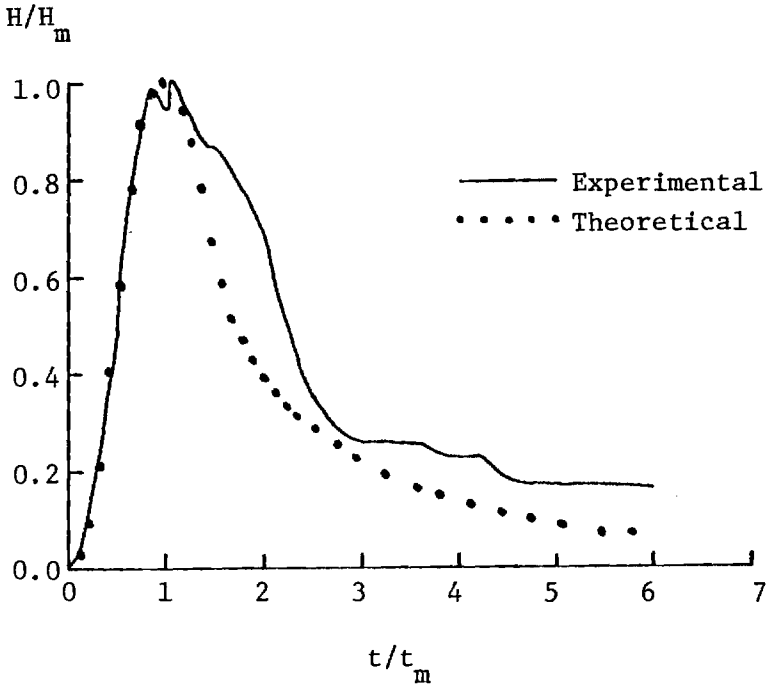

Figure 20. Experimental and Theoretical Pulse Shapes for Shutter Speed of 25 rpm.

TABLE IV

SIMULATED WEAPON SIZE AS A FUNCTION OF SHUTTER SPEED

Shutter Speed (rpm)	Time to Maximum Power (seconds)	Weapon Size (kilotons)
5	1.1	1180
14.8	0.30	88
25	0.17	28

TABLE V

COMPARISON OF NATICK AND GEORGIA TECH PULSE SHAPE AND WEAPON SIZE DATA

	Natick Data		Georgia Tech Data	
Shutter Speed (rpm)	t_m (sec)	W (kilotons)	t_m (sec)	W (kilotons)
5	-	-	1.1	1180
10	1.58	2440	-	-
14.8-15	0.69	468	0.30	88
25	0.29	82	0.17	28

This product should be a constant since the pulse rise time is inversely proportional to the shutter speed. That is,

$$t_m = \frac{k}{(rpm)},$$

where k is some constant. The results of these calculations appear as Table VI.

TABLE VI

PRODUCT OF SHUTTER SPEED AND PULSE RISE TIME AS A FUNCTION OF SHUTTER SPEED FOR THE NATICK DATA AND THE GEORGIA TECH DATA

Source of Data	Shutter Speed	t_m (rpm) Product
Georgia Tech:	5	5.5
	14.8	4.44
	25	4.13
Natick:	10	15.8
	15	10.35
	20	8.0
	25	7.25
	35	5.6

The Georgia Tech data is reasonably self-consistent with respect to the t_m(rpm) product. Such is not the case with the Natick data. The Georgia Tech product is constant within 14 percent for the three shutter speeds. The Natick product is constant only within 48 percent over an even smaller dynamic range of shutter speeds. The implication is that there is an error in the data as published by Penniman et al., or the time base of the oscilloscope used to collect the Georgia Tech data is incorrect by a factor of approximately two for some but not all sweep rates. Having an uncalibrated scope in the most recent experiment would not, however, explain the relatively large t_m (rpm) product spread exhibited by the Natick data.

Semiconductor Detector. An alternative candidate for measuring optical/thermal pulse shapes at the WSSF is the semiconductor detector.

Such a detector, based on the use of a phototransistor and an integrated circuit operational amplifier, was designed, built and checked out on the Georgia Tech campus and evaluated at the White Sands Furnace. Photographs of the detector appear as Figures 21 and 22 and a schematic as Figure 23.

The semiconductor detector was provided with three switch selectable gain positions to give a dynamic range of 100 for the amplifier gain; i.e., relative output gains of 1, 10 and 100 were provided. Power ($\pm$ 15 volts or $\pm$ 12 volts) was supplied to the detector through a 3 pin Jones connector. A 4.7 kΩ resistor in the collector circuit served to protect the phototransistor from excessive currents due to strong illumination. The spectral and angular response of the Motorola MRD 300 phototransistor used in this detector are shown in Figures 24 and 25.

Checkout of the detector, prior to the February visit to the solar furnace, consisted of determining its range of linearity for each of the three gain positions and determining that the response time was adequate for recording shutter pulse shapes. The linearity of the instrument was determined as a function of its output voltage by using the arrangement shown in Figure 26. Kodak neutral density filters were used to vary the light intensity onto the diffuser screen. The constant voltage line transformer was necessary to stabilize the intensity of the microscope lamp. This arrangement was used to determine the response and thus linearity of the detector for all three detector gain positions for both $\pm$ 12 and $\pm$ 15 volt supply voltages. Plots of electrical output versus relative light inputs for each gain position and each power supply voltage are shown in Figures 27 and 28. At each gain position the light intensity from the microscope lamp was varied to give detector saturation for a N.D. 0.1

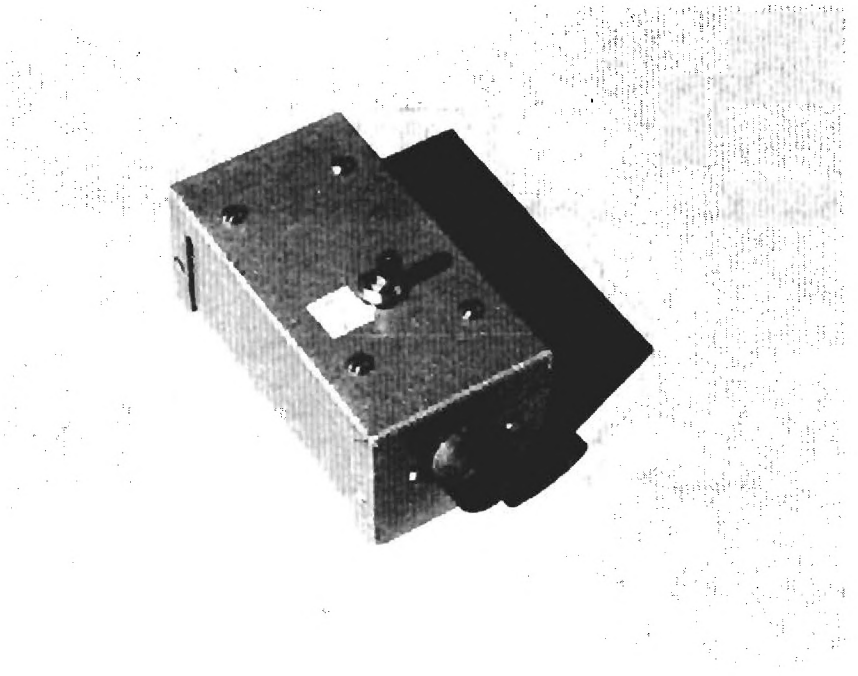

Figure 21. Photograph of Semiconductor Detector.

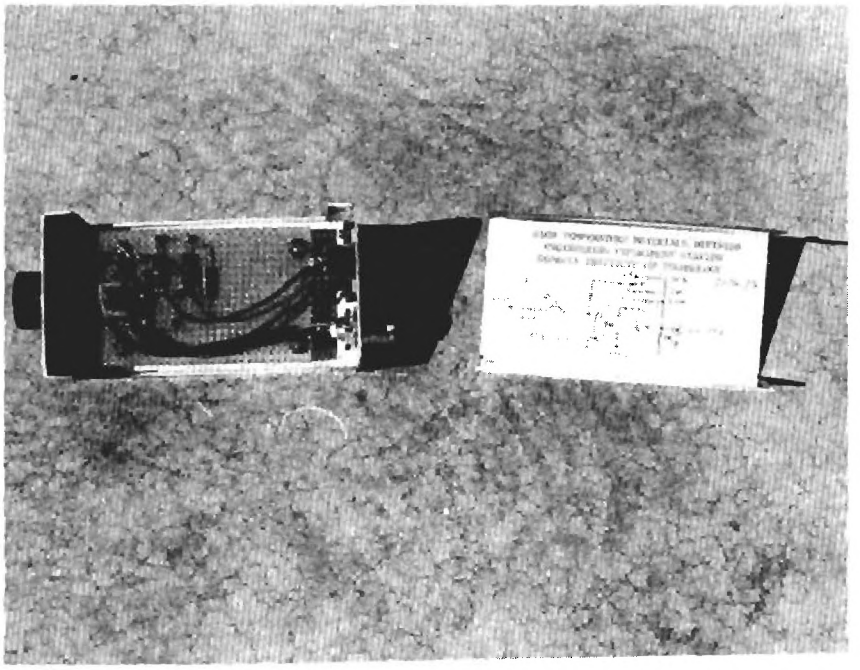

Figure 22. Photograph of Semiconductor Detector with Top Removed to Expose Circuit.

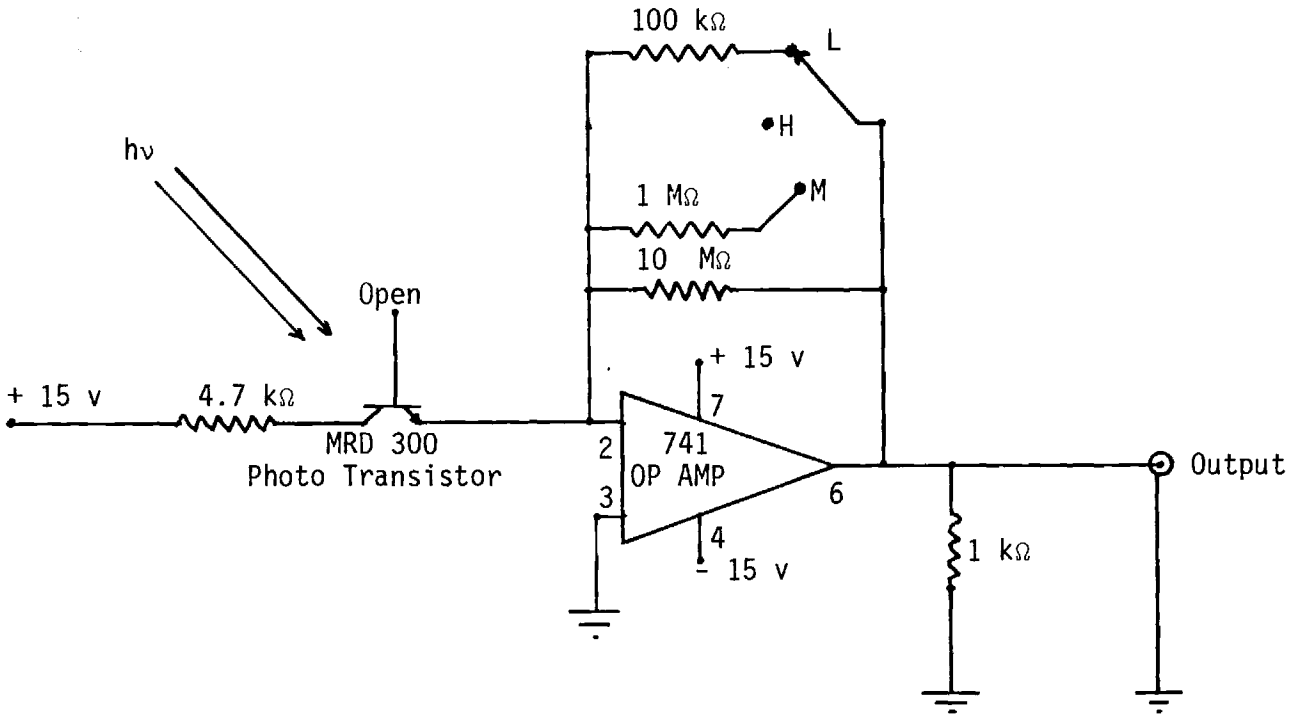

Figure 23. Schematic of Semiconductor Detector.

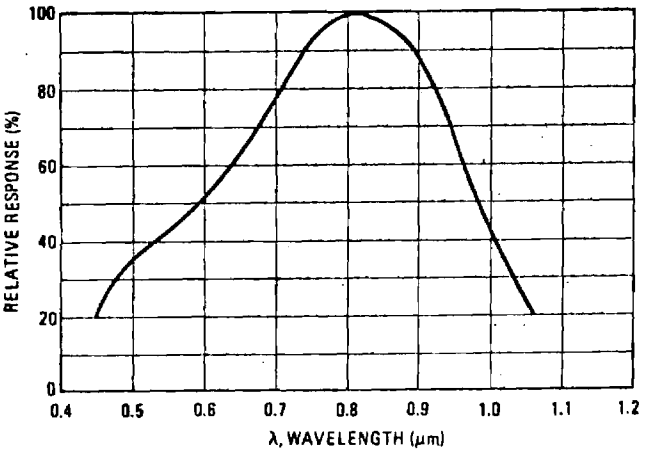

Figure 24. Spectral Response of Motorola MRD 300 Photo Transister 5/.

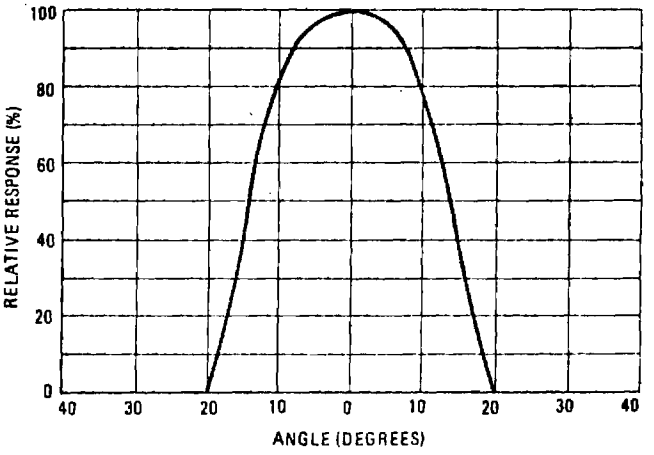

Figure 25. Angular Response of Motorola MRD 300 Photo Transistor 5/.

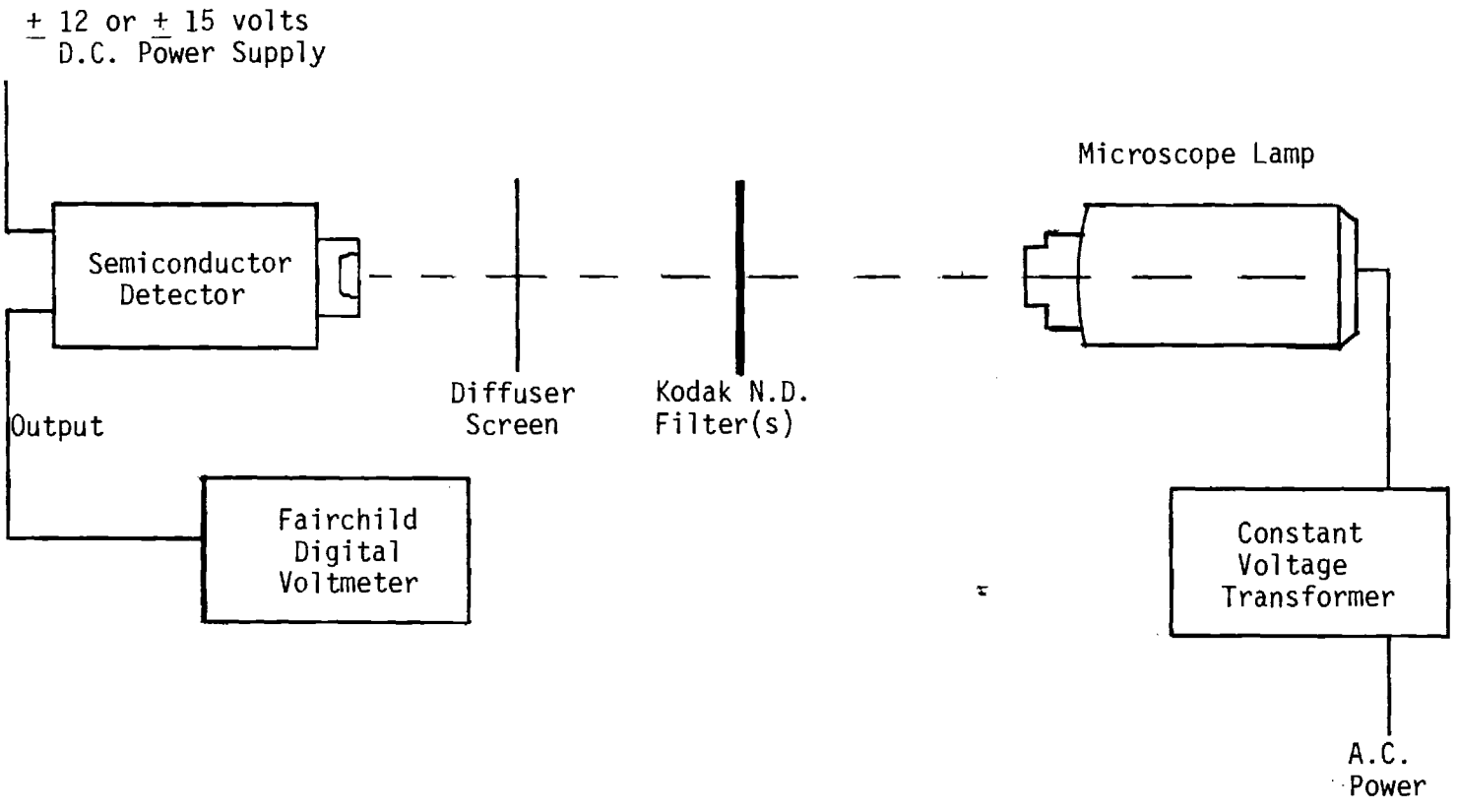

Figure 26. Arrangement for Determining the Range of Linearity of the Semiconductor Detector.

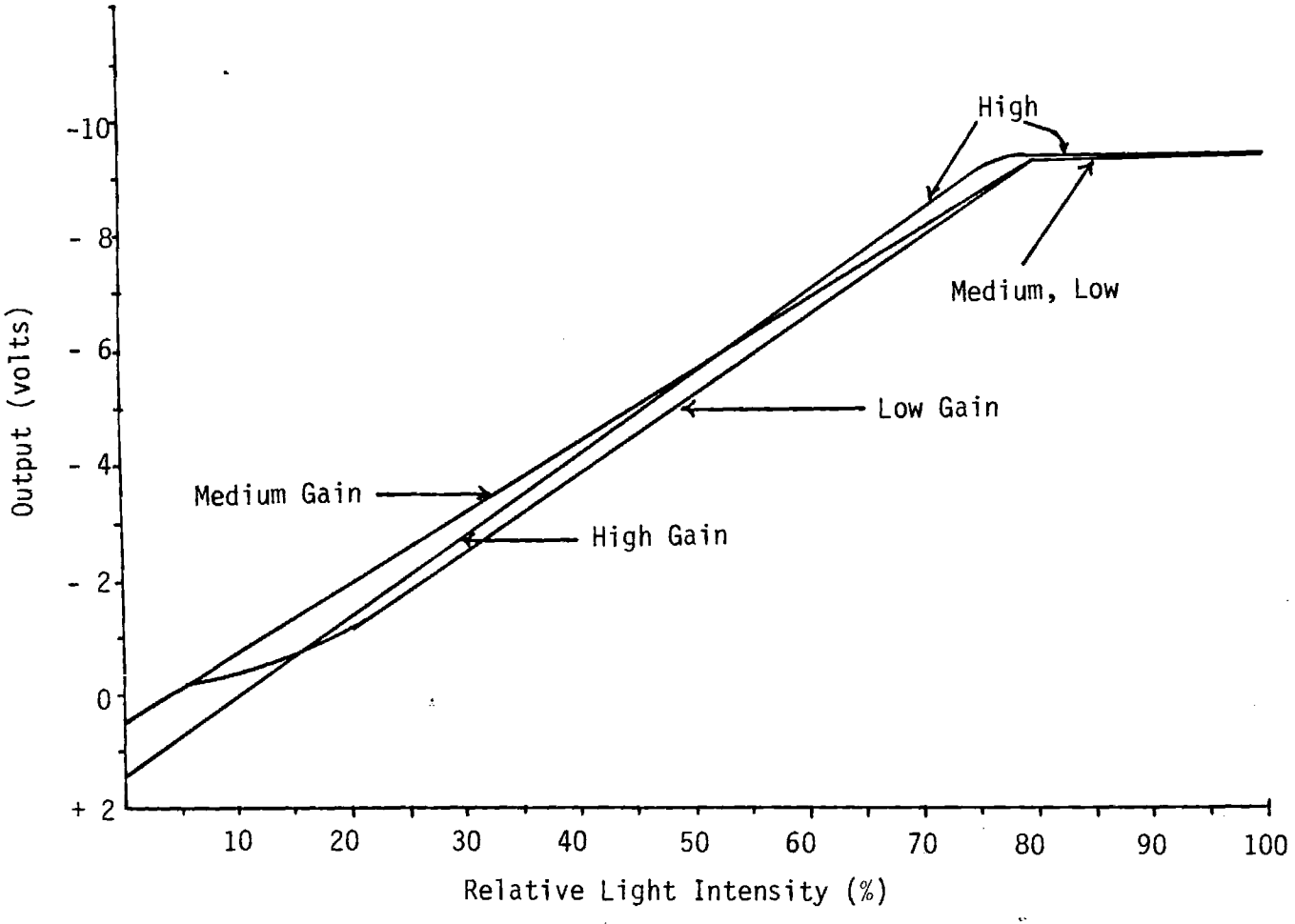

Figure 27. Electrical Output of Semiconductor Detector Versus Incident Light Intensity. ± 12 Volt Supply Voltages to Detector. Light Intensity Varied to Give Detector Saturation for N.D. 0.1 Filter.

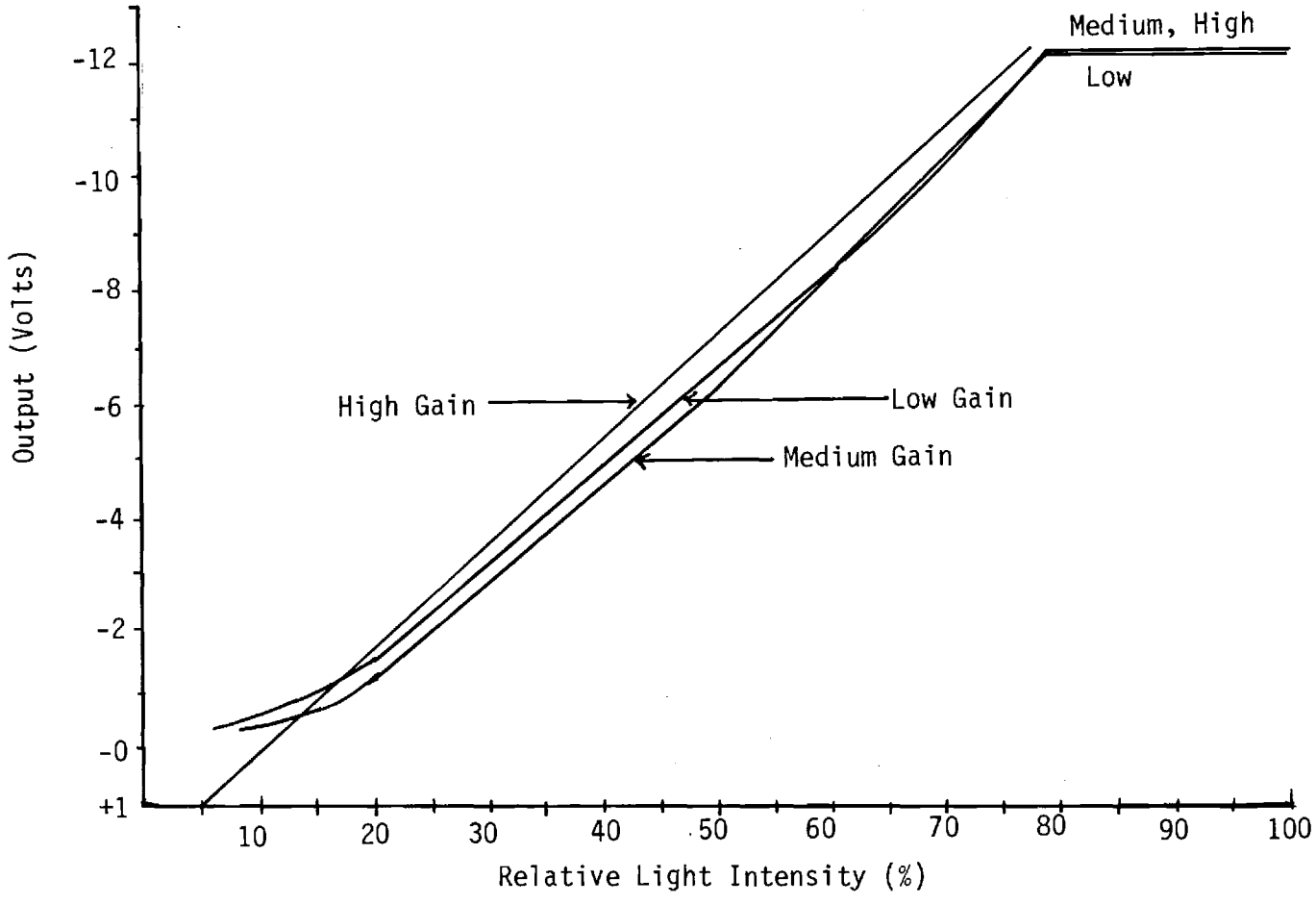

Figure 28. Electrical Output of Semiconductor Detector versus Incident Light Intensity. ± 15 Volt Supply Voltages to Detector. Light Intensity Varied to Give Detector Saturation for N. D. 0.1 Filter.

filter. No attempt was made to determine the absolute sensitivity of the detector.

The time response of the detector was determined only to the extent that it was shown to be satisfactory for the intended purposes. An upper limit response time of approximately 40 microseconds was determined for the detector by mounting a small mirror on the flat portion of the shaft of an ac motor and using the rotating mirror to sweep a reflected light beam across the detector.

The detector was evaluated at the WSSF during the February visit. Accessory equipment used during this evaluation included a $\pm$ 12 volt power supply to energize the detector, an oscilloscope and scope camera to facilitate the monitoring and recording of thermal pulses observed by the detector, and a digital voltmeter to monitor the output d.c. level from the detector under steady state illumination conditions.

Experimentation with the solid state detector followed the same general lines as that used in the evaluation of the photomultiplier tube system. In the first series of experiments, the detector was mounted to a vertical member of the fast shutter support structure and allowed to view a water cooled aluminum plate through a neutral density filter pack having an optical density of 2.3. Figure 29 shows the output of the detector for a nominal one second pulse from the fast shutter assembly. The full width half maximum (FWHM) value for this pulse was determined to be 1.0 seconds. The risetime of the one second pulse is shown in Figure 30. The 10-90 percent risetime associated with that pulse was determined to be 20 milliseconds - in agreement with the photomultiplier tube data.

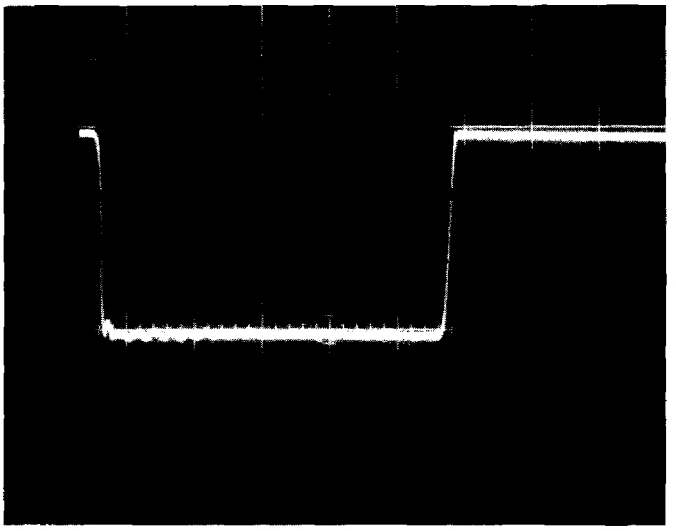

Figure 29. One Second Programmed Pulse From the WSSF Fast Shutter Assembly as Recorded by Semiconductor Detector. 200 msec/cm, 1 v/cm, Detector gain set at "medium."

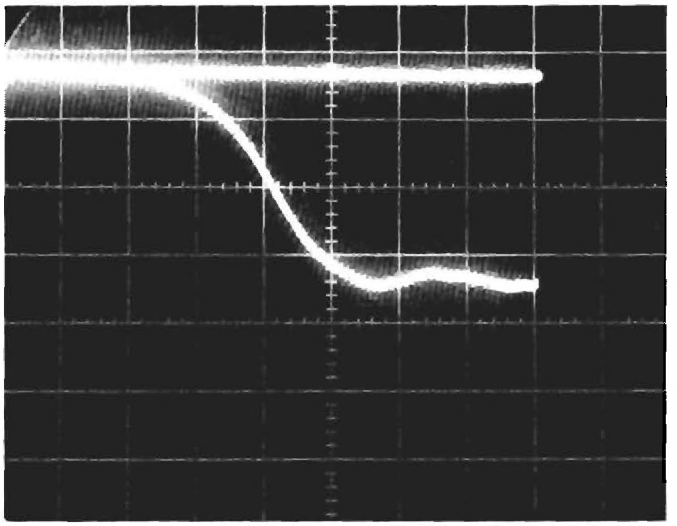

Figure 30. Risetime Associated with a One Second Programmed Pulse From the WSSF Shutter Assembly as Recorded by the Semiconductor Retector. 10 msec/cm, 1 v/cm, Detector gain set at "medium."

The compressed air supply used to drive the shutters was set at 87 psig for these experiments.

The pulse shape from the nuclear burst shutter was also recorded with the aid of the semiconductor detector (see Figure 31). The resulting shape for a shaper speed of 25 rpm, was not unlike that previously recorded with the PMT detector. Of particular interest in this figure, and also in Figures 12, 15 and possibly 11, is the evidence for a double peaked pulse. This artifact was determined to be the result of a light leakage problem. During normal operation of the vane shutter, light from the concentrator is being reflected off of the concentrator side of the vane shutters just as these shutters start to open. This light floods the focal building and is seen by the detector. To verify this hypothesis, the semiconductor detector was fitted with a 5-5/8 inch long by 3/4 inch diameter collimator tube, a large black cloth was placed behind the water cooled target and additional nuclear burst pulses were recorded. As illustrated in Figure 32, these modifications eliminated the double pulsing problem.

An attempt was also made to map the focal zone of the WSSF with the semiconductor detector while tracking the full moon. If such a flux map could be generated, it would be a straightforward task to renormalize it to the sun's intensity. In an attempt to carry out such a flux mapping, the detector was mounted on a three-axis table with its optical axis parallel to the optical axis of the furnace. With such an arrangement, the detector could be accurately positioned to any point in the vicinity of the focal zone. The voltage output of the detector, which is proportional to the

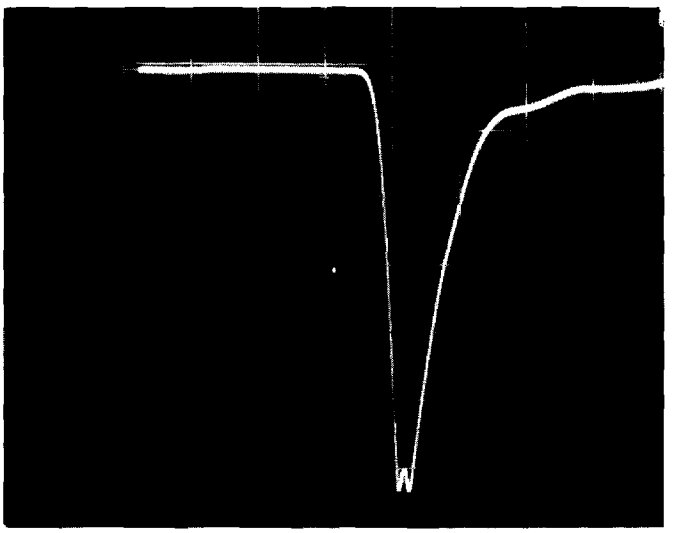

Figure 31. Nuclear Burst Pulse as Recorded by the Semiconductor Detector. Detector Collimator NOT in Use. Shaper Operated at 25 rpm and Furnace Attenuator set at "3". Oscilloscope: 200 msec/cm, 200 mv/cm.

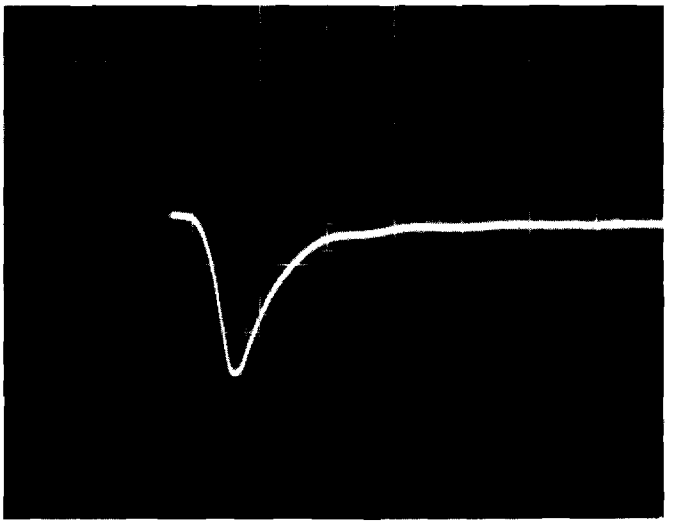

Figure 32. Nuclear Burst Pulse as Recorded by the Semiconductor Detector. 5-5/8" long by 3/4" Inside Diameter Collimator Mounted on Detector. Black Cloth Placed Beyond Target. Shaper Operated at 25 rpm and Furnace Attenuator set at "3", Oscilloscope: 200 msec/cm, 200 mv/cm.

flux received by the detector, was displayed by a digital voltmeter for manual recording. It was readily determined that the sensitivity of the detector was entirely adequate to allow such a flux mapping project, and several scan lines were generated before it became apparent that the furnace heliostat was not accurately tracking the moon. This problem was later traced to a prior failure of the optical tracking tube's sun filter, and with it, the probable damage of the tracking tube's quadrant detector. It was not possible to repair the damaged tracking system during the February visit and thus the optical flux mapping project was abandoned.

The semiconductor detector used in the above work was left at the WSSF to become a permanent part of the instrumentation for that facility.

B. Flux Map of Focal Zone

Probably the two most important characteristics of any solar furnace facility are the power level of the furnace and the distribution of that power in the neighborhood of the focal zone. For a facility such as the WSSF, the power level will be dictated by the insolation, the "size" of the facility and the quality or condition of the many mirrors which compose the heliostat and concentrator. Likewise, the distribution of that power in the vicinity of the focal zone will be dependent on the alignment and relative condition of these many mirrors.

Two attempts were made to map the focal zone of the WSSF. The first attempt, an optical scan with a solid state detector while tracking a full moon, failed because of the inability of the furnace to moon track. This approach was described above.

The second attempt to obtain a flux map was made while tracking the sun, and involved the use of a Hy-Cal Asymptotic® calorimeter mounted in a water-cooled aluminum jacket, which in turn was mounted on the previously described 3-axis table. The millivolt level output from this calorimeter was fed to a model 425 AR Hewlett Packard d.c. microvolt-ammeter for manual recording. A photograph of the experimental arrangement is shown in Figure 33.

Flux map data were collected for the three mutually perpendicular x-y, y-z and x-z planes. The orientations of these planes are defined in Figure 34. The number of data points collected in each plane and the spacing between data points was: the x-y plane - 340 points with Δx = 0.20 inches, Δy = 0.50 inches; the x-z plane - 275 points with Δx = 0.50 inches, Δz = 0.50 inches; and the y-z plane - 110 data points with Δy = 0.50 inches, Δz = 1.00 inches. A copy of the raw data appears as Appendix A. All data were collected at a furnace attenuator setting of "5" (37.5 percent transmission) and later extrapolated to "attenuator full-open" values. A plot of percent transmission versus attenuator setting was supplied by WSSF personnel for this purpose and has been included in this report as Figure 35.

For calibration purposes the calorimeter was frequently moved to the center of the focal zone, the attenuator was placed at "full-open," and a maximum flux reading was obtained. This value ranged from 69.5 to 82 cal/cm^2-sec with an average value of 76.3 cal/cm^2-sec. The above data were collected between 10:30 a.m. and 4:45 p.m. local time, February 25-March 1, 1975.

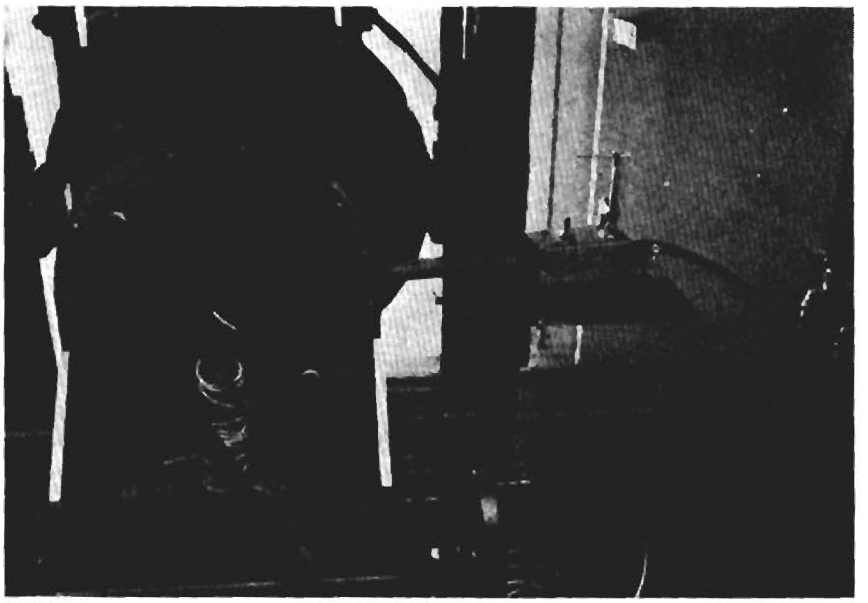

Figure 33. Calorimeter Arrangement Used to Map Flux Zone of the WSSF.

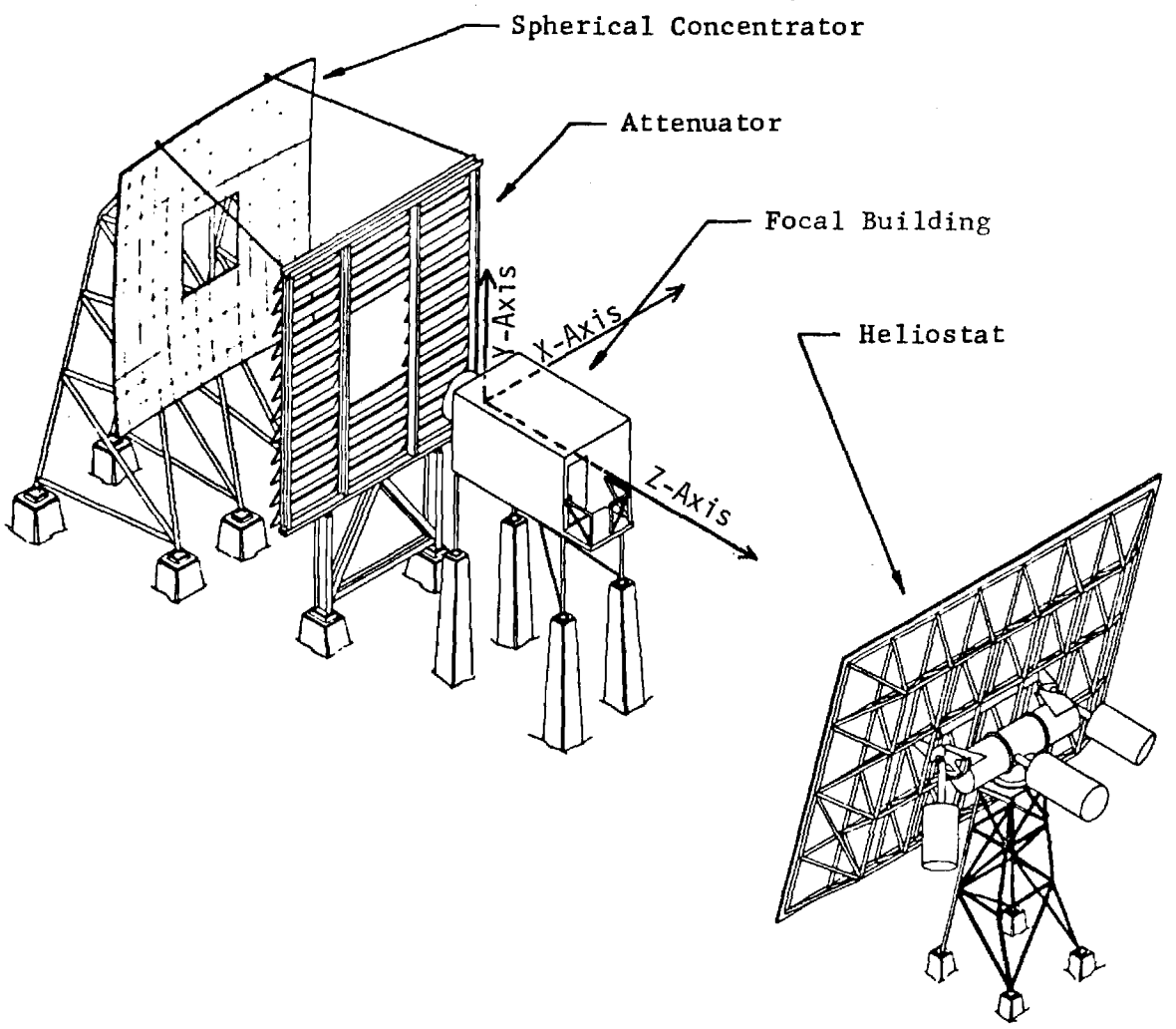

Figure 34. Orientation of Planes Used for Flux Map.

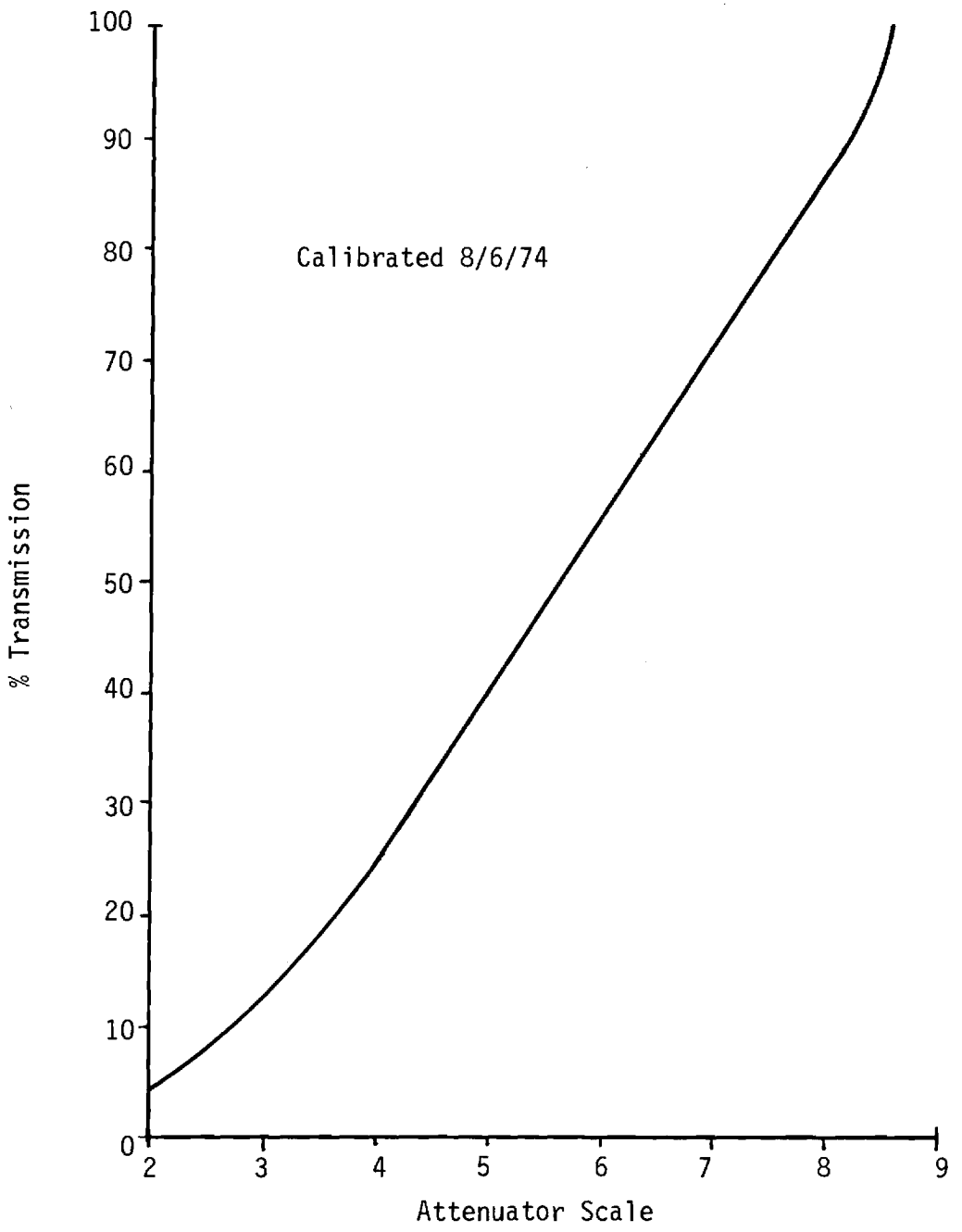

Figure 35. Attenuator Calibration Curve Provided by White Sands Solar Furnace Personnel.

The raw flux map data for each of the three planes was analyzed by a general purpose contouring program* which is operational on the Georgia Tech U-1108 computer. The results of that analysis appears as Figures 36, 37 and 38. For purposes of comparison, the equivalent x-z plane flux map reported by Cotton, et al. 2/ for the Natick furnace is shown in Figure 39.

Several conclusions can be drawn by comparing the two x-z flux maps. First, the contours of the two maps are surprisingly parallel to each other. This can be seen by overlaying one map with the other. Second, it appears that the White Sands facility is better focussed now (at least in the x-z plane) than it was when it was at Natick.

The power level for the WSSF was determined by graphically integrating the thermal flux over the x-y plane (see Figure 36). A planimeter was used to determine the areas between each pair of contour lines. Each area was then multiplied by the thermal flux associated with that area and these contributions were summed to give the power level of the furnace. The thermal flux associated with a given pair of contour lines was taken to be the average of the values of the two contours. When the above procedure was carried out, a value of 24 kW was obtained. Recall, however, that the average peak flux recorded during the flux mapping operations was 76.3 cal/cm^2-sec. According to WSSF personnel the maximum peak flux recorded at the furnace is 86 cal/cm^2-sec. Thus, under those conditions the peak power of the furnace would be 27 kW.

The design value for the power level of the furnace is 35 kW. The presently realized power level is thus approximately 77 percent of the

*Proprietary with California Computer Corporation.

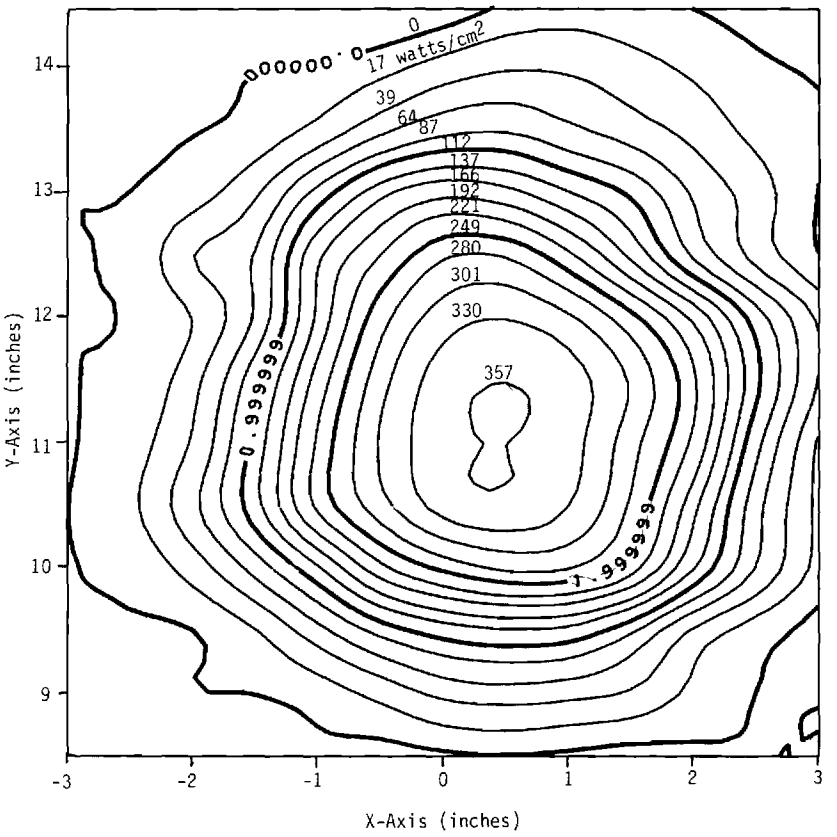

Figure 36. X-Y Plane Flux Map of the Focal Zone of the White Sands Solar Furnace. February 1975.

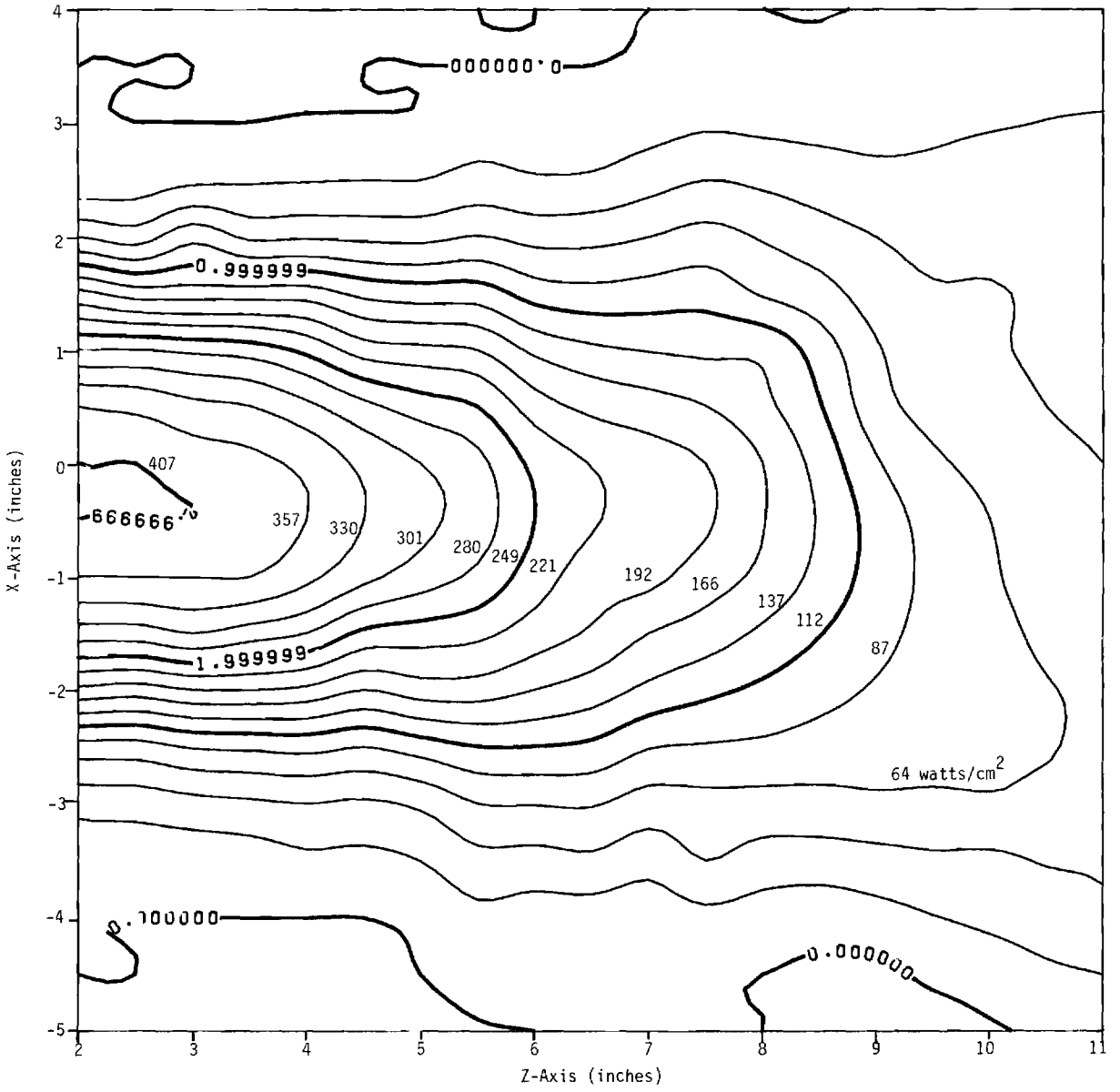

Figure 37. X-Z Plane Flux Map of the Focal Zone of the White Sands Solar Furnace. February 1975.

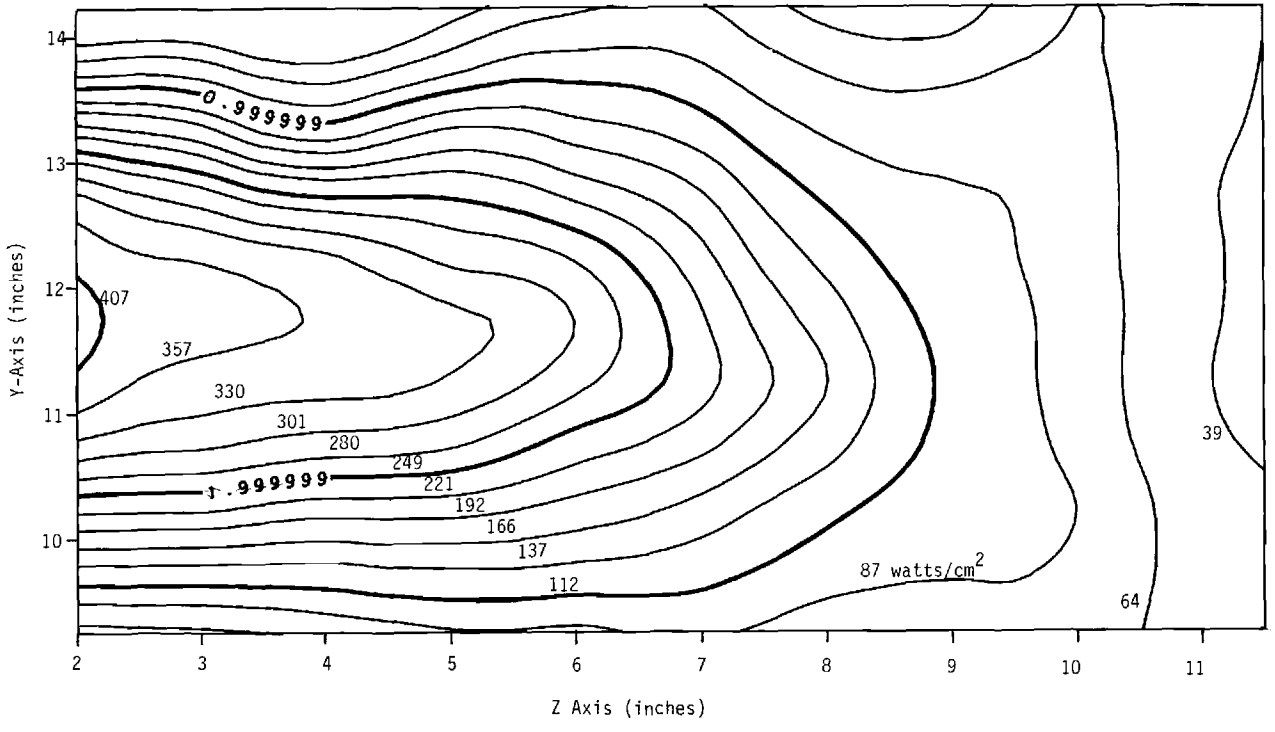

Figure 38. Y-Z Plane Flux Map of the Focal Zone of the White Sands Solar Furnace. February 1975.

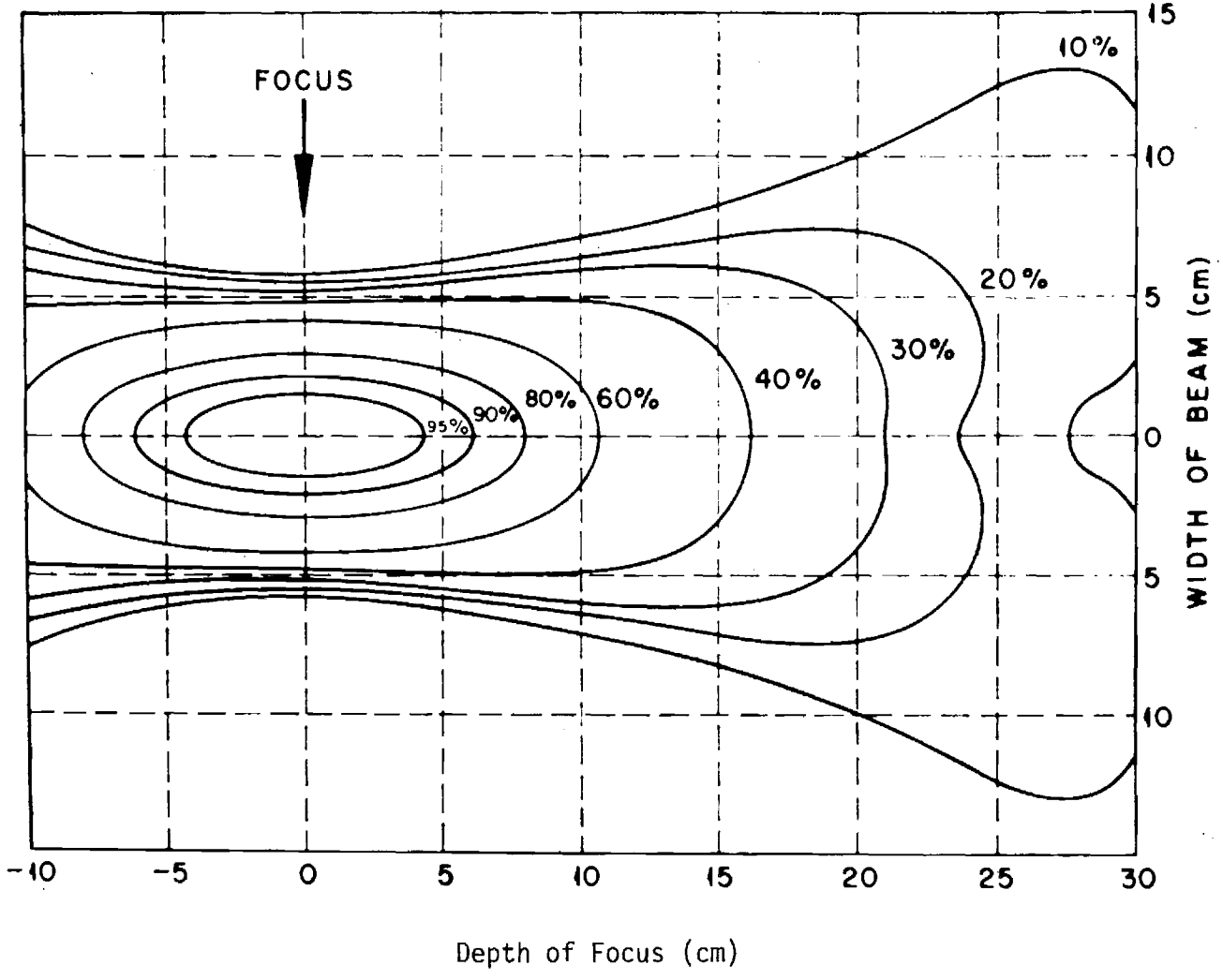

Figure 39. X-Z Plane Flux Map from the Natick Solar Furnace 2/.

design value. There are two major reasons for this difference. First, the concentrator is presently missing its entire bottom row of mirrors. This accounts for an 8 percent reduction in the power level. Second, many of the mirrors on both the concentrator and the heliostat are in a very bad state of repair. This could easily account for the remaining 15 percent or so reduction in power level.

C. Heliostat Tracking

In a facility such as the WSSF the purpose of the heliostat is to redirect the energy from the sun onto the concentrator along a direction parallel to the axis of the concentrator. If this is done accurately the result will be a stable image at the focal point of the concentrator. The White Sands facility is equipped with an optical/electronic tracking tube for control of its heliostat. This tube is mounted through the rear wall of the focal building and has its axis parallel to the optical axis of the concentrator, but displaced from it by approximately four feet. When the heliostat is properly positioned, the image of the sun, as seen through the heliostat, is centered on a quadrant photodiode detector in the rear of the tube. Control of the heliostat is affected by balancing the currents from each of the four detectors in the quadrant photodiode.

At the present time the WSSF heliostat tracking system is not capable of consistently producing a stable image at the focal point of the concentrator. This problem has been tentatively traced to the fact that during a large fraction of the day, or the night if moon tracking, the optical guidance tube sees the sun's image where four separate heliostat mirrors are joined. The result is a broken image of the sun during this

time. The path of the sun across the heliostat as seen by the tracking tube on February 27 and 28, 1974, is shown as Figure 40. The size of the discs on the plot, though not to scale, are characteristic of the size of the sun on the mirror. Note also the tendency of the image to move parallel to, and rather close to, the crack between adjacent north-south mirrors. This may prove to be an additional problem with the higher sun altitudes characteristic of the summer months.

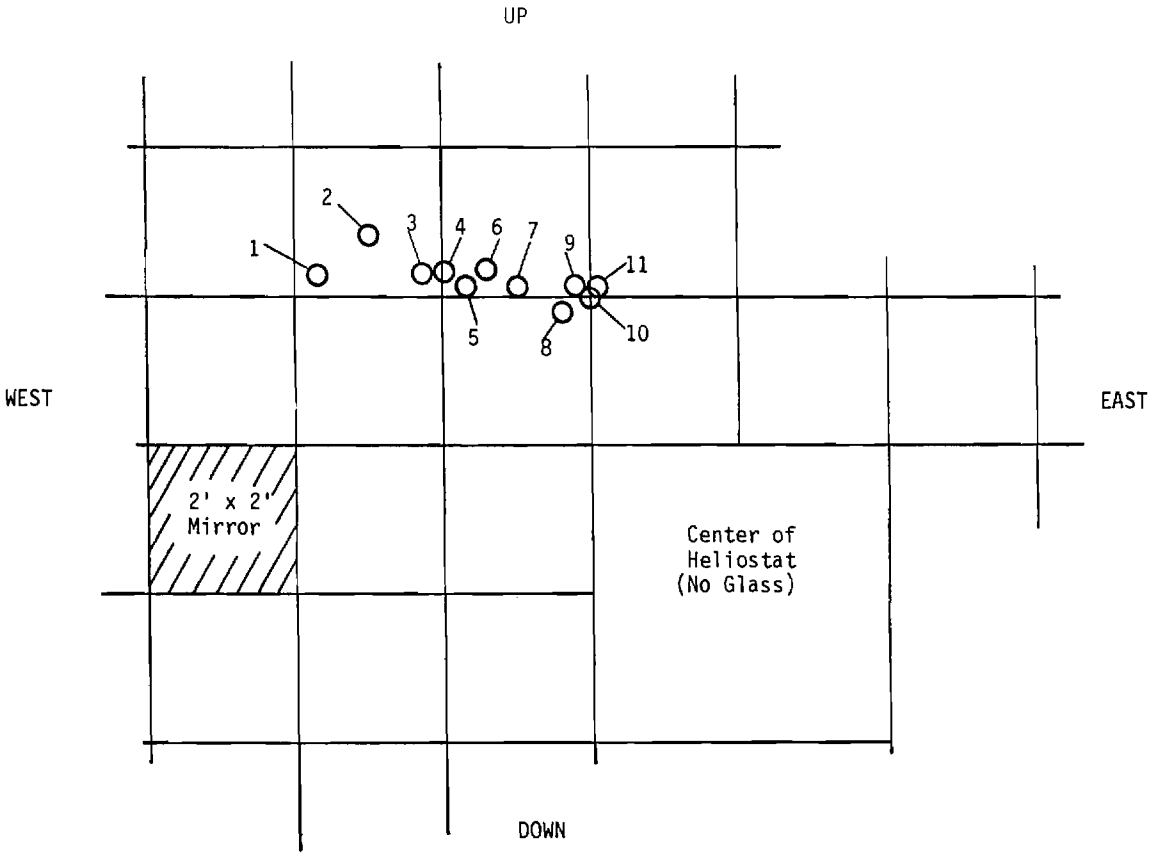

Local Time, February 27 & 28, 1975

1 - 8:00 a.m.
2 - 9:00 a.m.
3 - 9:30 a.m.
4 - 10:00 a.m.
5 - 10:55 a.m.
6 - 11:05 a.m.
7 - 11:40 a.m.
8 - 12:45 p.m.
9 - 1:20 p.m.
10 - 1:40 p.m.
11 - 1:45 p.m.
12 - 2:20 p.m. (same as 11)
13 - 4:00 p.m. (same as 11)

Figure 40. Position of Sun's Image on Heliostat as seen by Optical Guidance Tube as a Function of Time of Day. Only Those Mirrors of Interest are Shown.

SECTION III

EVALUATION OF EXPERIMENTAL TECHNIQUES FOR USE AT THE WHITE SANDS SOLAR FURNACE

A. Optical Pyrometry

The use of thermocouples on surfaces exposed to radiant heat fluxes presumes that the absorption characteristics of the thermocouple match those of the specimen. Our experience indicates that such an assumption is untenable in many situations; for example, translucent materials absorb energy in depth as well as on the surface and the emittance of a thermocouple may be quite different from that of the sample. Therefore, optical pyrometry is preferred for surface temperature measurements. In order to use optical pyrometry however, one must devise a means of accounting for the reflected incident radiation and separating it from the thermally emitted radiation which is to be measured. This separation can be accomplished by optically filtering the incident radiation at the operating wavelength of the pyrometer or by mechanically chopping the incident radiation for brief time intervals and obtaining optical temperature data while the incident beam is cut off. Either of these schemes involves the sacrifice of a portion of the incident energy from the concentrator of the solar furnace. Mechanical chopping is unacceptable during nuclear pulse simulation tests because the pulse time is the same order of magnitude as the chopping time.

It is sometimes possible to let natural phenomena accomplish the optical filtering at the pyrometer's operating wavelength so that temperature measurements can be made. At the CNRS 1000 kW furnace in southern France, Georgia Tech researchers have used this technique with pyrometers

operating at wavelengths around 5 μm in the infrared portion of the spectrum. Glass absorbs radiation strongly in this wavelength range, and all the mirrors at the CNRS installation are back-silvered glass. Therefore, energy reaching the focal point of that solar furnace contains no 5 μm radiation and the pyrometer observes no reflected solar energy at its operating wavelength. Thus, the pyrometer response can be attributed entirely to emitted radiation from the spectrum and temperature can thus be measured.

All of the concentrator mirrors and many of the heliostat mirrors at the WSSF are front-silvered glass, so that much of the energy in the focal area of the White Sands facility has not been filtered through glass. During the May 1974 visit to the White Sands Solar Furnace, Georgia Tech investigators brought a pyrometer which operates at 5.1 μm. The pyrometer measured apparent temperatures of about 2000^{o} F on a water cooled aluminum shutter plate, leading to the conclusion that pyrometry at 5 μm is not feasible at the WSSF because of interference by reflected radiation at that wavelength.

A second potential source for natural filtering of the incident sunlight is the earth's atmosphere. During the NSF International Seminar on Large Scale Solar Test Facilities in November 1974, Professor Sakuari, who operates the Japanese Solar Furnace noted that he had made temperature measurements with pyrometers operating in the water absorption bands at 1.38 and 1.8 μm. The success of this approach depends upon having strong absorption by water vapor in the atmosphere, and this in turn depends to some extent on local weather conditions.

Georgia Tech investigators, in reviewing published data 6,7/ on the spectral transmittance of the earth's atmosphere identified several carbon

dioxide and water vapor absorption bands which might be useful for optical pyrometry in the WSSF environment. In summary, there are combination CO_2/H_2O absorption bands at 1.4, 2.0 and 2.5-2.8 μm; a wide water vapor absorption band exists between 5.5 and 7.0 μm; and finally, a well defined CO_2 band exists between 4.20 and 4.30 μm.

The quantity and distribution of CO_2 in the atmosphere is rather constant with respect to time. Such is not the case with atmospheric water vapor. Thus, the CO_2 band at 4.20-4.30 μm was chosen for further examination.

The possibility of using the CO_2 absorption band to design a solar blind pyrometer was pursued experimentally during the February visit to the WSSF. Two filters which had pass bands in the vicinity of the 4.20-4.30 band were located on the Georgia Tech Campus. Unfortunately, a filter operating entirely within the 4.20-4.30 μm band could not be acquired in the time available. The two filters, one centered at 4.5 μm and the other at 4.3 μm, were adapted to fit a Barnes Engineering IT-4 pyrometer. After calibration with each filter, the instrument was taken to the White Sands furnace for evaluation.

The results of the evaluation were very encouraging. Two experiments were conducted with each filter. First the apparent temperature of the water cooled shutter was determined with the pyrometer while the shutter was receiving the full power of the furnace. Second, the apparent temperature of a new, highly polished stainless steel fast shutter blade was determined as a function of time as it was heated at the focal point of the furnace. The period of heating corresponded to a five second pulse at full furnace power.

The results of the experiments were as follows: the apparent temperature of the water cooled shutter was 1200° F for the 4-5 μm filter and 700° F for the 4.3 μm filter. In the pulsed heating experiment with the 4.5 μm filter, the apparent temperature of the stainless steel target jumped to approximately 1350° F as the fast shutters opened and then steadily rose to approximately 2500° F as the plate melted. The rather good agreement at the higher temperature is probably due to the decreased reflectivity of the target at the higher temperature. The results with the 4.3 μm filter were very similar to those of the 4.5 μm filter except the jump in temperature at the beginning of the thermal pulse was to 700° F.

B. Solar Spectrum Measurements

In August 1974, a representative of Tektronix, Incorporated demonstrated a spectrometer at the White Sands Solar Furnace and made solar spectrum measurements covering the range from 0.3 μm to 1.1 μm. Although this work was not done by Georgia Tech, it is shown in this report for reference. Figures 41 through 43 show the measured curves for direct sunlight, the reflected beam from the heliostat, and the reflected radiation from the concentrator. Figure 44 shows a set of curves published by Thekaekara 8/.

The spectra measured at White Sands are probably on a logarithimic scale, although this is not known for certain. Considering this probable difference in scales, they have an appearance similar to the "sea level" curve in Figure 44 except that they peak at a higher wavelength. An oxygen absorption band at about 0.76 μm and a water absorption band at about 0.94 μm are visible on the White Sands curves at relative intensities similar to Figure 44; thus it appears that the absorption bands at 1.38 and 1.8 μm may also be strong enough to permit optical pyrometry at those wavelengths.

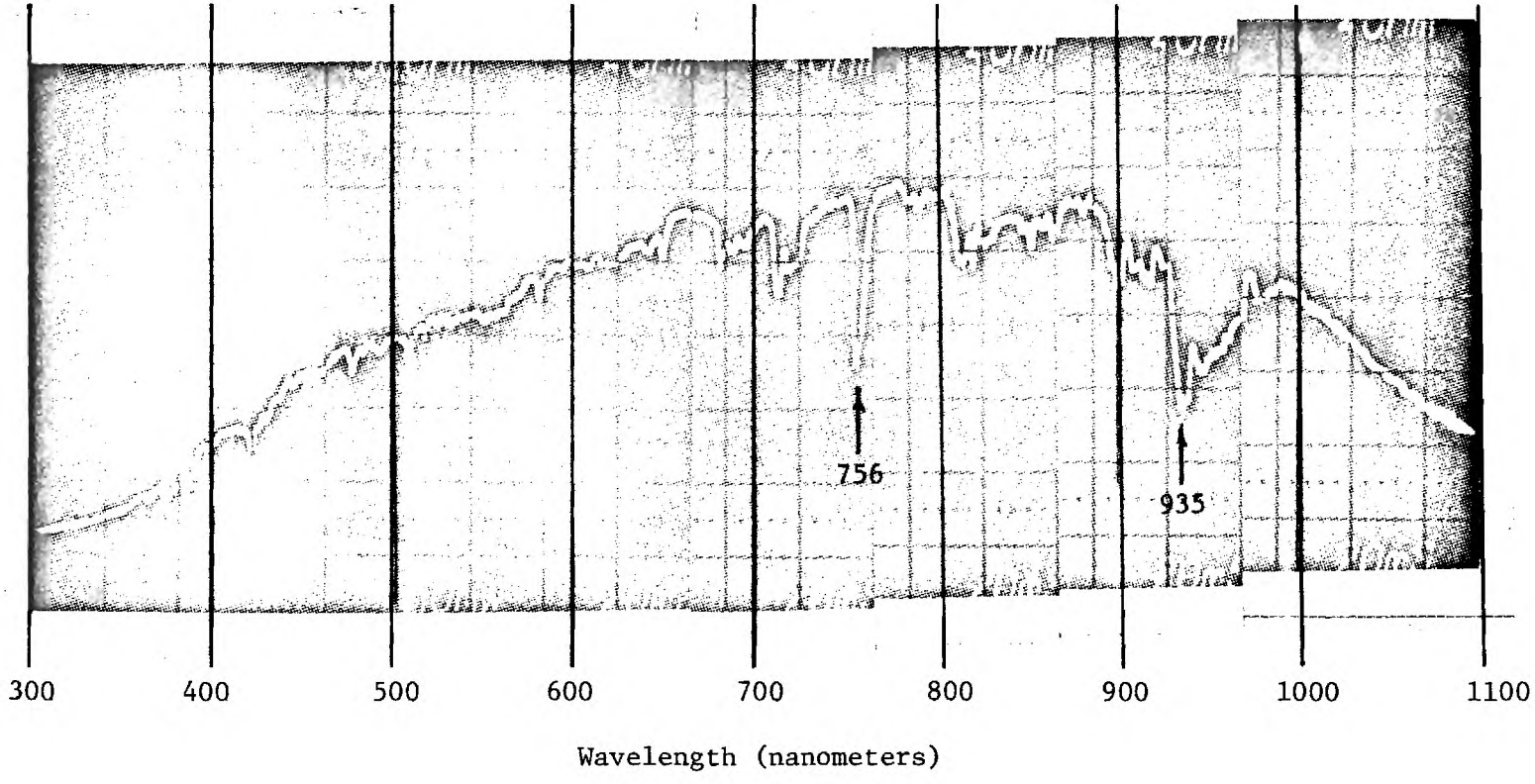

Figure 41. Solar Spectrum Taken at White Sands Solar Furnace, August 1, 1974.

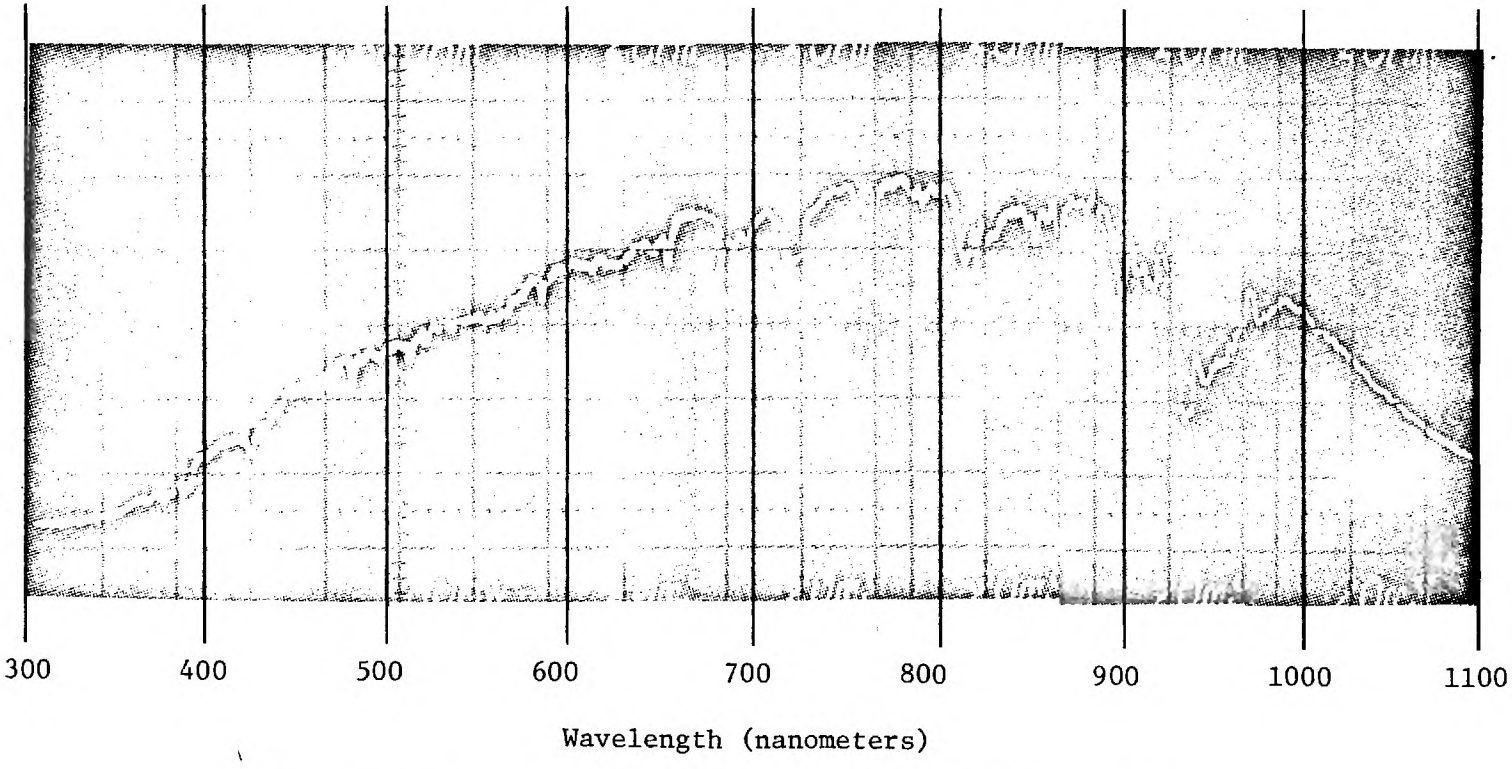

Figure 42. Spectrum of Solar Radiation Reflected from WSSF Heliostat, August 1, 1974.

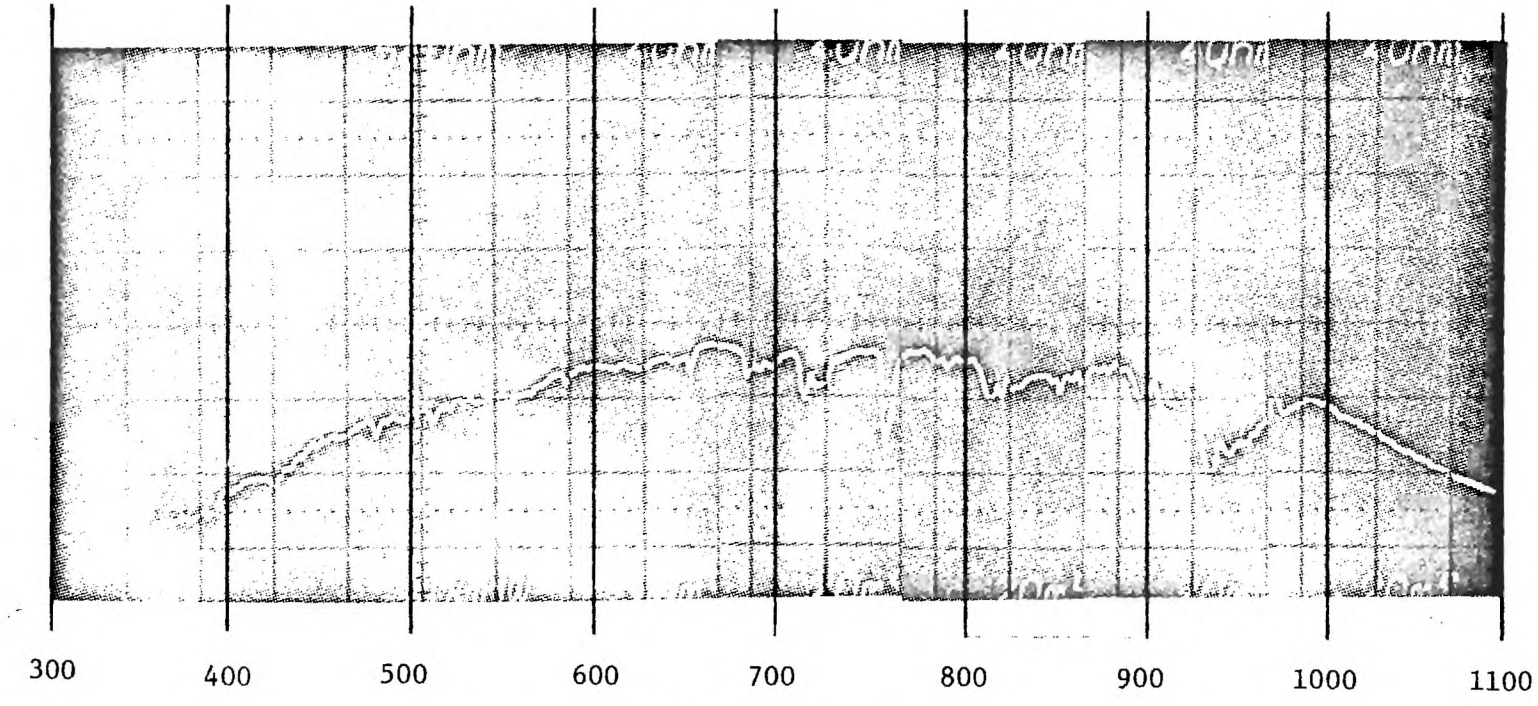

Figure 43. Spectrum of Solar Radiation Reflected from WSSF Concentrator, August 1, 1974.

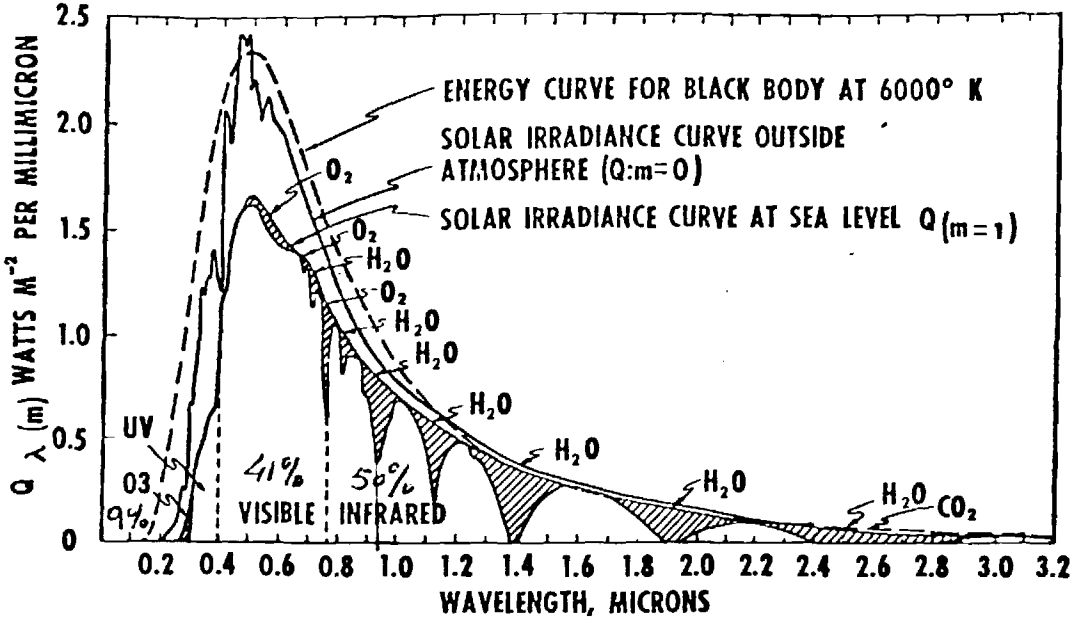

Figure 44. Solar Spectrum Data Published by Thekaekara 8/.

C. Optical Transformer

A light amplification device known as an optical transformer came to our attention earlier this year 9,10/. It is roughly a funnel-shaped device with a highly reflecting inner surface; it should have a particular wall curvature for maximum efficiency although even a straight sided funnel can give some amplification. In theory, the radiant flux arriving at the larger end is directed through the aperture at the smaller end with minimum losses, thereby giving an amplification of flux at the expense of illuminated area. It is a non-focussing device, and it may have considerable value in nuclear and laser effects testing.

In October 1974, two simple versions of the optical transformer were constructed at Georgia Tech for preliminary tests at the White Sands Solar Furnace. These were made by wrapping aluminum foil around a mandrel, covering the foil with epoxy-impregnated glass tape, and curing the structure at elevated temperature. The resulting device had thin glass reinforced plastic walls with a shiny but crinkled inner surface formed by the aluminum foil. No cooling was provided. The two optical transformers were inspected briefly at very low power levels at the solar furnace during a brief visit in October, and amplification of flux was detected.

Further experimentation designed to measure the optical gain of the two Georgia Tech optical transformers was conducted during the November visit to the WSSF. This work was carried out at night while manually tracking a half moon. First, the photomultiplier tube was placed at the focal point of the concentrator and a light intensity recorded. Then each optical transformer was placed with its mouth at the focal point and the light intensity at the small end recorded. In each case the intensity after

amplification was lower than the original intensity. Various alignment positions were tried, but without success.

In retrospect the above results appear to be reasonable. With the photomultiplier at the focal point of the concentrator, it was receiving approximately 65 percent of the incident radiation. With the photomultiplier/optical transformer in position the amount of direct radiation falling on the photomultiplier tube was only 10 to 20 percent of the incident radiation. Thus, for the optical transformer to have an apparent gain of one in the above experiments it would have had to redirect the remaining 80 to 90 percent of the radiation from the concentrator onto the photomultiplier with an efficiency of approximately 50 percent. Since optical gains approaching one were obtained, it follows that the transformer was redirecting the scattered radiation through the rear aperature with an efficiency of approximately 50 percent. Thus, with a highly polished cone it should be possible to approximately double the peak flux available at the White Sands Solar Furnace.

SECTION IV

CONCLUSIONS AND RECOMMENDATIONS

A. Conclusions

The subject program produced the following conclusions:

(1) The current maximum power level of the WSSF is approximately 27 kilowatts - approximately 77 percent of its design power level.

(2) The WSSF is better focussed now, at least in the x-z plane, than when it was at Natick.

(3) There is generally good agreement between the shape of the WSSF flux contours as determined by Georgia Tech personnel and the Natick contours published by Cotton, et al.

(4) The WSSF heliostat tracking system is not capable of consistantly producing a stable image at its focal point. This problem has been tentatively traced to the fact that during a large fraction of the day the optical guidance tube sees the sun's image where four separate heliostat mirrors are joined.

(5) Either a PMT detector or a solid state detector can be used to determine the shape of thermal pulses available at the WSSF. The solid state detector does have the advantages of smaller size and lower cost. The greater dynamic range associated with the PMT does not appear to be necessary for this particular application.

(6) The pulse risetime associated with the fast focal plane shutter is shorter than 30 milliseconds. In five trials the 10-90 percent risetime varied from 20 to 28 milliseconds with an average of 25 milliseconds.

(7) The pulse falltime associated with the fast focal plane shutter is approximately 30 milliseconds.

(8) The measured pulse width for the fast focal plane shutter is within five percent of its programmed value.

(9) Theoretical and experimental pulse shapes for the nuclear burst shutter compare very favorably for shutter speeds up to and including 14 rpm.

(10) The nuclear burst shutter appears to be closing much slower than required for the 25 rpm setting.

(11) There is evidence at all nuclear burst shutter speeds that the vanes are somewhat erratic in their rate of closing.

(12) There is a large discrepancy in shutter speed versus simulated weapon size between the Georgia Tech data and the data reported from Natick. For a given shutter speed, the weapon sizes reported by Georgia Tech are from 1/3 to 1/5 the sizes reported at Natick. Further calculations tend to discredit the Natick data.

(13) Light reflected from the concentrator side of the nuclear burst shutter floods the focal room just as the shutter opens. This light will usually be seen by a pulse shape detector and can result in an apparent double pulse being recorded.

(14) The semiconductor detector described in Section II has adequate sensitivity to be used for flux mapping of the focal zone under full moon conditions.

(15) An optical pyrometer operating in a pass band of 4.20 to 4.30 μm would probably be solar blind and thus could be used to measure the temperature of a sample during irradiation at the WSSF.

(16) The Winston optical transformer offers the possibility of increasing the maximum flux density of the WSSF by a factor of approximately two.

B. Recommendations

The WSSF is presently in a rather poor state of repair and is ill-equipped to undertake serious research. Implementation of the following recommendations would substantially restore the facility to its original capability:

(1) Install concentrator mirrors on the bottom row of the concentrator. These mirrors were broken during the move from Natick, but were never replaced.

(2) Replace or refinish all deteriated mirrors on the heliostat and the concentrator. Implementation of items (1) and (2) should restore the power level of the furnace to its original design value of $\sim$ 35 kW.

(3) Redesign the heliostat optical guidance system so that the sun's image, as seen by the guidance tube, never crosses a heliostat mirror boundary. This might be accomplished by placing the guidance tube nearer to the optical axis of the concentrator, or possibly by replacing several of the small heliostat mirrors with one larger mirror. A combination of the above approaches might yield some relief. A third possibility would be to move the tracking tube closer to the heliostat.

(4) Obtain a <u>volume</u> flux map of the focal zone of the WSSF. This might be accomplished by designing and constructing a mechanical system which could rapidly and accurately sweep the volume with a suitable detector. The analog output of the detector, along with certain timing signals, could be recorded on magnetic tape by an instrument recorder, and later digitized and analyzed. A similar scheme has been developed and used on the Georgia Tech campus to digitize and analyze scanning electron microscope images.

(5) Determine the cause for the sluggish operation of the nuclear burst shutter at high operating speeds and correct.

(6) Determine the cause for the erratic rate of closing of the nuclear burst shutter at all speeds and correct.

(7) Acquire a solar blind pyrometer for measuring the temperature of samples during radiant exposure. One such instrument would be a specially modified Model IT-7C available from Barnes Engineering Company*. The required instrument must operate in the 4.20-4.30 μm CO_2 absorption band. A quotation from Barnes Engineering Company for such an instrument yielded the following:

(a) Filter: half power points of 4.201 and 4.294 μm
1/10 power points of 4.194 and 4.312 μm
84 percent transmission

(b) Available 1 percent accuracy+

temperature ranges:	
	400 to 2300° F
	500 to 2600° F
	580 to 3000° F
	1500 to 4000° F

*Barnes Engineering Company, Industrial Products Group, 30 Commerce Road, Stanford, CT 06904.

+Accuracy is quoted as percent of span.

(c) Available 2 percent accuracy*

temperature ranges:	400 to 2500° F
	500 to 3000° F

It is recommended that White Sands purchase a one percent instrument having a temperature span of approximately 580° to 3000° F. The April 1975 cost of a one percent instrument is $3,505. The April 1975 cost of a two percent instrument is $3,930.

*Accuracy is quoted as percent of span.

REFERENCES

1. John M. Davies and Eugene S. Cotton, "Design of the Quartermaster Solar Furnace," Solar Energy 1, 16-22, (1957).

2. Eugene S. Cotton, William P. Lynch, Walter Zagieboylo and John M. Davies, "Image Quality and Use of the United States Army Quartermaster Solar Furnace," Vol. 6 of the Proceedings of the Conference on New Sources of Energy, Rome, 336-345 (Aug 1961).

3. Frederic G. Penniman, Robert J. Goff and John M. Davies, "A Pulse Shaper for the Natick Laboratories Solar Furnace," Solar Energy 12, 85-94 (1968).

4. Samuel Glasstone, The Effects of Nuclear Weapons, Revised Edition, U. S. Government Printing Office, April 1962.

5. Product Data Sheet for MRD 300 Photo Transistor, Motorola Semiconductors, Box 20912, Phoenix, Arizona.

6. Electro-Optics Handbook, RCA Commercial Engineering, Harrison, New Jersey, 1974, 81-84.

7. John A. Jamieson and others, Infrared Physics and Engineering, New York: McGraw-Hill, 1968, 75-82.

8. Matthew P. Thekaekara, "The Solar Constant and Spectral Distribution of Solar Radiant Flux," Solar Energy 9, 7-20 (1965).

9. H. Hinterberger and R. Winston, "Use of a Solid Light Funnel to Increase Phototube Aperture without Restricting Angular Acceptance," The Review of Scientific Instruments 39, 1217-1218 (1968).

10. R. Winston and J. M. Enoch, "Retinal Cone Receptor as an Ideal Light Collector," Journal of the Optical Society Society of America 61, 1120-1121.

APPENDIX A

RAW FLUX MAP DATA

z–AXIS (inches

x–AXIS (inches)	2.0	2.5	3.0	3.5	4.0	4.5	5.0	5.5	6.0	6.5	7.0	7.5	8.0	9	10	11	x–AXIS (inches)
4½																	4½
4								0	0		0	0	0			0.14	4
3½	0	0	0			0	0	0	0	0	0.04	0.04	0.03	0.10	0.10	0.12	3½
3	0	0	0	0	0.02	0.01	0.02	0.10	0.08	0.08	0.20	0.17	0.15	0.14	0.18	0.22	3
2½	0.6	0.1	0.16	0.18	0.19	0.20	0.195	0.27	0.22	0.23	0.57	0.4	0.36	0.25	0.3	0.3	2½
2	0.6	0.5	0.74	0.56	0.58	0.55	0.54	0.61	0.53	0.54	0.76	0.67	0.58	0.4	0.32	0.34	2
1½	1.45	1.3	1.3	1.3	1.3	1.15	1.1	1.1	0.91	0.86	1.05	0.92	0.78	0.5	0.40	0.32	1½
1	2.2	2.2	2.15	2.1	1.95	1.7	1.65	1.6	1.35	1.24	1.3	1.13	1.15	0.62	0.42	0.34	1
½	2.8	2.75	2.65	2.6	2.45	2.15	2.1	2.0	1.7	1.55	1.6	1.4	1.25	0.68	0.47	0.36	½
0	3.0	3.0	2.9	2.85	2.75	2.55	2.4	2.25	1.95	1.79	1.8	1.6	1.4	0.82	0.54	0.4	0
-½	3.0	3.0	3.0	2.9	2.8	2.6	2.45	2.3	2.0	1.82	1.8	1.63	1.41	0.92	0.60	0.45	-½
-1	2.8	2.8	2.8	2.8	2.65	2.45	2.3	2.15	1.90	1.7	1.65	1.5	1.35	0.92	0.62	0.47	-1
-1½	2.3	2.3	2.4	2.3	2.2	1.95	1.9	1.85	1.70	1.57	1.4	1.3	1.16	0.86	0.64	0.53	-1½
-2	1.55	1.5	1.6	1.6	1.55	1.4	1.5	1.5	1.4	1.30	1.15	1.05	0.96	0.78	0.64	0.58	-2
-2½	0.72	0.72	0.82	0.84	0.87	0.8	0.9	1.0	1.0	0.96	0.81	0.78	0.76	0.72	0.63	0.62	-2½
-3	0.28	0.29	0.34	0.37	0.4	0.37	0.44	0.60	0.61	.62	0.51	0.54	0.53	0.62	0.58	0.57	-3
-3½	0.04	0.06	0.08	0.1	0.16	0.15	0.2	0.34	0.33	0.36	0.27	0.40	0.31	0.50	0.36	0.43	-3½
-4	0	0	0	0	0	0	0.04	0.15	0.11	0.11	0.08	0.15	0.11		0.24	0.36	-4
-4½	0	0			0		0	0.06	0.03	0.02	0	0.02	0			0.20	-4½
-5									0	0	0	0	0				
	2.0	2.5	3.0	3.5	4.0	4.5	5.0	5.5	6.0	6.5	7.0	7.5	8.0	9	10	11	

z–AXIS (inches)

Figure A-1. Raw flux map data for x-z plane.
(calorimeter reading in millivolts)

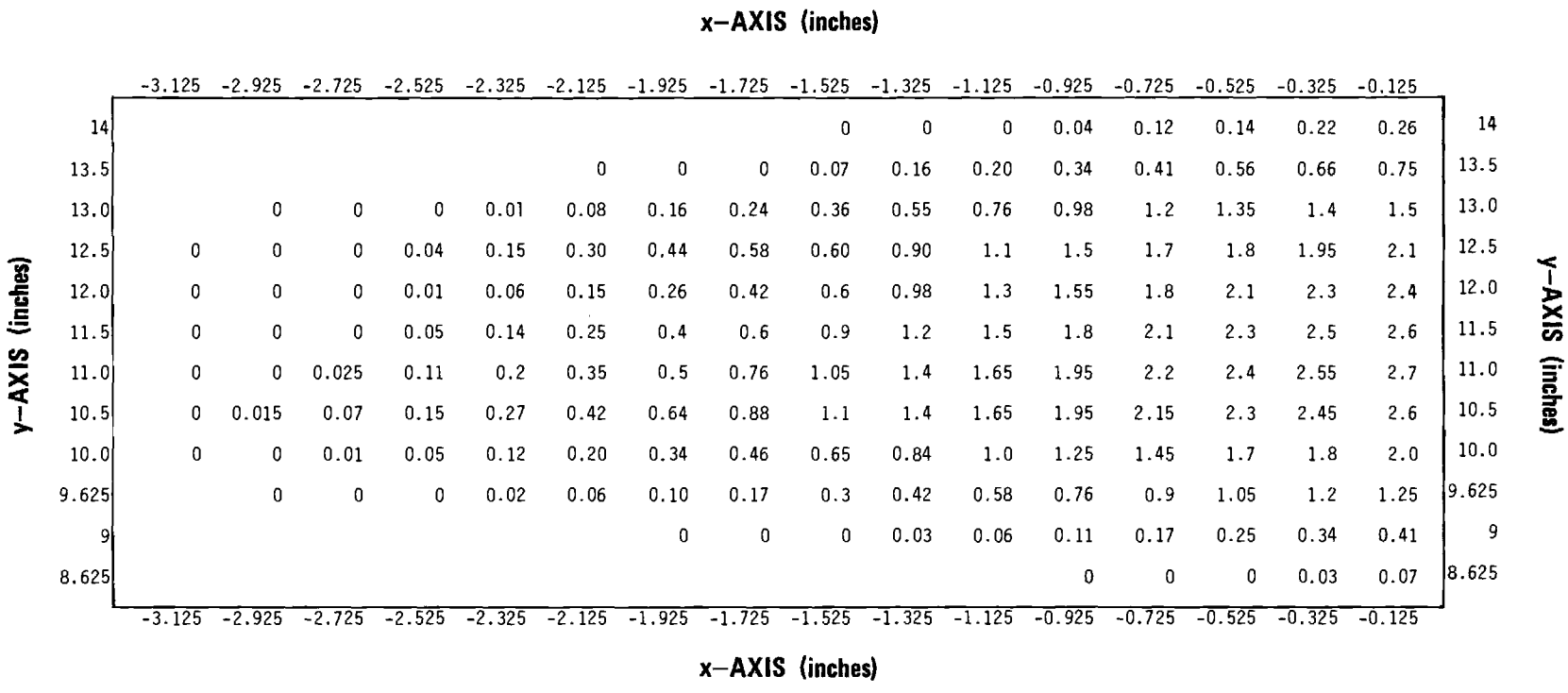

Figure A-2. Raw flux map data for x-y plane.
(calorimeter reading in millivolts)
(continued)

x–AXIS (inches)

y–AXIS (inches)	0.075	0.275	0.475	0.675	0.875	1.075	1.275	1.475	1.675	1.875	2.075	2.275	2.475	2.675	2.875	y–AXIS (inches)
14	0.33	0.38	0.40	0.40	0.40	0.37	0.33	0.29	0.25	0.2	0.15	0.1	0.05	0	0	14
13.5	0.78	0.81	0.81	0.78	0.70	0.64	0.59	0.52	0.45	0.38	0.32	0.25	0.16	0.03	0.07	13.5
13.0	1.6	1.6	1.5	1.5	1.3	1.2	1.1	1.0	0.81	0.66	0.54	0.43	0.32	0.2	0.07	13.0
12.5	2.2	2.2	2.2	2.1	1.95	1.8	1.6	1.4	1.2	0.91	0.70	0.55	0.36	0.21	0.11	12.5
12.0	2.55	2.6	2.6	2.6	2.5	2.4	2.25	2.1	1.9	1.7	1.5	1.2	0.95	0.71	0.5	12.0
11.5	2.75	2.8	2.8	2.8	2.75	2.65	2.5	2.4	2.2	2.0	1.75	1.45	1.1	0.82	0.55	11.5
11.0	2.75	2.8	2.8	2.8	2.7	2.65	2.5	2.3	2.1	1.9	1.65	1.25	0.9	0.6	0.35	11.0
10.5	2.7	2.75	2.75	2.7	2.65	2.55	2.4	2.2	1.9	1.65	1.35	1.05	0.71	0.46	0.29	10.5
10.0	2.05	2.15	2.2	2.2	2.2	2.15	2.0	1.9	1.7	1.4	1.1	0.9	0.62	0.42	0.24	10.0
9.625	1.35	1.4	1.4	1.5	1.4	1.35	1.25	1.1	0.9	0.65	0.53	0.38	0.24	0.14	0.06	9.625
9	0.46	0.49	0.5	0.5	0.48	0.44	0.41	0.38	0.29	0.2	0.13	0.01	0	0	0	9
8.625	0.09	0.11	0.12	0.12	0.1	0.07	0.06	0.03	0	0	0	0	0	0	0	8.625
	0.075	0.275	0.425	0.675	0.875	1.075	1.275	1.475	1.675	1.875	2.075	2.275	2.475	2.675	2.875	

x–AXIS (inches)

Figure A-3. Raw flux map data for x-y plane. (calorimeter reading in millivolts) (concluded)

y–AXIS (inches) \ z–AXIS (inches)	2.0	3.0	4.0	5.0	6.0	7.0	8.0	9.0	10.0	11.0	11.3
14.0	0.38	0.38	0.26	0.55	0.74	0.73	0.44	0.38	0.61	0.48	0.43
13.5	1.05	1.05	0.70	1.00	1.10	0.94	0.68	0.65	0.64	0.46	0.42
13.0	2.40	1.90	1.50	1.85	1.50	1.25	0.86	0.58	0.71	0.42	0.40
12.5	2.70	2.70	2.40	2.05	1.95	1.55	1.05	0.84	0.70	0.43	0.38
12.0	3.00	3.20	2.70	2.55	2.30	1.72	1.20	0.90	0.71	0.43	0.40
11.5	3.00	2.75	2.70	2.60	2.35	1.85	1.35	0.94	0.74	0.43	0.37
11.0	2.75	2.55	2.50	2.40	2.05	1.80	1.40	0.96	0.71	0.42	0.36
10.5	2.20	2.20	2.00	1.95	1.70	1.45	1.10	0.91	0.78	0.48	0.45
10.0	1.45	1.40	1.35	1.40	1.35	1.20	1.00	0.86	0.80	0.50	0.47
9.5	0.80	0.85	0.92	1.00	0.94	0.96	0.78	0.76	0.71	0.50	0.49

Figure A-4. Raw flux map data for y-z plane.
(calorimeter reading in millivolts)